A DISSERTATION FOR THE DEGREE OF DOCTOR OF PHILOSOPHY

Stochastic model for predicting the bending strength distribution of glued laminated timber based on knot area ratio in lamination

층재 내 옹이면적비를 반영한 구조용집성재의 휨강도분포 예측모델

By

Sung-Jun Pang

August, 2015

DEPARTMENT OF FOREST SCIENCES

GRADUATE SCHOOL

SEOUL NATIONAL UNIVERSITY

A DISSERTATION FOR THE DEGREE OF DOCTOR OF PHILOSOPHY

Stochastic model for predicting the bending strength distribution of glued laminated timber based on knot area ratio in lamination

층재 내 옹이면적비를 반영한 구조용집성재의 휨강도분포 예측모델

Professor: Jun-Jae Lee

By

Sung-Jun Pang

August, 2015

DEPARTMENT OF FOREST SCIENCES

GRADUATE SCHOOL

SEOUL NATIONAL UNIVERSITY

Abstract

The aim of this study was to develop a stochastic glued laminated timber (glulam) beam model for predicting the glulam bending strength distribution. The glulam model adds to the understanding of glulam behavior and enables the influence of parameters on the load-bearing capacity to be investigated. As model applications, size effect, effect of knot size restriction, and reliability analysis of glulam were investigated using the developed glulam model.

The developed glulam beam model requires localized modulus of elasticity (MOE) and localized tensile strength of lamination as input variables. Since the localized tensile strength cannot obtain without destructive testing, the tensile strength was calculated using material regression model based on localized MOE and localized knot area ratio (KAR). The localized MOE was obtained by MSR machine and the localized KAR was obtained by image process system. Since the lengthwise variation on lamination is reflected in the lengthwise input variables, the developed glulam beam model can investigate the glulam

size effect and influence of knot limitation by reflecting tensile strength of finger joint instead of the tensile strength reduced by knot.

The bending strength distributions in four types of glulams were simulated using the developed glulam beam model; these four types included: (1) glulam beams without finger joint, (2) glulam beams with finger joints, (3) glulam beams with different lamination size. (4) glulam beams with different lamination grade. The simulated bending strength distributions were validated with actual bending strength distributions tested with full size glulam beams. The Kolmogorov-Smirnov goodness-of-fit test results showed that all of the simulated bending strength distribution were fit well with the tested bending strength distributions. Especially, the difference of 5% point estimate was approximately 1%.

As the model applications, the size effect of glulam beams was investigated using the developed glulam model. The size effect exponent was determined as approximately 16.9 and the calculated bending strength using size effect function fits well with the simulated bending strength. The effect of knot size restriction investigated using the developed glulam model shows that there is a specified knot size

restriction for optimizing the glulam bending strength due to the possibility of that the tensile strength of finger-jointed lamination inserted instead of knots can be lower than the original tensile strength. In other words, the phenomenon means that the quality of finger joint is important since the glulam bending strength can be increased as increasing the finger joint strength and reducing the strength variation. Reliability analysis has been carried out using the load distributions in Korea and the simulated glulam bending strength distributions with Monte Carlo simulation. Reliability indexes of all glulam Types were bigger than 3.0 at the resistance factor, 0.8.

Keywords : glued laminated timber, bending strength, tensile strength, probabilistic model, transform section method, reliability analysis, Monte Carlo simulation

Student number : 2011-30341

Contents

List of Tables

List of Figures

Nomenclature

Abbreviations

ASD	allowable stress design
COV	coefficient of variation
glulam	glued laminated timber
ISO	the International Organization for Standardization
JAS	Japanese Agricultural Standard
KAR	knot area ratio
KAR restriction	the maximum allowable knot size (%)
KBC	Korean building codes
KFRI	Korea Forest Research Institute
KICT	Korea Institute of Civil Engineering and Building Technology
LSD	limited state design
MinLenLa	the minimum length between finger joints (mm)
MOE	modulus of elasticity (MPa)
MOR	modulus of rupture (MPa)
RBD	reliability-based design
ULAG	Ultimate Load Analysis of Glulam

Latin upper-case letters

A_i	Cross section area of the i^{th} lamination (mm^2)
D	the uniformly distributed dead load (random variables) (N)

D_n the design dead load (N)

E_T the modulus of elasticity of the virtual glulam (MPa)

E_i MOE of the i^{th} lamination (MPa)

GL_i grade of lamination (i = # of lamination)

G_b : the bending failure limit state of a simply supported beam of rectangular cross-section

I the moment of inertia (mm^4)

I_T the moment of inertia of the virtual glulam cross section (mm^4)

I_k the moment of inertia of the knots at a cross section (mm^4)

I_g the moment of inertia of the beam cross section (mm^4)

L the beam span (mm)

L_1 length of glulam 1 (mm)

L_2 length of glulam 2 (mm)

M maximum bending moment ($N \cdot mm$)

M_{ult} ultimate moment carrying capacity of entire virtual glulam ($N \cdot mm$)

$M_{ult,S}$ ultimate moment carrying capacity of virtual glulam at a segment ($N \cdot mm$)

P_{max} applied maximum load (N)

P_f the probability of failure, $G_{bending} \leq 0$ in Eq. (6.13)

Q_{DL} the uniformly distributed load (N)

Q the uniformly distributed live load (random variables) (N)

Q_n the design live load (N)

R the bending strength (random variables) (MPa)

R_g random variables taken from simulated glulam bending strength (MPa)

$R_{0.05}$ the characteristic strength (the nonparametric 5th percentile) (MPa)

S the section modulus of virtual glulam (mm^3)

T thickness of beam (mm)

T_1 thickness of glulam 1 (mm)

T_2 thickness of glulam 2 (mm)

W width of beam (mm)

W_1 width of glulam 1 (mm)

W_2 width of glulam 2 (mm)

X_1 independent variable (herein, knot area ratio)

X_2 independent variable (herein, modulus of elasticity) (MPa)

Y the predicted tensile strength (MPa)

Latin lower-case letters

d random variables, the dead loads normalized with respect to their corresponding design values (mm)

q random variables, the dead loads normalized with respect to their corresponding design values (mm)

$f_{b,i}$ modulus of rupture of the i^{th} lamination (MPa)

$f_{t,i}$ tension strength of the i^{th} lamination (MPa)

k ratio of MOR and tensile strength of lamination

k_{size} the size effect exponent

l load span in machine stress grader (600 mm)

t thickness of lamination (mm)

w width of lamination (mm)

y the distance from the neutral axis to the location of a extreme fiber stress (mm)

$y_{i,c}$ distance between a neutral axis of virtual glulam and a centroid of ith lamination (mm)

$y_{i,t}$ distance between a neutral axis of virtual glulam and a tensile stress of ith lamination (mm)

$y_{i,end}$ distance between a neutral axis of virtual glulam and an end of ith lamination (mm)

Greek upper-case letters

Δy deflection at center of load span in machine stress grader (4 mm)

Φ^{-1} the inverse cumulative distribution function (CDF) of the standard normal distribution

$\emptyset$ resistance factor, a deterministic parameter for calibrating a probability of failure

Greek lower-case letters

σ_b : the maximum bending stresses of a beam (MPa)

$\sigma_{i,b}$ the bending stress component of the *i-th* lamination (MPa)

$\sigma_{i,glulam}$ the stress of the *i-th* lamination in glulam (MPa)

$\sigma_{i,t}$ the tensile stress component of the *i-th* lamination (MPa)

σ_1 the strength of glulam 1 (MPa)

σ_2 the strength of glulam 2(MPa)

β_i regression coefficients

ϵ the error term

γ dead-live load ratio, a deterministic parameter and herein chosen to be 0.25, 0.5, 1, 1.5, 2 (KICT, 1989)

Chapter 1. Introduction

1.1 Background

Reliability-based design (RBD) based on the reliability analysis has become a global trend due to the demands of cost-effective and reasonable optimized design with the tendency of multifunctional and large-scale of modern architecture. The RBD allows the consistent, economical, and efficient design by evaluating quantitatively the safety of structures using the probability of failure and the target reliability index. The probability of failure and the reliability index is calculated through the reliability analysis of databases established by researches. Especially, the collapse of a large facility leads the lumber of precious lives and astronomical direct or indirect economic loss. Thus, it is required to ensure a reasonable level of safety from the design stage. The RBD allows to ensure the required safety in the design process by considering the uncertainties of design variables related to material properties, applied load, and analytical models.

The RBD procedures for engineered structures, civil engineering structures as well as machinery, shipbuilding, have been developed and accepted throughout the world. Since the announcement of structural reliability theory (Freudenthal, 1947; Pugsley, 1955), the structural design codes based on

reliability has been actively researched. Reliability-based design has been widely recognized as a design code in the structural engineering field and applied to actual structural design based on a number of studies over the past 50 years. In addition, the RBD has been applied for engineered wood structures and the design concept has been included in the design standards of the International Organization for Standardization (ISO) as well as in the national design code of United States, Canada, Europe, Australia, New Zealand and China.

Korean building codes (KBC) for wood structures are based on allowable stress design (ASD). ASD is a traditional design philosophy and is based on the accumulation of knowledge and experience collected over a long period of time. Thus, although a larger cross section member is used in a structure, the actual safety of the structure cannot be quantified. On the contrary, limited state design (LSD), which is one of RBD, allows to control the probability that structures collapse and/or that they cannot maintain functionalities by calculating the failure probability based on the applied load and resistance distribution.

In order to derive suitable safety factor, reliability analysis is required using load and resistance variables. The load variables for LSD are already established in building codes and commonly used regardless of materials. However, the resistance variables are different depending on materials, especially, the material variables reflect regional characteristics. Currently, resistance factor and characteristic values for domestic steel (Sin et al., 2007), concrete (Kim et al., 2007), and foundation piles (Park et al. 2011) have been investigated based on domestic data. Strength distribution of domestic timber has been investigated through full-scale test by several researchers. However, the strength distribution of domestic glued laminated timber (glulam) has not investigated yet.

Glued laminated timber (glulam) is most widely-used engineered-wood-products and predominately used for beam elements in large scale structures, such as stadium, station, conference room, and swimming pool. glulam is manufactured by bonding laminations in longitudinal direction. Thus, glulam can be designed for the required performance by control of the lamination species, grade, thickness, width, etc. Meanwhile, experimental evaluation for establishing design values is clearly too expensive due to the diversity of lamination size, grade and combination. Therefore, using a predictive model,

which makes it possible to estimate the properties of glulam from those of the laminations, is required. In addition, a rational model adds to the understanding of glulam behavior.

Development of LSD code for domestic wood design is required for promoting domestic wood structures. To do this, the specified design stress of domestic wood species should be provided by evaluating the structural characteristics. In case of glulam, experimental approach is not possible due to too large sample size for full scale tests. Thus, using validated prediction model is required for developing resistance factor and characteristic values of glulam. Moreover, the prediction model can provide a good solution for improving a quality standards of glulam by considering visual quality level and design of a large size glulam by considering size effect.

1.2 Objectives

The main objective of this study was to develop a stochastic glued laminated timber beam model for reliability assessment of domestic glulam beams. Specifically, sub-objectives were to investigate as follows:

1) Stochastic model for predicting glulam bending strength distribution
2) Size effect and knot size restriction on glulam bending strength distribution
3) Reliability analysis based on glulam bending distributions and loads distribution in Korea

Chapter 2. Literature Review

2.1 Reliability analysis and resistance factor for timber engineering

The concept of using the probability of failure as a criterion for structural design was presented in the late 1920s by the Russians N. F. Khotsialov and N. S. Streletskii, and the classical structural reliability theory became widely known through a few influential publications such as Freudenthal (1947) in USA and Pugsley (1955) in UK (Paikowsky, 2002). The reliability research for structural design has been actively conducted Mainly in Europe, the USA, Canada and other developed countries. In addition to the above, the structural reliability analysis have been presented in the structural design for civil, geotechnical, mechanical, and shipbuilding engineering by many researches (Cornell, 1969; Ang and Cornell, 1974; Hasofer and Lind, 1974; Rackwitz and Fiessler, 1978; Ellingwood et al., 1980; Haldar and Mahadevan, 2000; Wen, 2001; Huh and Haldar, 2001). Based on these research results, limited state design (LSD) and load resistance factor design (LRFD) have been developed and applied for actual structural design.

For the design of engineered timber structures, the concept of partial safety factor has been applied in Denmark (Danish Standards Institute, 1983) and the

draft Eurocode adopted the formats of LSD codes (European Committee for Standardization, 1990), including Eurocode 1 “Basis of Design and Actions on Structures” and Eurocode 5 “Design of Timber Buildings” to ensure the safety of structures. The researches for LSD codes for timber structures has been presented in several countries, Canada (Canadian Standards Association, 1989), Australia (Leicester 1990), New Zealand (Standards Association of New Zealand, 1991), and USA (Goodman, 1990) and the countries adopted the LSD codes for timber structures. Finally, the internationally harmonized codes for wood structures have been emphasized through reviewing the state-of-the-art on LSD procedures and exchanging ideas and approaches used with various construction materials.

The effort for developing the LSD codes and converting from ASD codes to LSD codes has been done for engineered wood structures throughout the world (Figure 2-1). Currently, the application of reliability-based design codes for wood structures has become the global trend. The domestic design code for wood structures is based on ASD that applies uniform safety factor based on experience and do not take into account the uncertainty of applied loads and structural materials. The LSD codes allow to consistent reliability level of a particular structural element or system by reflecting target reliability levels

or the probability of failure. The LSD codes permit a more economical design while ensuring acceptable reliability and lead to harmonization with other structural codes by establishing a common conceptual framework to address reliability issues. Thus, the design codes for structural engineering has been converted to the LSD codes in many countries and domestic design codes for steel and concretes has been also converted to LSD codes.

Load and resistance factors for domestic reinforced concrete structures has been developed by Korea Institute of Civil Engineering and Building Technology (KICT, 1989). Even though the structures codes for steel and concrete has been converted to limited state design in 2005, currently, the appropriate resistance factor for steel (Sin et al., 2007), concrete (Kim et al., 2011), foundation structures (Jang, 2009, Park et al., 2011) has been presented through research results based on domestic data. Thus, the researches for converting domestic timber design codes to limited state design are required for promoting a convergence research with other structures, designing structures using state-of-the-art structural technologies and cooperation between domestic and foreign scientists.

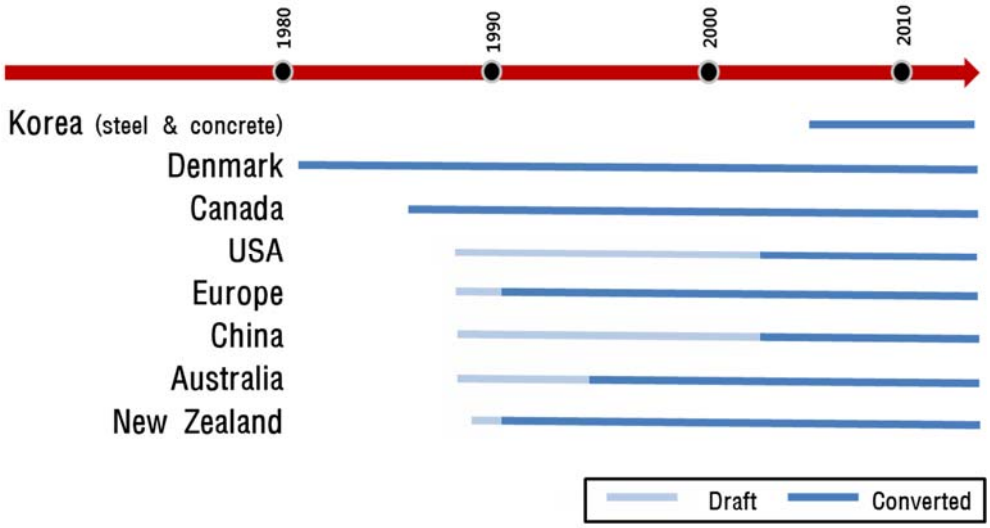

Figure 2-1 Countries adopted reliability-based design codes for timber structures

2.2 In-grade testing and LSD researches for domestic timber

In order to promote the use of domestic wood species as a structural purpose, grading rules and standards related to in-grade timber, testing and statistical processing methods for domestic timber based on full-size test data, timber grading and marking system for controlling the identification and certification of timber has been investigated and analyzed. The reliable strength distribution of structural timber is required for adopting LSD using reliability analysis. The strength distributions of full-sized domestic timber has been investigated through several researchers. However, the strength distribution of domestic glulam has not yet presented.

2.2.1 Domestic grading rules

Oh et al. (1993, 1995) mentioned that became grading rules of North America is not suitable for grading domestic lumber, careful consideration is required in order to adopt the grading rules of North America. He suggested that new grading system for domestic wood species is required and design values of domestic species should be derived to meet the new grading system. Since then, the first lumber grading rule (Korea Forest Research Institute, KFRI, notification 1995-27) for softwood structural lumber was promulgated (KFRI,

1998). The grading rule was reviesd twice in 2000 and 2007 and the term, standard dimensions, and tolerance ect. has been revised at the most recently version (KFRI notification 2009-1). Especially, the range of knot ratio of each grades was modified. Since the knot ratio is the greatest strength reducing factor among wood defects, the review of design values for the in-grade lumber has been required (Oh et al. 2010). The distribution characteristics of bending strength was investigated with rivised visual grading rule and the previous grading rule, respectively, based on domestic softwood in-grade test data (Pang et al. 2010). Meanwhile, the grading rules and grading system of several countries has been reviewed for domestic quality certification and marking system (Yeo et al. 2012). The irrationalism of two domestic grading rules (KS F 3020, KFRI 2009-1) has been revealed and the two national grading rules by different agencies are likely to cause confusion among manufacturers, users, and agencies.

2.2.2 In-grade test and statistical process

In-grade testing and statistical precessing methods are different by countires. The difference among Korea and other countires has been reviewed and the difference of bending strength distribution has been presented based on tested data (Pang et al., 2013a). It was revealed that the statistical processing methods

for deriving characteristic values in domestic standard (KS F 2152) is more strict than other standards (ASTM D 1990, ISO 13910, AS/NZS 4063.2) (Pang et al., 2013b). Most countries apply the 75% confidence level to derive characteristic values of structural timber, however, 95% conficence level is adopted in domestic standard.

Structural properties of domestic species has been investigated for use as a structural building material. Oh et al. (1993) derived the allowable stress of in-grade Korean pine (38×89 mm) and compared to the design value of major imported species such as, Douglas-fir-Larch, and S-P-F. Lee et al. (2003) investigated the bending strength distribution of domestic Japanese larch (38×140 mm) and Lim et al. (2010) evaluated the the feasibility of domestic hardwood (yellow poplar dismension lumber) for structural purpose. Meanwhile, traditional Korean wood buildings have been built with large-size structural timber. Thus, the bending stregnth distribution of large-size structural timber (Korean pine, 120×180 mm) has been investigated (Pang et al., 2011). The researches mentioned above used parametric models (normal, lognormal, weibull) for deriving characteristic values and the characteristic values based on non-parametric models has been investigated (Pang et al., 2013a, b)

2.2.3 Code implementation to limited state design

In order to establish LSD code of domestic wood structures, researches for code conversion has been carried out and more effective use of domestic species with higher design valus has been presented in LSD (Lee et al. 2003, Park et al. 2004, Park et al. 2010). As a basic research for code conversion, Park et al. (2009) compared the ASD and LSD for engineered wood design, and Kim (2009) mentioned the necessity of code conversion to LSD. Pang et al. (2012) investigated the charateristic values of domestic in-grade timber by ASTM D 5457, soft conversion standard, however, the resistance factors of the domestic species should be reviewed with domestic loads distribution by hard conversion.

The LSD researches for wood structures in KBC was focused on structural solid timber. Glued laminated timber (glulam), among engineered wood products, is mainly used for beam element. Thus, a research for estimating the strength distribution of glulam is required for converting design value.

A sufficiently large sample size is required to derive strength distribution on a statistical basis. Testing of a number of glulam members is clearly too expensive due to the many parameters influencing the properties of glulam

(e.g. timber species, grade, lamination thickness, finger joint, glulam depth). Thus, a model which makes it possible to estimate the strength properties of glulam from those of the laminations is required.

2.3 Modeling of glulam structural behavior

2.3.1 Glulam model for hand calculation

The mechanical modeling for estimating glulam behavior has been carried out for reviewing structural stability and effecient use of wood resources. The glulam stiffness can be estimated using transformed section methods based on beam theory and the glulam strength can be estimated using I_k/I_g-method. In order to investigate the structural characteristics of domestic glulam, these method has been used by several researchers (Kim et al, 2000, Lee et al. 2005)

The I_k/I_g-method was empirically developed by Freas et al. (1954) and adopted ASTM D 3737. This method uses a reduction in the moment of intertia due to knots as a way of taking the strength-reducing effects of knots into accout. I_k and I_g are the moment of inertia of the knots at a cross-section, and the moment of inertia of the beam cross-section, respectively. This method is simple and can estimate the allowable stress of glulam for allowable stress design by hand calculation.

However, this method does not allow the influence of finger joints and assign the same strength reducing effect for knots, whether they are placed in the tensile zone or in the compressive zone, which is unrealistic. Moreover, the

method does not allow the glulam beam strength distribution to be calculated. Thus, this mehod is not suitable for investigating the resistance factor by reliability analysis with charicteristic distribution of glulam.

2.3.2 Glulam models for computer analysis

Several computer simulation models has been developed, not intended for predicting the strength of a particular glulam beam, but rather to estimate population statistics for similar beams and to derive data to be used for the estimation of design values. The models for the determination of mechanical performance are based on stochastic analysis using Monte Carlo simulations.

These models are slightly different from generating input variables modelling. The tensile strength and modulus of elasticity (MOE) were considered as the most critical material properties, since glulam beam failures usually initiate in the tension zone of the beams.

All glulam beam models require the localized properties of the lamination, as well as the correlations among these properties (Richburg et al. 1992). Previous researchers have focused on the within member variation of tensile strength parallel to grain in lamination. Several approaches has been attempted for generating tensile strength and, generally, the tensile strength relationship

between several sections within lamination has been focused on. Showalter et al. (1987) developed length effect model for representing the within member variation of tensile strength of timber. Lam et al. (1991a and b) used window analyses for developing the tensile strength distribution of lamination segments of various lengths. Taylor et al. (1991) developed a stochastic model based on the relationship of lamination segments for simulating localized MOE and tensile strength. Takeda et al., (1999a and b) showed that the length effect on tensile strength was dependent on the mechanical grade of the lumber and governed by the presence of knots.

2.3.2.1 Foschi's model

Foschi and Barrett (1980) presented a more flexible apparoch for predicting a strength and strength distribution of the Douglas-fir glulam beam using Monte-Carlo simulations. A virtual beam was subdivided into 152 mm long cell and having the depth and width of a lamination. Each cell was randomly assigned a density from the assumed normal distribution and a knot diameter from the corresponding knot frequency data which was developed by the Canadian Institute of Timber Construdction for use with the I_k/I_g-method. After allocating a density, both MOE and strength of clear wood were assigned and adjusted for the influence of knot size using the allocated knot diameter.

Foschi‘s model was not reflected the influcence of finger joins. and as a basic data, requires a distribution of knots (knot-size frequencies) within each grade, and tensile test results on the different lamination grades. Thus, in order to apply this model for other speices the basic data should be developed.

2.3.2.2 Karlsruhe model

This model used a subdivison of a virtual glulam beam into 150 mm long cells (Ehlbeck et al., 1985a-c). The lamination was assumed to consist of two materials, wood and finger joints. The basic input variables were density and KAR. A section of a lamination between two finger joins are assigned a density and a KAR value. The specific KAR and density value are then used to calculate the MOE and strength of each cell using regression equations containing random elements. The finger joints are modelled in the same method as described above.

2.3.2.3 Bender‘s model (Prolam)

Bender et al. (1985) and Hernandez et al. (1992) developed a glulam beam model for predicting the statistical distribution of glued laminated beam strength. The model was based on actual lamination properties rather than clear wood stresses and knot information. As input data, lamination properties

(MOE and tensile strength) and finger joint properties (MOE and tensile strenght) were used. The lamination properties were simulated with 610 mm long MOE and tensile strength values using a correlate random variable (Taylor and Bender, 1991). Meanwhile, the finger joint MOE and tensile strength was simulated as functions of the 610 mm lamination MOE values on each side of the joint. The finger joint MOE was simulated using a regression approach that relates the finger joint MOE to the MOE values of the two segments on each side of the joint. The finger joint tensile strength was assinged using a regression model related finger joint tensile strength to the finger joint MOE.

2.3.2.4 Folz's model (ULAG)

Folz (1997) presented a glulam beam model, entitled Ultimate Load Analysis of Glulam (ULAG). The requisite input material properties of the model were the tensile strength and the corresponding mean elastic modulus from each lamination test specimen as well as the end-joint strength and the mean elastic modulus from each end-joint specimen. The tensile strength and the elastic modulus of the lamination material were modeled as one-dimensional homogeneous stochastic fields and a spectral approach was used for generating the input variables. The realizations of each material property were

simulated using a series representation of the stochastic field as a summation of cosine series involving random phase angles and amplitudes weighted according to the spectral density function.

2.3.2.5 Lee's model

Lee et al. (2005) presented a predition model for bending properties of glulam using optimized knot and MOE distributions of lamination. The bending strength of virtual glulam beam was predicted using I_k/I_g-method and Monte Carlo simulation. This model developed for simulating the bending strength distribution, however, the effect of finger-jointed lamination and lengthwise variation of lamination was not reflected.

2.3.2.6 Nakamura's model (SiViG)

Nakamura and Fujita (2011) presented a simulation method of strengths for glulam using correlated random variables. This model is optimised for the compatibility conditions for each lamination grade in the JAS and uses a tested strength distribution of finger-jointed lamination which is manufactured and tested according to Japanese Agricultural Standard (JAS). Thus, the glulam manufacturer uses this model for certifying the glulam beams producted

according to the JAS. However, this model does not consider the size effect of glulam.

2.3.2.7 Fink's model

Fink (2014) developed a glulam beam model for the probabilistic representation of the material properties. The lamination was subdivided into two types of section, knot sections and clear wood section. Two indicators were selected due to the large correlation between the global indicators: dynamic MOE to consider the between-member variability and KAR to consider the within-member variability.

Taking into account the two indicators, the tensile stiffness and the tensile strength of knot was predicted and the tensile strength of finger joint was assumed to be equal to the tensile strength of a specific knot. The distribution of distence between knots was generalized using Gamma distribution. This model attempted to reflecting natural growth characteristic of timber for assigning the position of knot and finger joint connections. These efforts make the probability of inappropriate configurations, such as knot, can be controled.

2.4 Conclusions

Several researches for adopting reliability-based design to domestic wood structures has been presented. However, few researches has been carried out for domestic glulam distribution. In order to estimate the population statistics for domestic glulam beam, a computer simulation model is required based on lamination properties. Several glulam beam models has been developed overseas based on lamination properties. The models are based on the same principle, however, the different input variables and the different method for generating the lamination characteristics are used. The previously developed model requires tensile strength of lamination as a input properties, and uses correlated random variables for generating the tensile strength. Thus, the generated tensile strength would be difference with actual tensile strength variation of lamination and the knot effect can not be considered.

Domestic wood species have a high frequengy of knots. Since the knot is the most strength reducing defects, the knots are removed and connected with finger joints. Thus, domestic lamination have a high frequency of finger joints. Reducing the high frequency of finger joint is required for saving the manufacturing cost. Meanwhile, the glulam standard, KS F 3021, provides the combination of laminations for manufacturing glulam and low-quality

laminations can not be used for manufacturing glulam. In order to maximize the benefits of glulam that various combinations are possible, a way for using the low-quality laminations should be considered. Usually, the low-quality laminations determined by a big knot. Thus, a new glulam model that considers the influence of knots on glulam is required for increasing the utilization of low-quality domestic wood.

Chapter 3. Development of glulam beam model

3.1 Basic concept

In Korea, graded laminations and finger-jointed laminations are manufactured based on orders received and the graded laminations cannot be obtained in the market. It means that the quality of manufactured lamination and glulam can significantly vary depending on the manufacturer. A few manufacturers produce glulam beams in accordance with a standard regulation and the regulation for graded lamination can be revised in order to better reflect the domestic situation. The strength properties of graded lamination for domestic wood species were not sufficiently researched and can be changed depending on the visual quality level in the regulation.

Thus, in this study, the glulam model was developed to reflect the growth characteristics of lamination and to review the glulam bending strength distribution by changing the knot size to be removed. As input properties, the localized KAR and MOE of lamination were used, and the localized tensile strength is calculated by the KAR and MOE of same location of lamination. Thus, the actual tensile strength variabion of lamination is reflected into the virtual glulam beam and high prediction accuracy can be expected.

Moreover, effect of knot on glulam bending strength distribution can be investigated by removing bigger knots than a specific KAR and connecting the divided lamination using finger joints. Due to the use of localized MOE and KAR, the possibility of weak zone is increased as much as the lamination length and lamination layer are increased. Thus, the size effect of glulam is reflected at the simulated bending strength distributioin.

For the developed glulam beam model, the following assumptions were used for simulating glulam bending strength distribution.

1) Tension failure :

   Glulam bending strength is governed by the tensile strength of lamination or finger joint. The failure of glulam beam is originated at a knot or a finger joint (E. Serrano, 2003). To simplify the model, only tension failure at lamination or finger joint was assumed in this study. In reality, some compression failure could be occur in compression side of beam. But in this study the influence of compression side was not considered in this study.

2) Elastic behavior :

Under the first assumption, behavior under tension can be assumed as elastic behavior.

3) Tensile strength of lamination :

The tensile strength of lamination can be predicted by the combination of KAR and MOE (Johansson et al., 1992, Glos et al., 1982, and Johansson, 1976)

4) Finger joint :

Manufacturer makes finger joint when the knot larger than visual quality (VQ) restraint was found and also some serious defects/serious drying problem was found. In this study, knot was focused; hence, if there is larger knot than predefined knot restraint, the knot was removed then the divided two pieces of laminae were finger jointed.

5) Weakest link theory :

The moment carrying capacity of glulam beam is governed by the weakest section of glulam beam.

6) Layup of lamination for virtual glulam :

Model generates a virtual glulam in the same manner as the actual glulam are made.

7) Laminating effect :

Bending strength distribution of glulam beams has a higher mean value and a lower coefficient of variation (COV) than the tensile or bending strength distribution of the lamination (Falk, 1995). In this model, the reflecting laminating effect is reflected as follows:

- Distance between a neutral axis of virtual glulam and tensile stress in the outer lamination was determined using combined stress of tensile strength and bending stress (Figure 3-7), in order to reflect the tensile stress of a glulam in bending which is not uniform through the beam depth.

- In a segment, a higher stress is applied at a higher MOE lamination than a lower MOE lamination by Eq. (3.2). Thus, reinforcing effet (when laminations are bonded in a glulam, defects and low-stiffness areas are reinforced.) is reflected.

- In this model, lengwise KAR and MOE of a lamination are assigned to a virtual glulam beam. Thus, a weak zone in lamination which governs tensile strengh of lamination will not be placed in a high-stressed location in virtual glulam beam. Thus, a possibility that the lowest strength in lamination will initiate beam failure is decreased.

3.2 Theoretical model for estimating glulam bending strength distribution

The calculation process of developed glulam beam is as follows (Figure 3-1);

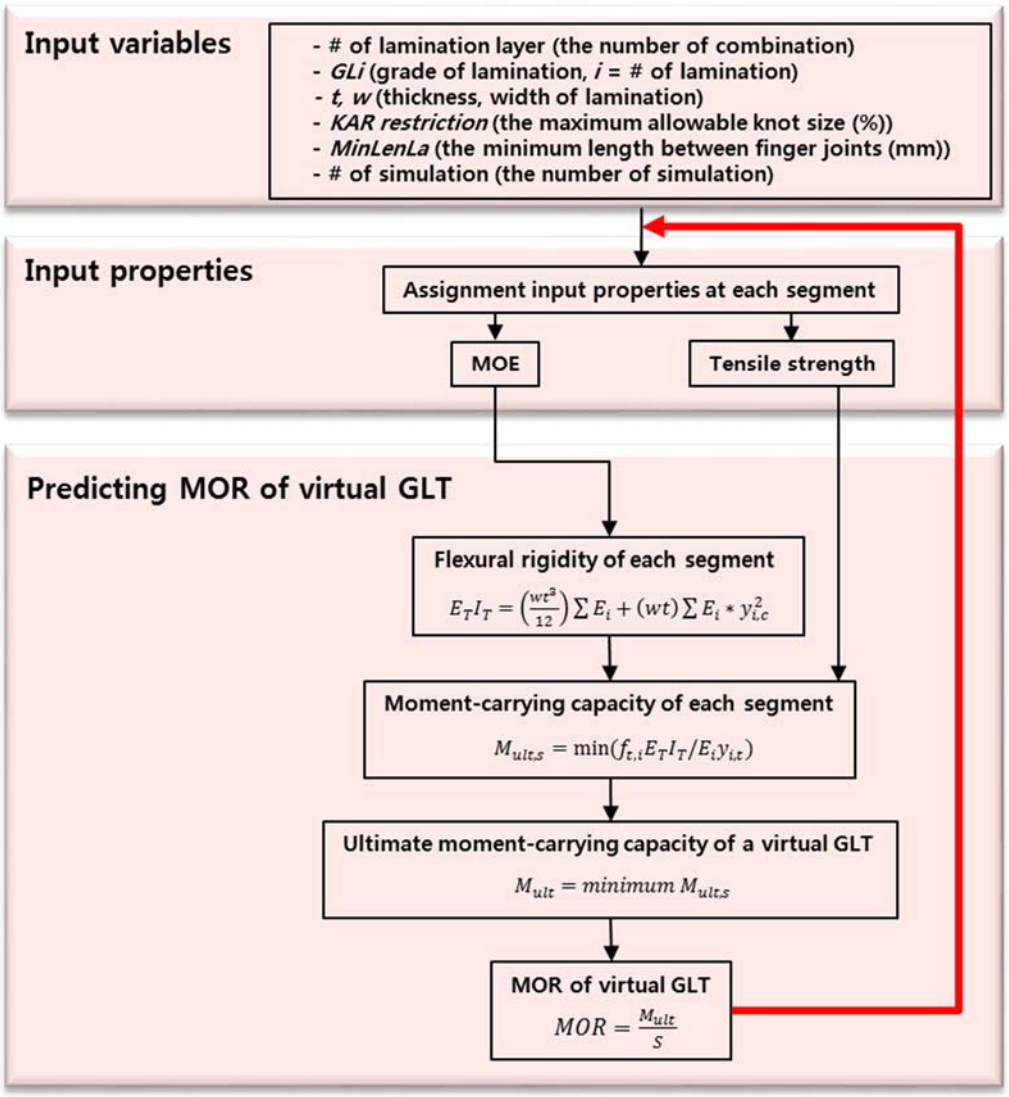

Figure 3-1 Flowchart to predict MOR

3.2.1 Input properties

In order to assign the input properties to virtual segments of glulam, lamination database was constructed as shown in Figure 3-2. The localized KAR and MOE of each lamination was obtained using image process system and MSR, respectively. The localized tensile strength was calculated from the localized KAR and MOE using the tensile strength predicting model (Figure 3-3).

3.2.2 Generating the virtual glulam

In order to reflect an actual manufacturing site condition, a virtual glulam beam was generated in the same manner as the actual glulam are made. As input variables for generating a virtual glulam beam, the number of lamination combination, grade of lamination layer, thickness and width of each lamination layer, the number of simulation, allowable knot size for inserting finger joint, and a minimum length between finger joints are required. The virtual glulam depth is determined by the information of the number combination and thickness of each lamination layer and the virtual glulam length is determined 18 times the glulam depth. The segment of virtual glulam was divided into 1mm on lengthwise for reflecting lengthwise variation of lamination.

3.2.3 Assigning the input properties from lamination database

The virtual segments of glulam were assigned with localized MOE and tensile strength of lamination database. In order to reflect the manufacturing condition, each lamination of same grades was linked in longitudinal direction (Figure 3-4) and the virtual lamination MOE and tensile strength of glulam were taken into from same lamination grade database as much as the virtual length of glulam (Figure 3-5). The first assigned lamination properties for a specific lamination layer grade were randomly selected from the same lamination grade database. The next assigned lamination properties for other lamination layer were taken into from the next to the previously extracted lamination part.

The input properties of finger joint were inserted instead of tensile strength of lamination. The position of finger joint was determined by a knot size. If a knot size is bigger than a designated allowable knot size, a tensile strength of finger joint was used instead of a tensile strength calculated by KAR and MOE on lamination. In a finger joint manufacturing process, too short lamination cannot be jointed. Thus, the information of minimum length between finger joints is required for preventing the generation of finger joints next to the previously generated finger joints.

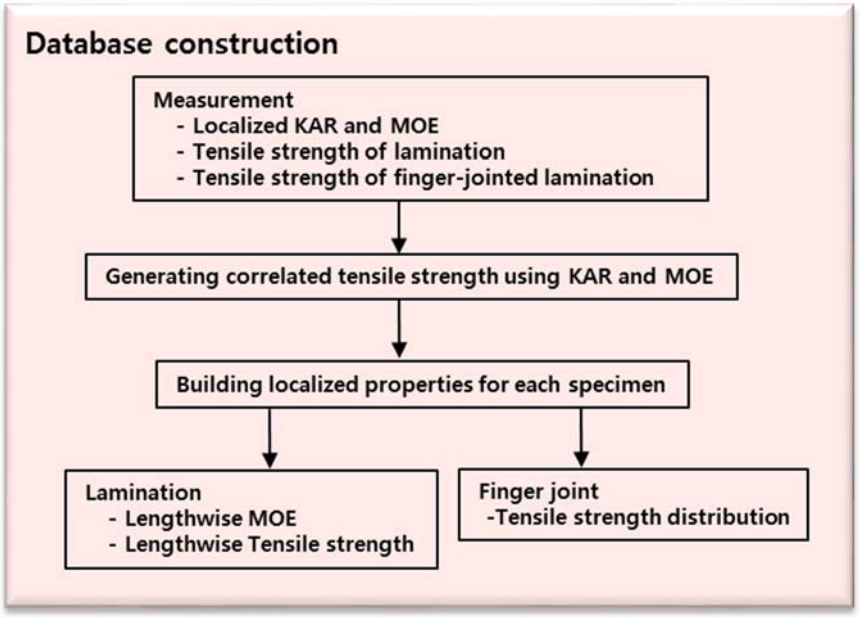

Figure 3-2 Flow chart of database construction

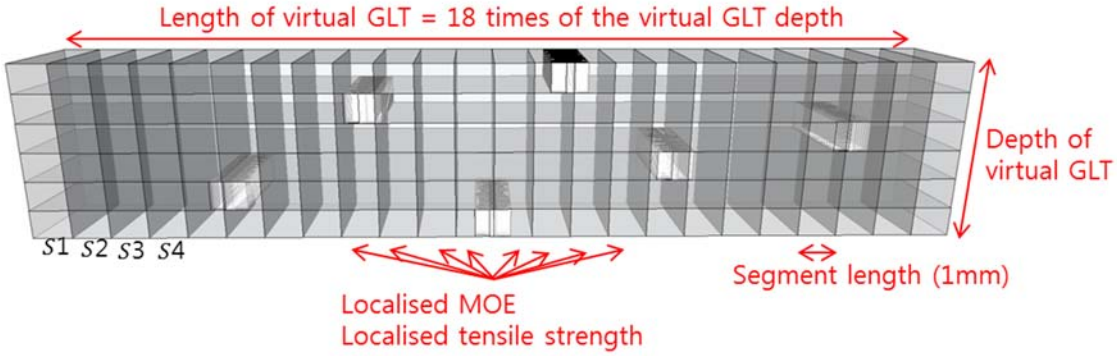

Figure 3-3 Generation of virtual glulam

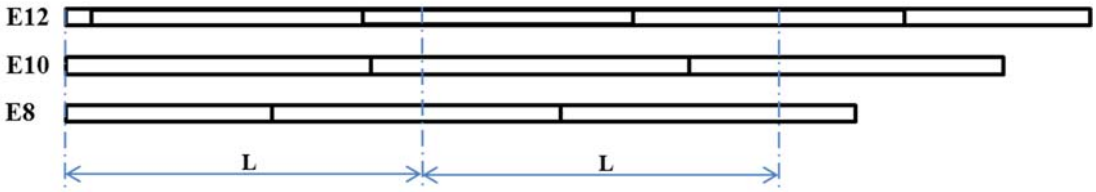

Figure 3-4 Laminations were connected with same grades

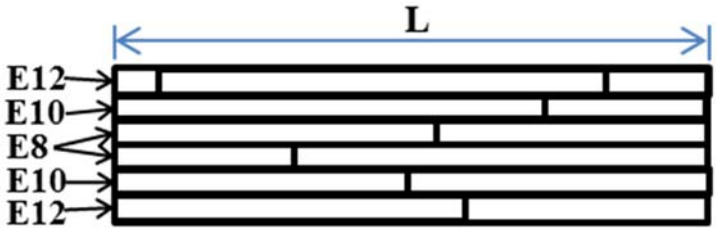

Figure 3-5 Example of virtual glulam beam assembly from lamination stock database

3.2.4 Predicting MOR of virtual glulam

The bending stiffness and strength of virtual glulam was predicted using transform section method. According to transform section method, the flexural stiffness for laminations of constant thickness, *t*, is given by Eq. (3.1) and the stress in the i^{th} lamination is given under moment, *M*, by Eq. (3.2)

$$E_T I_T = \left(\frac{wt^3}{12}\right)\sum_i E_i + (wt)\sum_i E_i\, y_{i,c}^2 \tag{3.1}$$

Where,

$E_T =$ the modulus of elasticity of the virtual glulam (MPa)

$I_T =$ the moment of inertia of the virtual glulam cross section (mm^4)

$w =$ width of lamination (mm)

$t =$ thickness of lamination (mm)

$E_i =$ MOE of the i^{th} lamination (MPa)

$y_{i,c} =$ distance between a neutral axis of virtual glulam and a centroid of i^{th} lamination (mm)

$$\sigma_{t,i} = \left(\frac{E_i\, M\, y_{i,t}}{E_T I_T}\right) \tag{3.2}$$

Where,

$\sigma_{t,i} =$ tensile stress of the i^{th} lamination (MPa)

$E_i =$ MOE of the i^{th} lamination (MPa)

$M =$ bending moment of virtual glulam ($N \cdot mm$)

$y_{i,t} =$ distance between a neutral axis of virtual glulam and tensile stress of i^{th} lamination(mm)

E_T = the modulus of elasticity of the virtual glulam (MPa)

I_T = the moment of inertia of the virtual glulam cross section (mm^4)

The neutral axis of each segment is calculated using localized MOE of each lamination and the moment capacity of each segment is calculated using the localized tensile strength of each segment (Eq. (3.3)). This procedure is repeated along the length of entire virtual glulam beam as shown in Figure 3-6. Finally, the minimum moment obtained from all of the analyses along the length of the beam defines the ultimate moment-carrying capacity of the virtual glulam beam.

$$M_{ult,s} = min\left(\frac{f_{t,i}E_T I_T}{E_i y_{i,t}}\right) \quad (3.3)$$

Where,

$M_{ult,S}$ = ultimate moment carrying capacity of virtual glulam at a segment ($N \cdot mm$)

$f_{t,i}$ = tension strength of the i^{th}lamination (MPa)

E_T = the modulus of elasticity of the virtual glulam (MPa)

I_T = the moment of inertia of the virtual glulam cross section (mm^4)

E_i = MOE of the i^{th} lamination (MPa)

$y_{i,t}$ = distance between a neutral axis of virtual glulam and tensile stress of i^{th} lamination (mm)

Once the ultimate moment-carrying capacity of the glulam beam is determined, the apparent modulus of rupture (MOR) of the beam is calculated using Eq. (3.4).

$$MOR = \frac{M_{ult}}{S} \tag{3.4}$$

Where,

$MOR =$ the apparent modulus of rupture (MPa)

$M_{ult} =$ ultimate moment carrying capacity of entire virtual glulam ($\mathrm{N \cdot mm}$)

$S =$ the section modulus of virtual glulam ($\mathrm{mm^3}$)

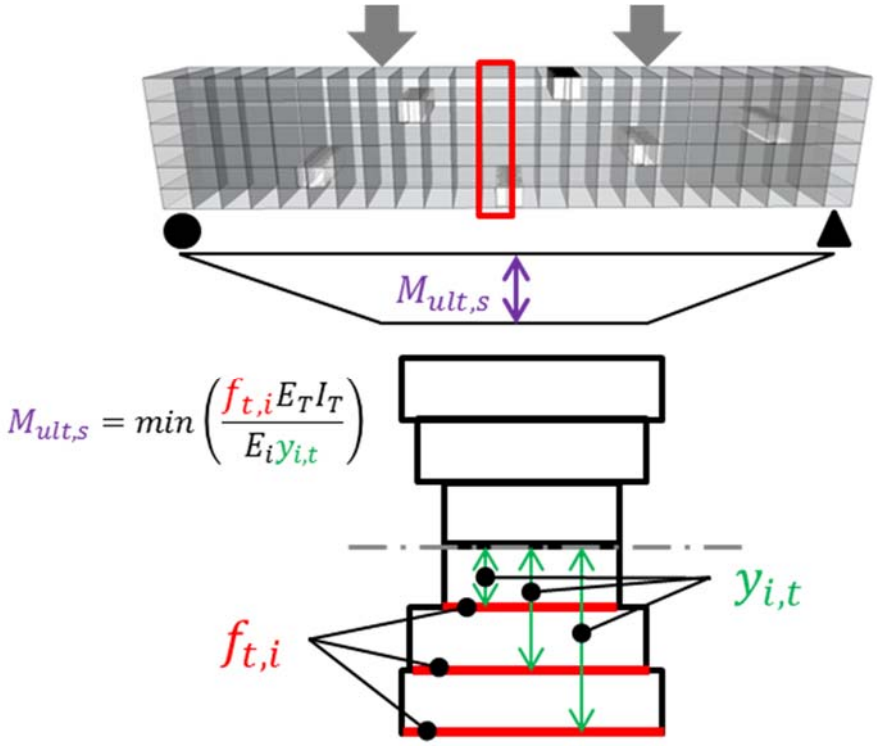

Figure 3-6 Determination of ultimate moment-carrying capacity

3.2.5 Distance between a neutral axis of virtual glulam and tensile stress in the outer lamination

The tensile strength of the lamination is determined in a uniaxial tensile test. The tensile stress of a glulam in bending is not uniform through the beam depth (Figure 3-7). Thus, the distance between a neutral axis of virtual glulam and a tensile stress in the outer lamination is should be considered. Bender et al. (1985) and Colling (1990) used the mid-depth stress criterion and Serrano et al. (2000) shows that the mid-depth stress criterion is suitable only for large beam depths. Meanwhile, Mihashi et al., (1996) compared three different criteria and showed that a combined failure criterion (MOR and tensile strength) gave the best agreement with the corresponding experimental results.

In this study, the distance between a neutral axis of virtual glulam and a tensile stress of ith lamination ($y_{i,t}$) was determined by Eq. (3.5) which was derived from the combined stress, bending and tensile stress (Figure 3-7).

$$y_{i,t} = \frac{\sqrt{(ky_{i,c})^2 + {y_{i,c}}^2 + {y_{i,end}}^2 - 2y_{i,c}y_{i,end}}}{k} \qquad (3.5)$$

Where,

$y_{i,t}$ = distance between a neutral axis of virtual glulam and tensile stress of ith lamination (mm)

$y_{i,c}$ = distance between a neutral axis of virtual glulam and a centroid of ith lamination (mm)

$y_{i,end}$ = distance between a neutral axis of virtual glulam and an end of ith lamination (mm)

k = ratio of MOR and tensile strength of lamination (herein 1.45 was used as references of Nakamura et al. (2011), Forest Products Society (1997), West Coast Lumber Inspection Bureau (2004), Barrett et al. (1994)

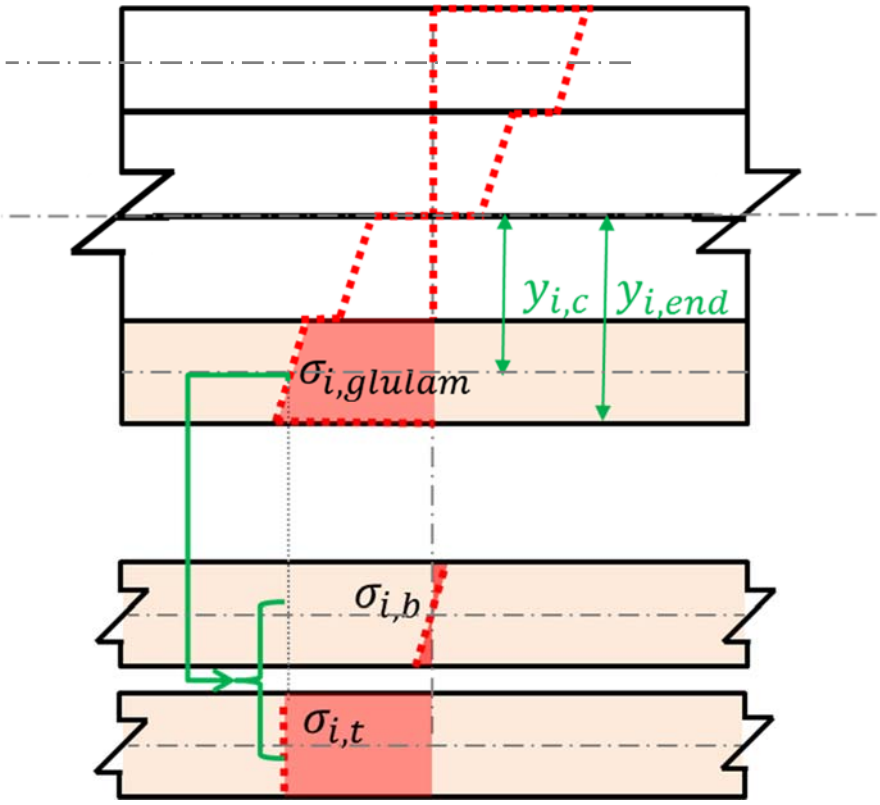

Figure 3-7 A linear stress in glulam beam were considered combined stress by bending ($\sigma_{i,b}$) and tension ($\sigma_{i,t}$) in lamination

Chapter 4. Material model for generating the localized tensile strength using the knot area ratio and localized MOE in lamination

4.1 Introduction

Most glulam beam models require input on the localized material properties of the lamination, as well as the correlations among these properties. Previous researchers have focused on the within member variation of tensile strength parallel to grain in lamination. Showalter et al. (1987) developed length effect model for representing the within member variation of tensile strength of timber. Lam et al. (1991a and b) used window analyses for developing the tensile strength distribution of lamination segments of various lengths. Taylor et al. (1991) developed a stochastic model for simulating localized MOE and tensile strength, Takeda et al., (1999a and b) showed that the length effect on tensile strength was dependent on the mechanical grade of the lumber and governed by the presence of knots.

In the previous researches, the developed models were based on statistical correlation among segments by testing short or long span specimens. Thus, for generating variation of long span lamination than tested specimens, the

statistical parameters should be extrapolated. It means that limitation for reflecting real variation of properties on lamination.

In this study, the developed glulam beam model also requires the tensile strength of lamination like previous models. The localized KAR and MOE of lamination can be measured by machine, but tensile strength can not be measured without destructive test. Thus, a material model should be required for generating tensile strength of lamination by KAR and MOE. The aim of this chapter is to develop the material model for generating the tensile strength used as an input property of glulam beam model.

4.2 Materials and methods

4.2.1 Localized MOE

4.2.1.1 Specimens

The commercially important softwood species, Japanese larch (*Larix kaempferi Carr*., oven- dry density: 540 kg/m^3) grown in Gangwon Province were used as specimens. After kiln drying, the surfaces were planed so that the final cross-sections were 38×89 mm and 38×140 mm with the length (3,600 mm). The moisture content of the specimens was approximately 10-13%. The specimens for input properties data were in Table 4-1.

Table 4-1 Specimens for input properties database

Wood species of specimens	Size (mm)	Number of specimens
Japanese larch	38 × 89 × 3600	890
	38 × 140 × 3600	1032

4.2.1.2 Experimental procedures

The MOE of specimens was measured by machine stress grader (MGFE-251, Figure 4-1) and the specimens were graded by the average MOE of each specimen. Especially, the localized MOE was measured for reflecting the lengthwise variation of each lamination.

Figure 4-1 Machine stress grader (MGFE-251, Japan)

4.2.1.3 Distribution of machine grade

The specimens were graded by average modulus of elasticity of lamination and classified as 10^3 N/mm^2 units (Table 4-2). As an outermost lamination, four grades, E12, E14, E16, and E18, are used in Korean standard (KS) F 3021. When the graded lamination were classified by outermost lamination grade, approximately 20% of lamination was assigned to E12 grade in both two cross section lamination.

Meanwhile, small percentage of lamination, 1% of 38×89 mm lamination and 8% of 38×140 mm lamination, was assigned to E14 grade as shown in Figure 4-2. It shows that it is difficult to make up glulam with E14 or higher grade as an outermost lamination grade. Thus, when considering the in-grade lamination distribution, 12S-30B glulam grade was reasonable for verifying a simulated distribution using the developed glulam beam model.

Table 4-2 Number and ratio of machine graded lamination

Grade	38×89×3600 mm		38×140×3600 mm		Minimum MOE (10^3 N/mm^2)
	Number (EA)	Ratio (%)	Number (EA)	Ratio (%)	
E4	0	0.0	4	0.4	4
E5	4	0.4	5	0.5	5
E6	14	1.6	24	2.3	6
E7	45	5.1	80	7.8	7
E8	113	12.7	100	9.7	8
E9	153	17.2	146	14.1	9
E10	201	22.6	186	18.0	10
E11	177	19.9	166	16.1	11
E12	127	14.3	141	13.7	12
E13	44	4.9	91	8.8	13
E14	11	1.2	61	5.9	14
E15	1	0.1	26	2.5	15
E16	0	0.0	2	0.2	16
Total	890	100.0	1032	100.0	

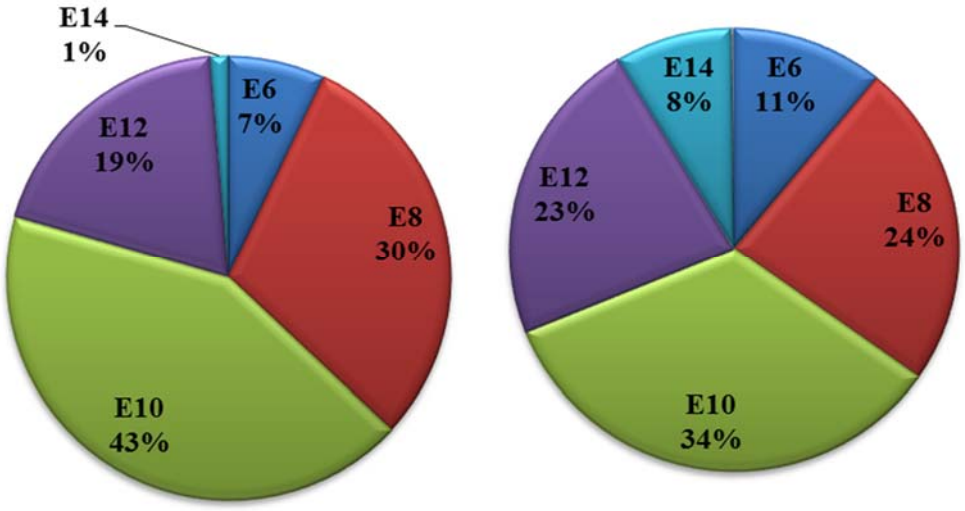

(a) 38×89×3600 mm (b) 38×140×3600 mm

Figure 4-2 Distribution of machine graded lamination (%)

In order to predict bending strength of glulam, the localized MOE of each specimen was measured as shown in Figure 4-3. An applied load was recorded by load cell of machine grader, when 4 mm displacement of the load cell was happened (Figure 4-4). Localized MOE was calculated by Eq. (4.1) and at both end side of specimen, 300 mm from the end, could not be measured due to the limitation of machine as shown in Figure 4-4.

$$MOE = \frac{P_{max} l^3}{4\, w\, t^3\, \Delta y} \tag{4.1}$$

Where,

$MOE =$ modulus of elasticity (MPa)

$P_{max} =$ applied maximum load (N)

$l =$ load span in machine stress grader (600 mm)

$w =$ width of lamination (mm)

$t =$ thickness of lamination (mm)

$\Delta y =$ deflection at center of load span in machine stress grader (4 mm)

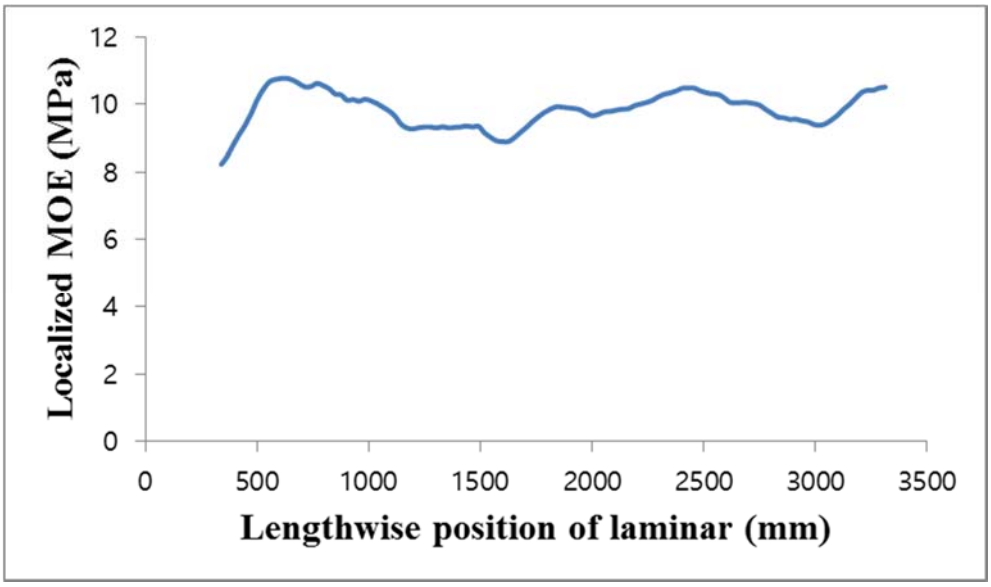

Figure 4-3 An example of localized MOE measured by machine stress grader

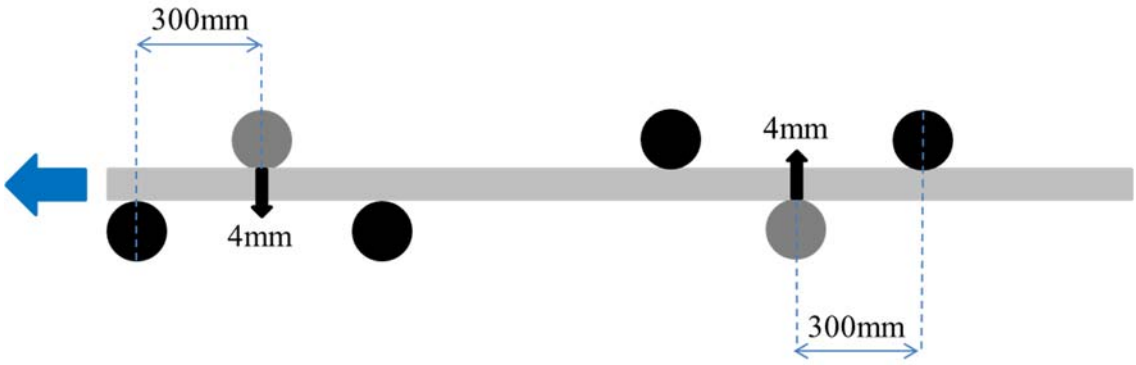

Figure 4-4 Measurement process of machine stress grader

4.2.2 Localized KAR

4.2.2.1 Specimens

The specimens need for localized KAR were the same for localized MOE in Section 4.2.1. (p.42).

4.2.2.2 Experimental procedures

Knot Area Ratio (KAR) is defined as the ratio of knot-area to the cross sectional area (Figure 4-5). A knot of which diameter was larger than 6 mm on wide or narrow face of lamination was detected by using knot detecting program. The processes for measuring localized KAR in lamination were as follows;

1) Four surfaces of each specimen were identified as shown in Figure 4-6.
2) Each surface was scanned using image processing system which was developed by Kim et al. (Kim et al., 2009a, Kim et al., 2009b) (Figure 4-7).
3) Knots of each surface were detected using knot detecting program (Figure 4-8) and two points (Figure 4-9) for identifying each knot was recorded.

4) A knot in lamination might appear on several surfaces. In order to recognize the knots on several surfaces as a single knot, a knot on a surface which was identified by two points was linked with the other knot on the other surface using knot linking program (Figure 4-10)

5) The KAR types of each knot was calculated according to Appendix (p.184) using the recorded points (Figure 4-9) on surface of lamination.

6) Finally, the localized KAR of each knot on longitudinal direction was obtained (Figure 4-11).

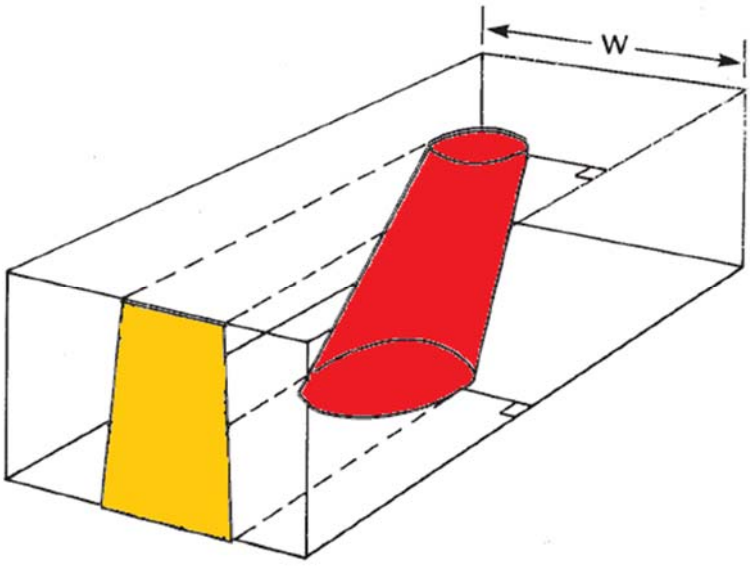

Figure 4-5 Knot area ratio

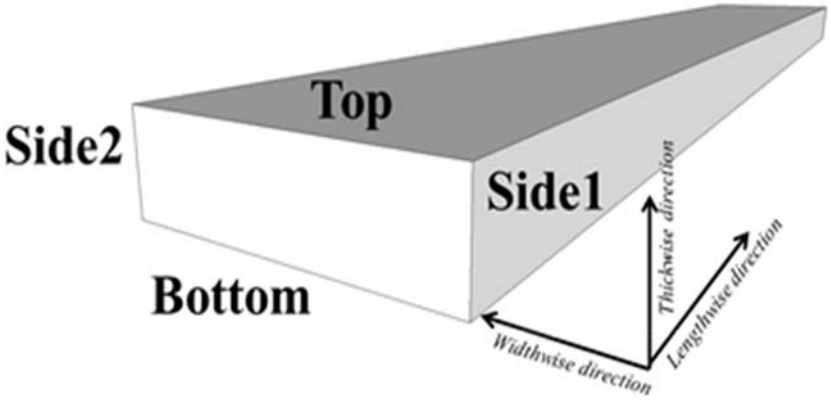

Figure 4-6 Four surface of specimen

Figure 4-7 Image processing system (Kim et al., 2009a, Kim et al., 2009b)

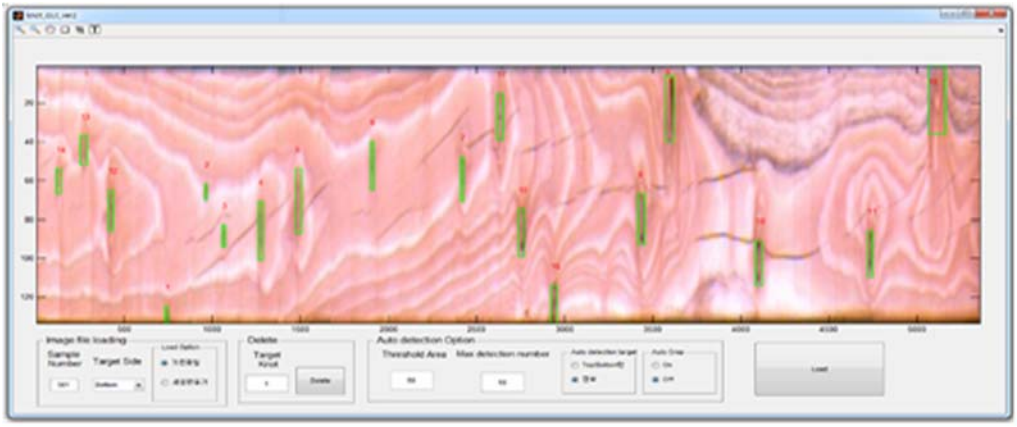

Figure 4-8 Knot detecting program

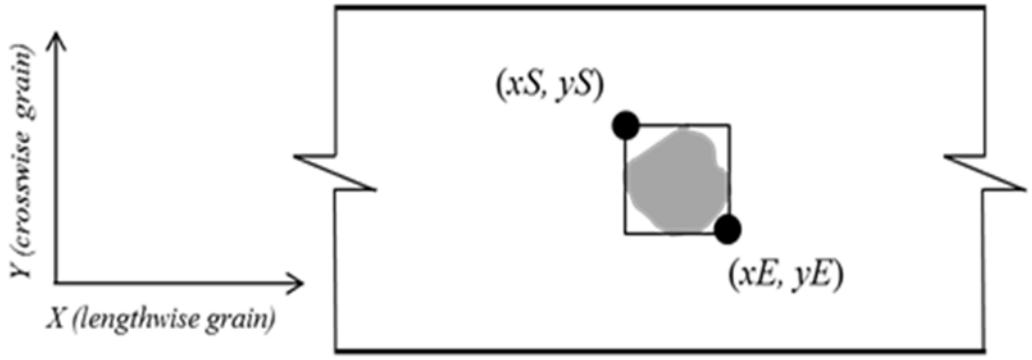

Figure 4-9 Two points for identifying Knot

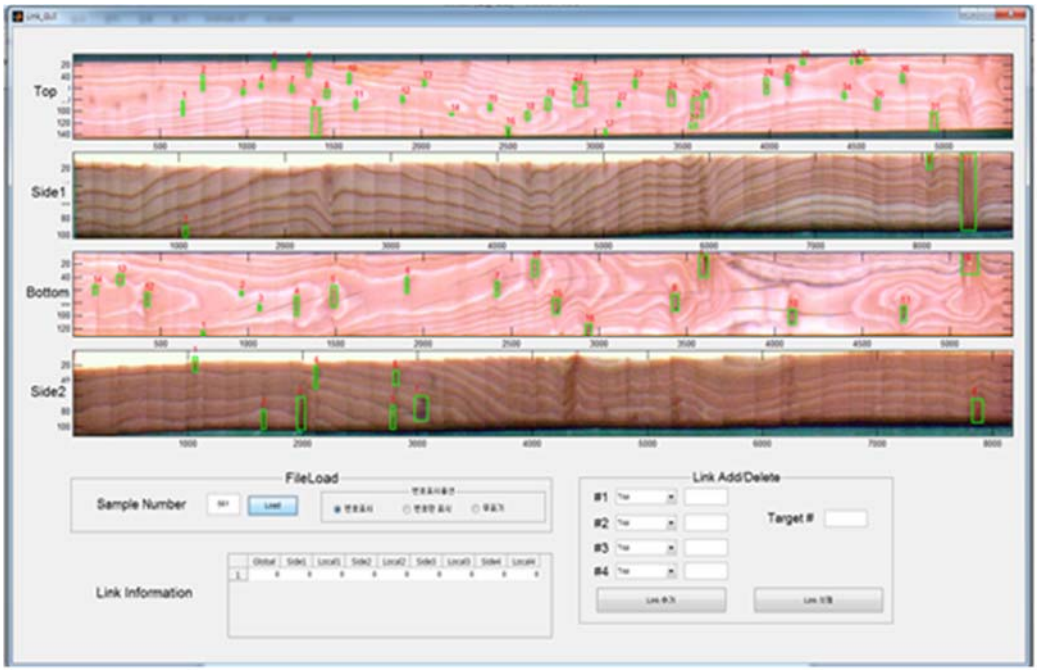

Figure 4-10 Knot linking program

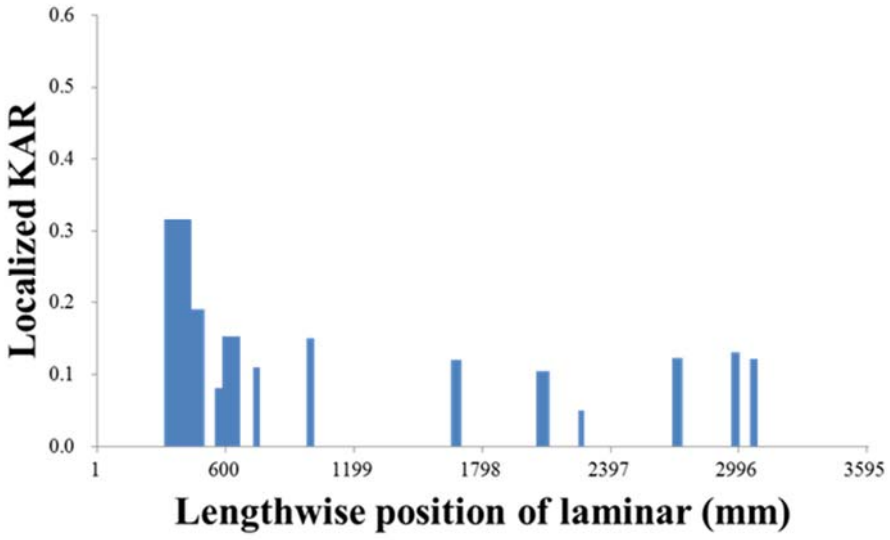

Figure 4-11 An example of localized KAR on longitudinal direction of lamination

4.2.3 Tensile strength test

4.2.3.1 Specimens

In order to develop the material model for generating tensile strength by KAR and MOE, the tensile strength test was carried out with randomly selected lamination (Table 4-3) among the specimens (Table 4-2) that the KAR and MOE were measured.

Table 4-3 Specimens for tensile strength test

Dimension	Grade	Number of specimens	
38×89×1800 mm	E8	34	99
	E10	35	
	E12	30	
38×140×1800 mm	E8	12	220
	E10	107	
	E12	101	

4.2.3.2 Experimental procedures

Tensile strength of lamination was measured using tensile testing machine (Kyoungsung testing machine co., LTD., Korea) as shown in accordance with KS F 3021 (Figure 4-12). The loading speed was 5 mm/min and the tests were ended in 5 min. The length of specimens for measuring KAR and MOE of lamination was 3600 mm (Table 4-1). The length of grip for holding the specimen was 600 mm and a tensile strength test span between grips was also 600 mm (Figure 4-13). Thus, tensile strengths of two parts in a lamination were tested. The tensile strength was calculated using Eq. (4.2).

$$f_{t,lamina} = \frac{P_{max}}{w \cdot t} \tag{4.2}$$

Where,

$f_{t,lamina}$ = tensile strength of lamination (MPa)

P_{max} = applied maximum load (N)

w = width of lamination (mm)

t = thickness of lamination (mm)

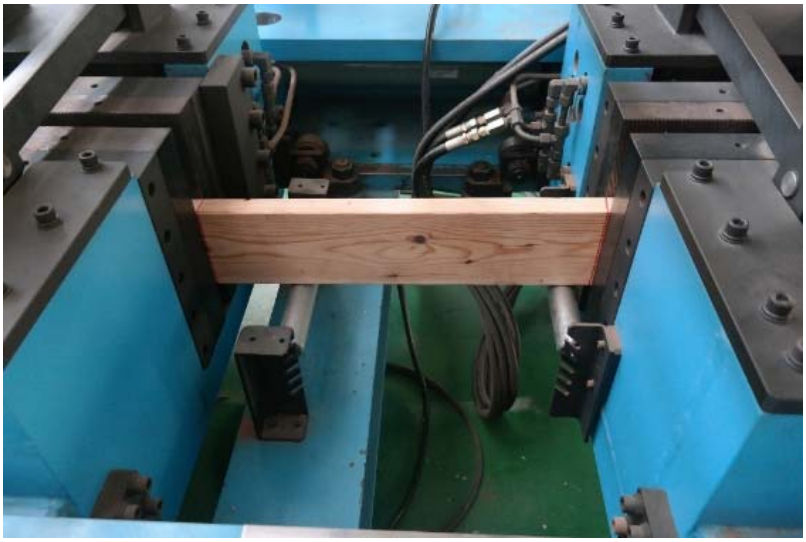

Figure 4-12 Tensile strength test setup
(Korea Forest Research Institute)

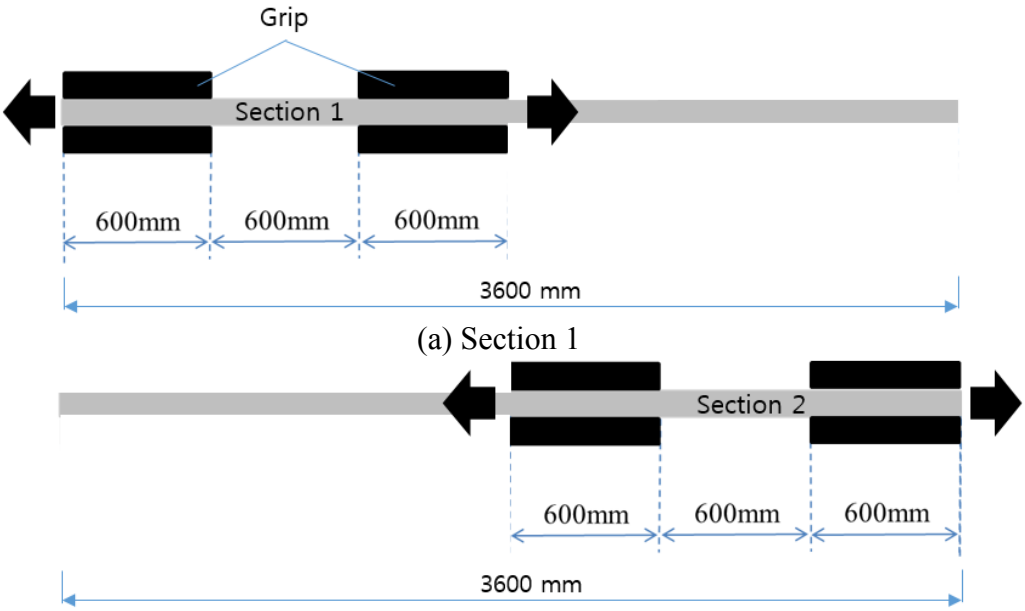

(a) Section 1

(b) Section 2

Figure 4-13 Tensile test arrangement for in-grade tested lamination

4.2.4 Multiple regression model

For considering both KAR and MOE as estimators, a linear multiple regression model (Eq. (4.3)) is used. The regression coefficients were derived by both ordinary least squares (OLS) and the partial least squares (PLS) using Minitab software (Minitab Inc., PA).

$$Y = \beta_0 + \beta_1 X_1 + \beta_2 X_2 + \epsilon \tag{4.3}$$

Where,

Y = the predicted tensile strength (MPa)

β_i = regression coefficients

X_1 = independent variable (herein, knot area ratio)

X_2 = independent variable (herein, modulus of elasticity) (MPa)

ϵ = the error term

4.3 Results and discussion

4.3.1 Correlation between a tensile strength and an estimator

The correlation between segments (Figure 4-13) within lamination has been analyzed. The correlation of tensile strength was different depends on its size and showed lower correlation than MOE (Figure 4-14). In order to generate the tensile strength of lamination, the correlation among segments by testing short or long span specimens has been considered statistically by many researchers (Showalter et al., 1987, Lam et al., 1991a and b,, Taylor et al., 1991, Hernandez et al., 1992). However, the correlation among segments depends on species, grades, and size. In addition, for generating variation of long span lamination than tested specimens, the statistical parameters should be extrapolated. It means that limitation for reflecting actual variation of properties on lamination.

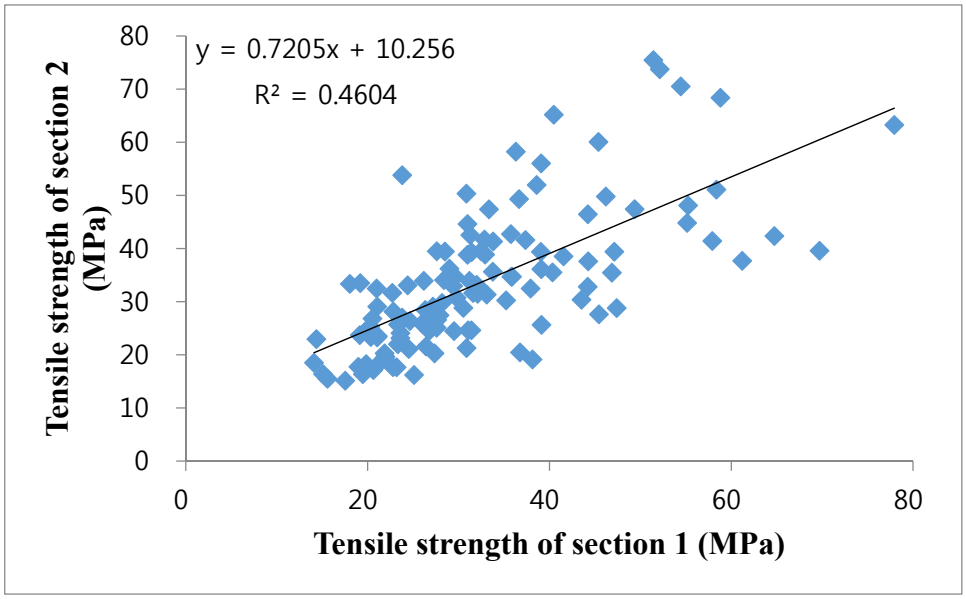

(a) Correlation of tensile strength within 38×89 mm cross section lamination

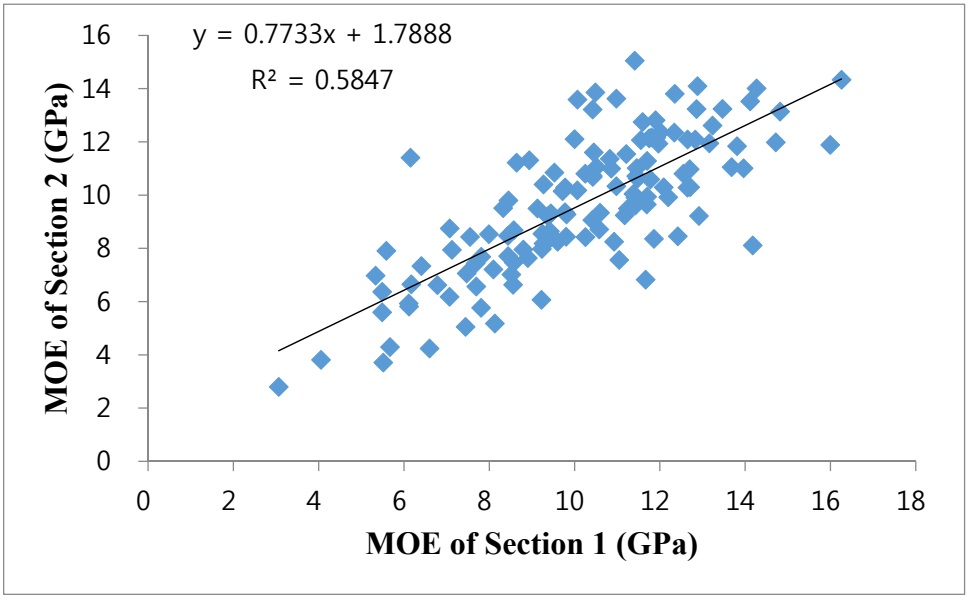

(b) Correlation of MOE within 38×89 mm cross section lamination

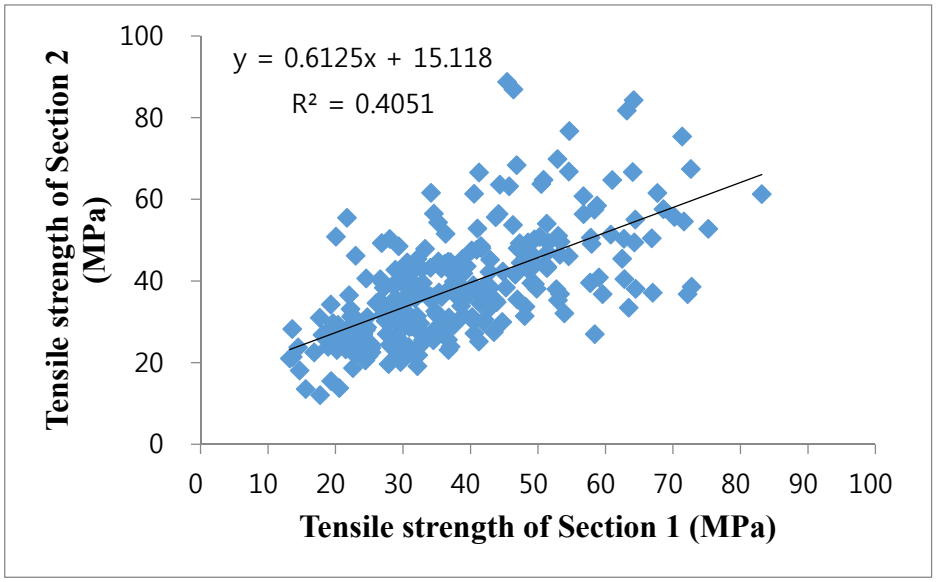

(c) Correlation of tensile strength within 38×140 mm cross section lamination

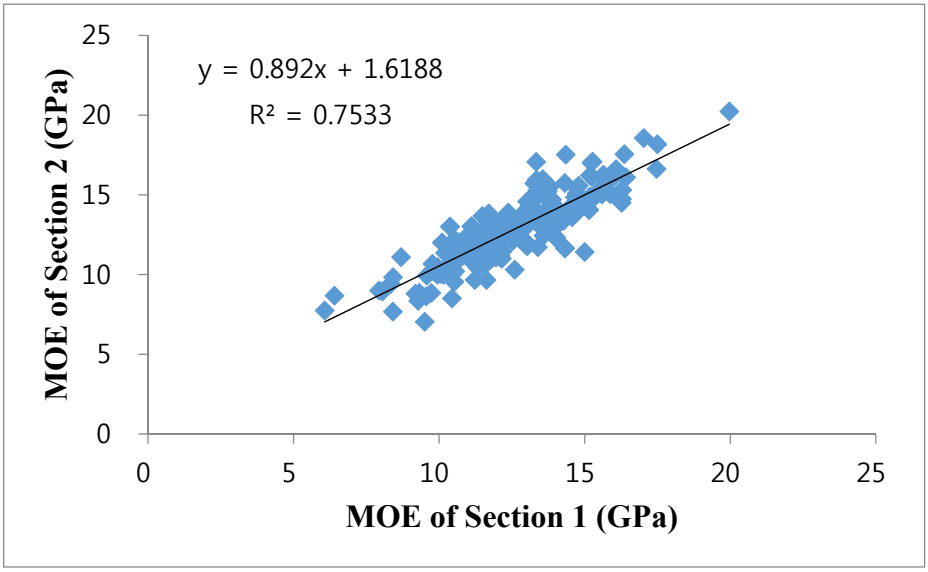

(d) Correlation of MOE within 38×140 mm cross section lamination

Figure 4-14 Correlation between segments within lamination

In order to generate the lengthwise tensile strength of lamination, a tensile strength prediction model has been considered based on localized knot and MOE. Knot area ratio (KAR) is well known as the most major strength reducing defect for tensile and bending strength. In order to improve the prediction accuracy of the tensile strength, localized KAR was considered with localized MOE. The specimens that failure occurred around knot were used for analyzing the effect to the tensile strength of lamination (Figure 4-15 a). Specimens, failure occurred in grips and caused by other defects, such as slope of grain, were excluded (Figure 4-15 b and c).

Localized knot area ratio on longitudinal direction was obtained and the maximum KAR used as an estimator (Figure 4-16). The coefficient of determination (R^2) of the equation for the least-squares regression line using the KAR to predict the tensile strength was approximately 0.55-0.60. Meanwhile, the R^2 of the regression line using the MOE to predict the tensile strength was approximately 0.19-0.35 (Figure 4-17). The relationship of flatwise MOE and tensile strength was low. The low relationship between flatwise bending stiffness and knot size was presented by Samson, M. and Blanchet, L. (Samson et al., 1992). Thus, the flatwise MOE has less influence to tensile strength of lamination than KAR.

(a) Failure caused by knot

(b) Failure caused by slope of grain

(c) Failure caused by grip

Figure 4-15 Failure modes in tensile strength test

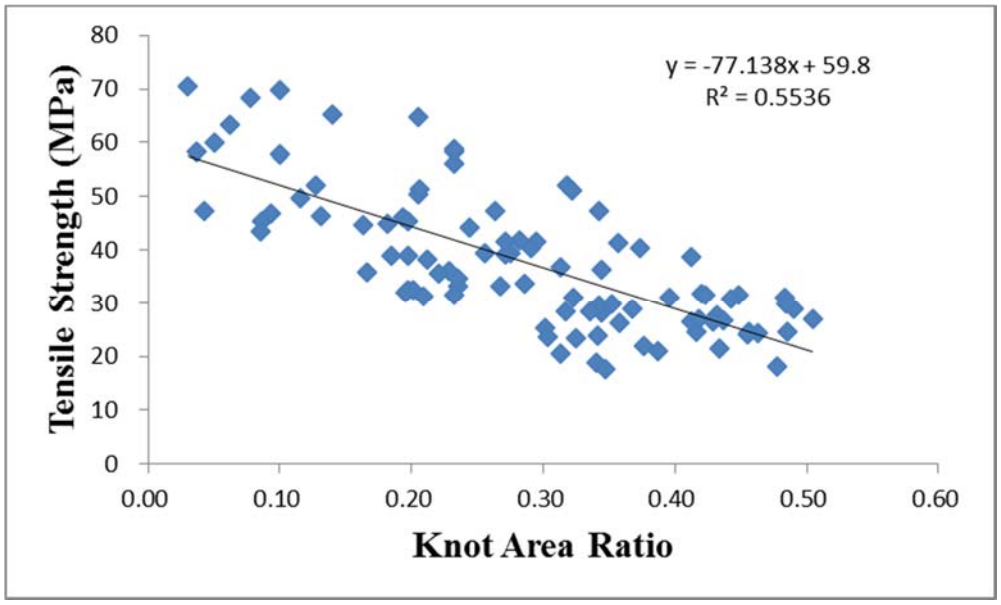

(a) 38×89 mm

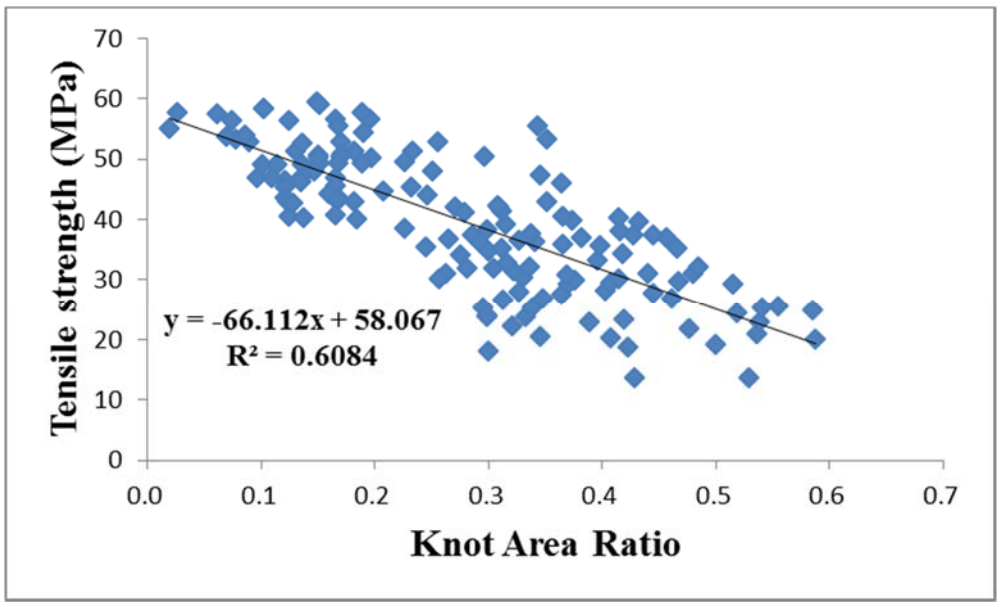

(b) 38×140 mm

Figure 4-16 Relationship between KAR and tensile strength (MPa)

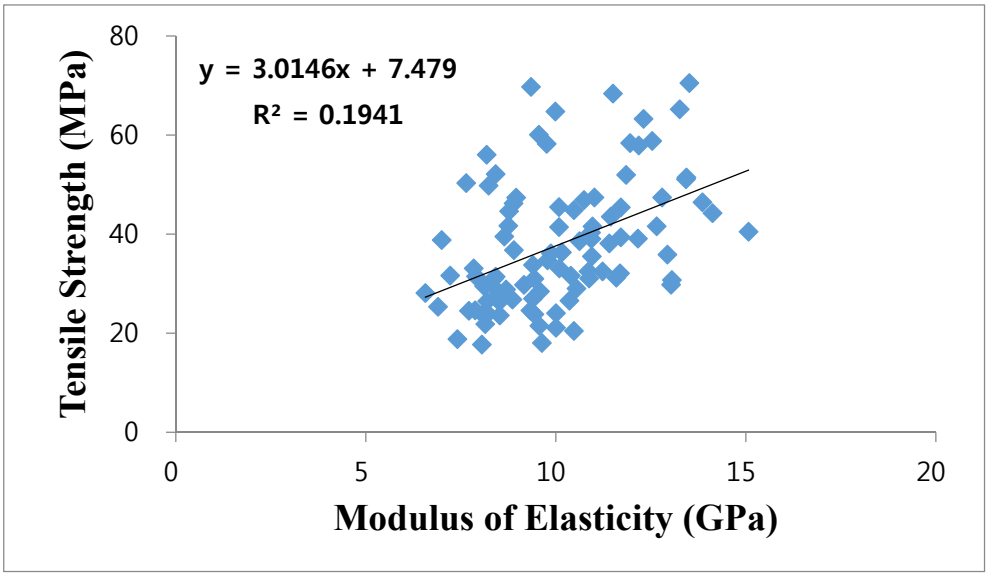

(a) 38×89 mm

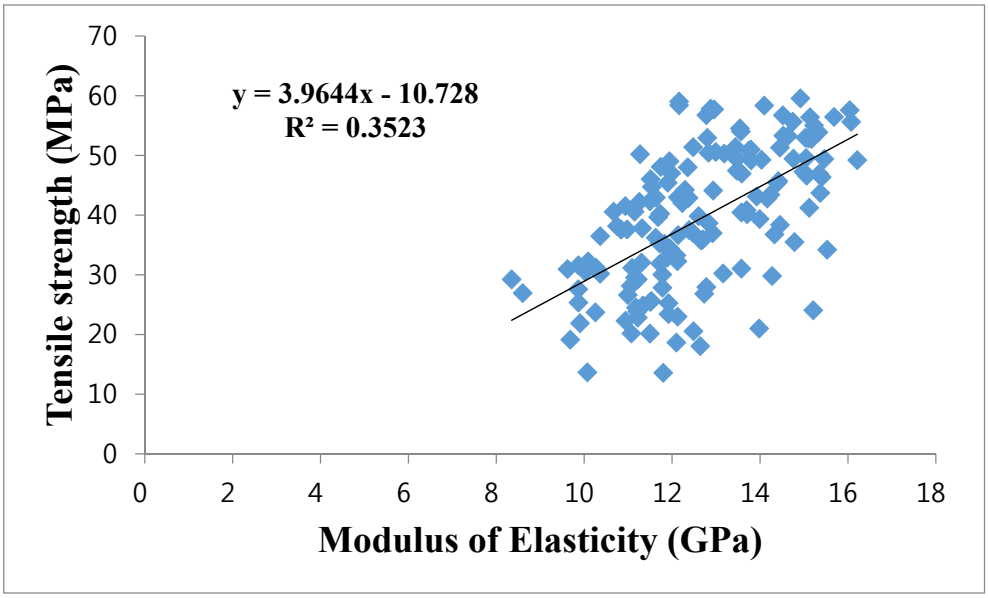

(b) 38×140 mm

Figure 4-17 Relationship between MOE and tensile strength (MPa)

4.3.2 Material model to predict tensile strength

A material model to predict tensile strength of lamination was developed using localized MOE and KAR. In multiple regression, the coefficient estimates can be changed erratically in response to small changes in the model or the data. Thus, a multicollinearity, a phenomenon in which two or more predictor variables are highly correlated, should be checked. In case of multi regression using ordinary least squares, the multicollinearity can be quantified using a variance inflation factor (VIF). The VIF is calculated using Eq. (4.4) and a VIR of 5 or 10 and above indicates a multicollinearity problem.

$$VIF = \frac{1}{1 - R_j^2} \tag{4.4}$$

R_j^2 = the coefficient of determination of a regression of explanator j on all of the explanators, $0 \leq R_j^2 \leq 1$

The derived VIF values (Table 3-7) using the ordinary least squares multiple regression were lower than 5, so there is not a multicollineartity problem. Thus, the derived coefficients of multiple regression using localized MOE and KAR is valid for estimating tensile strength in statistically. This result is similar with another research result by Samson, M. and Blanchet, L. (Samson et al., 1992).

They evaluated the relationship between flatwise bending stiffness and knot size and found out that the effect of knots on flatwise bending stiffness is very small.

Table 4-4 Ordinary least squares multiple regression result with KAR, MOE, and tensile strength

Lamination size	Predictor	Coef	SE Coef	P-value	VIF
38×89 mm	Constant	41.23	7.17	0.000	
	KAR	-69.71	7.23	0.000	1.20
	MOE	1.63	0.55	0.000	1.20
38×140 mm	Constant	39.40	6.47	0.000	
	KAR	-56.38	5.41	0.000	1.59
	MOE	1.26	0.43	0.004	1.59

When the predictor variables are highly collinear, PLS regression is usually considered. Even though the VIF values of ordinary least square regression show that there is a low collinearity between predictors, PLS regression was carried out for checking a main component and driving a more reliable regression without the multicollinearity problem. The coefficient of PLS regression was same with OLS regression as shown in Table 3-8. It means that

the correlation between KAR and MOE was very low. The standardized coefficients, the relative importance of each predictor in the model, shows that KAR was main component. When adding MOE, the multiple determination, R^2, using KAR was increased and it means that considering both the components is optimal to predict tensile strength. The predicted R^2 to determine how well the model predicts new observations was approximately 63% (Figure 4-18).

Table 4-5 Partial least squares multiple regression result with KAR, MOE, and tensile strength

Lamination size	Predictor	Coef	Standardized Coef	R^2
38×89 mm	Constant	41.23		
	KAR	-69.71	-0.62	0.62
	MOE	1.63	0.30	0.63
38×140 mm	Constant	39.40		
	KAR	-56.38	-0.67	0.61
	MOE	1.26	0.19	0.63

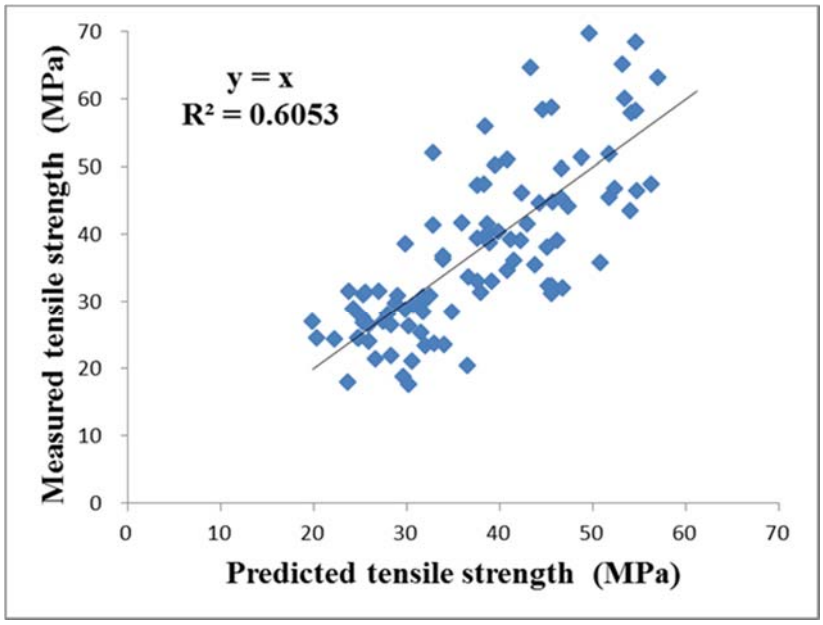

(a) 38×89 mm

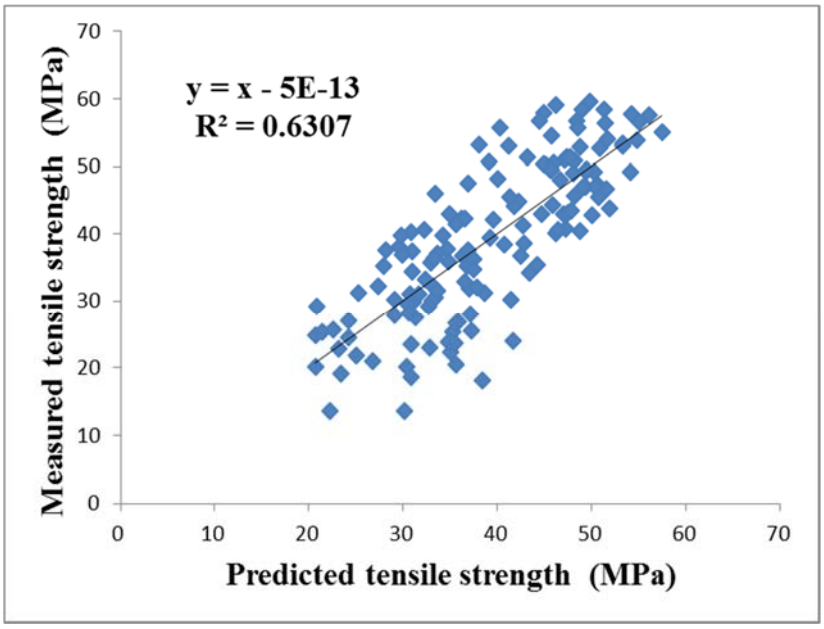

(b) 38×140 mm

Figure 4-18 Comparison between measured and predicted tensile strength using multiple regression

4.4 Conclusions

Tensile strength of two segments in a lamination was evaluated, and the correlation among segments was different depends on the lamination size. Moreover, for generating variation of long span lamination than tested specimens, the statistical parameters should be extrapolated and a lot of tests are required with various test span. Thus, there is a limitation to reflect actual tensile strength of lamination into glulam model using correlation of segment.

Material model to predict tensile strength of lamination using MOE and KAR was developed. When adding MOE, the multiple determination using KAR was increased and it means that considering both the components is optimal to predict tensile strength. The predicted R^2 was approximately 63%. For using the coefficent of multiple regression model, the multicollinearity was checked, and there was not a multicollineartity problem.

Chapter 5. Validation of the developed glulam beam model

5.1 Introduction

In this chapter, a simulated bending strength distribution of glued laminated timber (glulam) by the developed glulam model in Chapter 3 was validated with a experimental bending strength distribution by full-scale glulam beams test.

In case of the simulated glulam bending strength distribution, as the input properties, localized MOE and tensile strength of lamination, and tensile strength of finger joints are required. For the localized MOE and tensile strength of lamination, the measured localized MOE of lamination and the material model for generating tensile strength using MOE and KAR in Chapter 4 were used. Meanwhile, the tensile strength of finger joints was measured by an additional full-scale tensile strength test in this chapter.

In case of the experimental glulam bending strength distribution, four types of glulam beam was manufactured and tested. For deriving the bending strength distribution, 30 EA of glulam beam for each glulam type were manufactured. For validating the simulated bending distribution, a goodness-of-fit test was carried out, and an errer of 5% point estimate (PE) between simulated and experimental bending strength distribution was compared.

5.2 Materials and methods

5.2.1 Input properties database

5.2.1.1 Localized MOE and tensile strength of lamination

The input properties database for simulating glulam beam were conducted based on inherent characteristics of lamination. Since the localized MOE and tensile strength of lamination are required, material models (Table 4-5) for generating tensile strength was developed based on localized MOE and KAR. The MOE profile of lamination was obtained using MSR machine (Figure 4-1) and the KAR on lamination was obtained using image processing machine (Figure 4-7). Finally, the database of MOE and tensile strength of lamination was conducted at each grade as shown in Table 5-1.

Table 5-1 Length of established database

Grade	Database (Unit : m)	
	38×89 mm	38×140 mm
Under E8	97.2	212.4
E8	223.2	738.0
E10	900.0	810.0
E12	230.4	630.0
Total	1450.8	2390.4

5.2.1.2 Tensile strength of finger-jointed lamination

The end of lamination is connected with finger joints and the tensile strength of finger-jointed lamination is different with a lamination without finger joints. For deriving the tensile strength distribution of finger-jointed lamination, 30 pieces of finger-jointed lamination were manufactured at each grade (Table 5-2). The same grade laminations were connected using finger joint and the finger joint was placed in the middle of test span (Figure 5-1). The experimental procedures was same in Section 4.2.2.2. (p.54).

Table 5-2 Specimens for tensile strength of finger-jointed lamination

Dimension	Grade	Number of specimens	
38×89×1800 mm	E8	30	120
	E10	30	
	E12	30	
38×140×1800 mm	E8	30	120
	E10	30	
	E12	30	

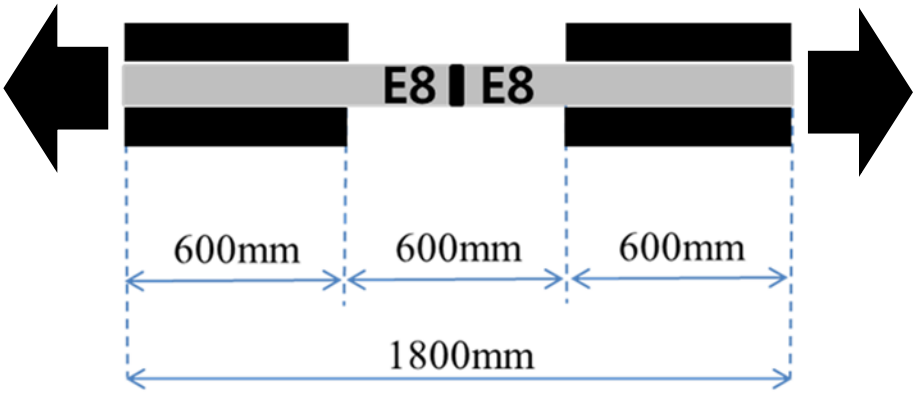

Figure 5-1 An example of tensile test for finger-jointed lamination

5.2.2 Prediction of bending strength by simulation

A virtual glulam beam was generated in the same manner as the experimental glulam beam are made. The bending strength calculation processing of virtual glulam beam in Figure 3-1 was carried out using Matlab software (2014a, The Mathworks, Natick, MA) and a thousand virtual glulam beams were simulated. The localized MOE and KAR of lamination and tensile strength of finger-jointed lamination were assigned from the corresponding lamination grade in the input properties database.

5.2.3 Experimental test for validation of the glulam beam model

5.2.3.1 Specimens

The glulam beam model developed can reflect the effect of finger joints, size effect, and combination of lamination. Thus, four sets of glulam beams designed for validating the glulam beam model were manufactured as follows:

1) Set 1 : to verify the basic model without finger joint
2) Set 2 : to verify the reflection of finger joint as comparing to Set 1
3) Set 3 : to verify size effect as comparing to Set 2
4) Set 4 : to verify the different combination of lamination

All laminations for manufacturing glulam were selected randomly among the specimens for establishing input properties. However, in the process of manufacturing a glulam beam, a lamination, especially finger-jointed laminations, was planned in order to bond the surface to the other lamination. The final sizes and specification of glulam to validate the glulam model were in Table 5-3.

Table 5-3 Specimens for validating simulated glulam bending strength distribution

	Finger joint	glulam grade	Final dimension (mm)			Number of specimens
			Width	depth	Length	
Set1	No finger joint	10S-30B	80	130	2400	30
Set2	With finger joint	10S-30B	80	130	2400	30
Set3	With finger joint	10S-30B	130	250	4800	30
Set4	With finger joint	7S-27B	80	250	4800	30

5.2.3.2 Experimental procedures

Third-point loading test was carried out for evaluating the bending strength of glulam (Figure 5-2) by a universal testing machine (Zwick GmbH & Co., Ltd., Ulm, Germany). The span to depth ratio was 1:18. The load speed was 10mm/min. The failure was occurred in 5 min. The MOR value was calculated with the maximum bending moment at the failure position from the following equations:

$$MOR = \frac{M_{max} y}{I} = \frac{6M_{max}}{WT^2} \quad (5.1)$$

where,

MOR = modulus of rupture (MPa)

M_{max} = maximum bending moment (N•mm)

y = the distance from the neutral axis to the location of a extreme fiber stress (mm)

I = the moment of inertia of the cross section (mm^4)

W = width of beam (mm)

T = thickness of beam (mm)

When a failure occurred in maximum moment zone (MMZ), the maximum bending moment was calculated using Eq. (5.2).

$$M_{max\ in\ MMZ} = \frac{P_{max} L}{6} \quad (5.2)$$

where,

$M_{max\ in\ MMZ}$= maximum bending moment in maximum moment zone (N•mm)

P_{max}= applied maximum load (N)

L= length of the test span (mm)

Meanwhile, when a failure occurred at out of MMZ, the maximum bending moment was calculated using Eq. (5.2).

$$M_{\max\ out\ of\ MMZ} = \frac{P_{max}}{4}(L - 2L_v) \qquad (5.3)$$

where,

$M_{\max\ out\ of\ MMZ}$= maximum bending moment out of maximum moment zone (N•mm)

P_{max}= applied maximum load (N)

L= length of the test span (mm)

L_v = the horizontal distance from the center of the test span to the point of failure ($L_v \geq L/6$) (mm)

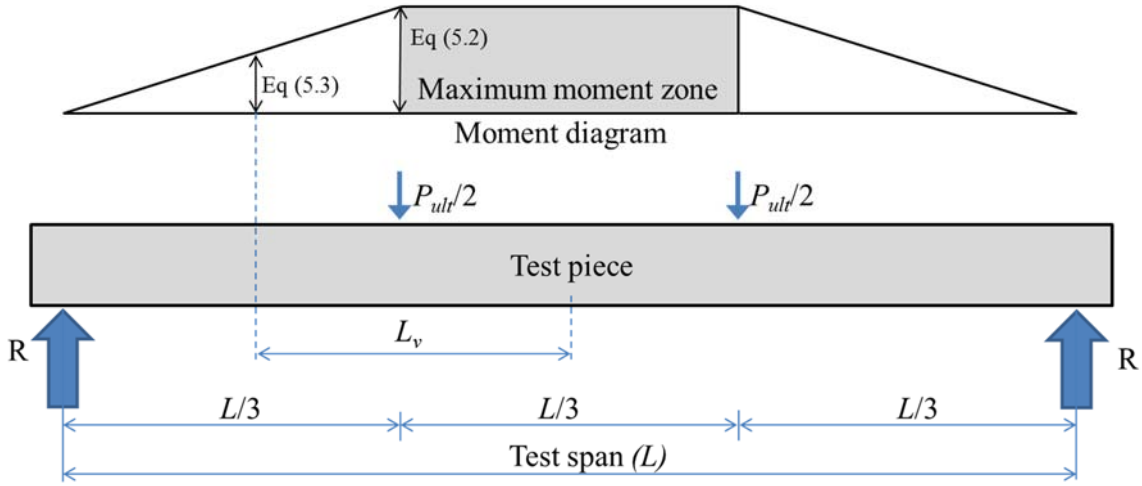

Figure 5-2 Moment diagram with test set-up for measuring bending strength

5.2.4 Lower 5th percentile strength

5.2.4.1 Nonparametric point estimate

The sample nonparametric 5th percentile point estimate (5% NPE) was interpolated from the tested specimens. The test values were arranged in ascending order. Beginning with the lowest value, $i/(n + 1)$ was calculated. The 5% NPE was interpolated by Eq. (5.4).

$$5\%\ \text{NPE} = \left[\frac{5}{100}(n+1) - (j-1)\right]\left[x_j - x_{(j-1)}\right] + x_{(j-1)} \tag{5.4}$$

where,

n: total number of samples

j: the lowest order of the test value when $i/(n + 1) \geq 0.05$

i: the order of the test value

x_i: ith value

5.2.4.2 Parametric point estimate

The parametric point estimate are based on fitting a two parameter (2P) Weibull distribution to the lower tail portion of the empirical cumulative frequency distribution of the test data. Eq. (5.5) is intended to be used to calculate any percentile of a two-parameter Weibull distribution. The percentile of interest depends on the property being estimated.

$$Weibull\ point\ estimate = \eta[-ln(1-p)]^{1/\alpha} \quad (5.5)$$

where,

η = Weibull scale parameter

p = percentile as a decimal

α = Weibull shape parameter

The regression method of fitting the two-parameter Weibull was applied by first sorting the data, in ascending order, as $f_1, f_2 \cdots f_n$. To each of these values is assigned a plotting position $p_i = (i - 0.5)/n$. Then coordinate pairs (X_i, Y_i) were computed using the transformations, $X_i = \ln[-\ln(1-p_i)]$, and $Y_i = \ln f_i$. Once the coordinate pairs (X_i, Y_i) have been computed, one can use linear regression to estimate the intercept and slope parameters a and b of a straight line at the form $y = aX_i + b$. The parameters $\eta = \exp(b)$ and $\alpha = 1/a$.

5.3 Results and discussion

5.3.1 Input properties database

5.3.1.1 Tensile strength distribution of lamination stock

The higher machine grades shows the higher tensile strength distribution (Figure 5-3). This trends appeared 5% point estimate (PE) as well as shown in Figure 5-4. The reason can be explained by the knot effect as investigated by Takeda (1999). Takeda (1999) showed that the lower grades have more knots than higher grades and the knots were the most important influence on tensile strength.

All of the tensile strengths of lamination stock were higher than the two pass criterion, mean and 5% PE, tabulated in KS F 3021 (Table 5-4). It means that the graded lamination satisfied the KS F 3021. Especially, for the comparison of 5% PE, two types of 5% PE, nonparametric point estimate (NPE) and parametric point estimate using Weibull distribution fit (WPE), were compared.

Table 5-4 Empirical tensile strengths of lamination and pass criterion in KS F 3021

Size	Grade	Number of specimens	Empirical tensile strength (MPa)				KS F 3021 (MPa)	
			Mean	COV	5% NPE	5% WPE	Mean	5% PE
38×89 mm	E8	68	28.9	0.26	17.8	17.3	21	16
	E10	69	35.2	0.29	23.1	21.8	24	18
	E12	57	44.2	0.28	29.6	28.8	28	21
38×140 mm	E8	21	29.1	0.29	16.0	16.4	21	16
	E10	213	31.5	0.28	19.5	19.7	24	18
	E12	202	40.7	0.29	23.9	24.5	28	21

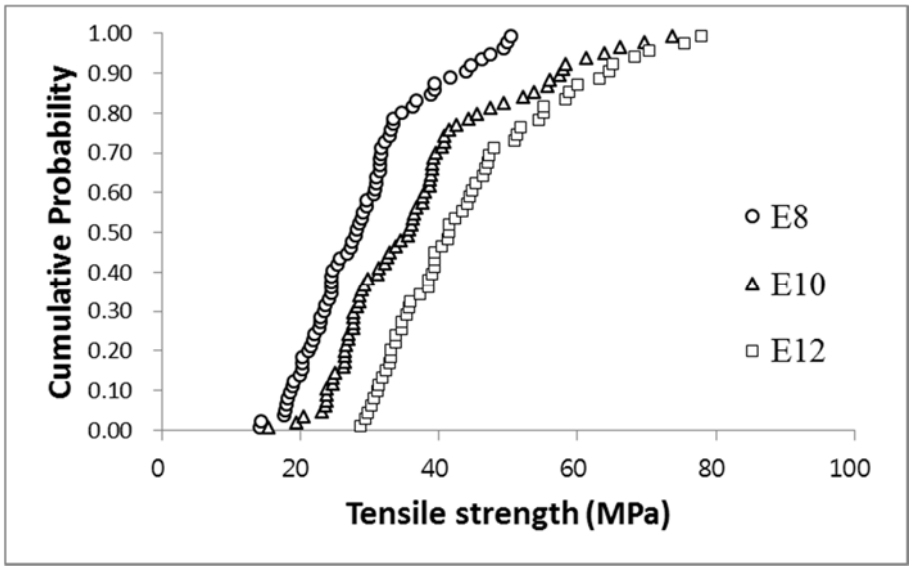

(a) 38×89 mm

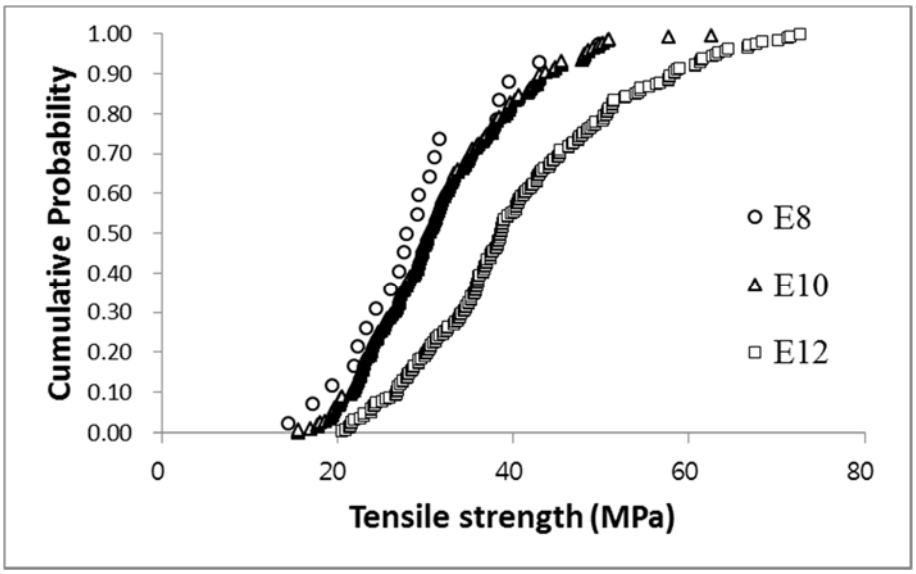

(b) 38×140 mm

Figure 5-3 Empirical cumulative probability distribution for tensile strength

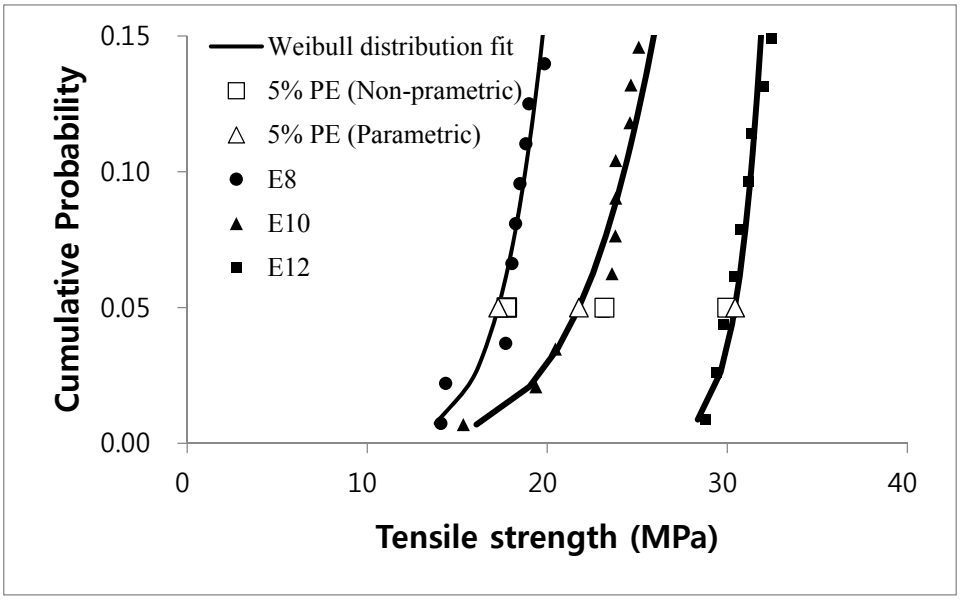

(a) 38×89 mm

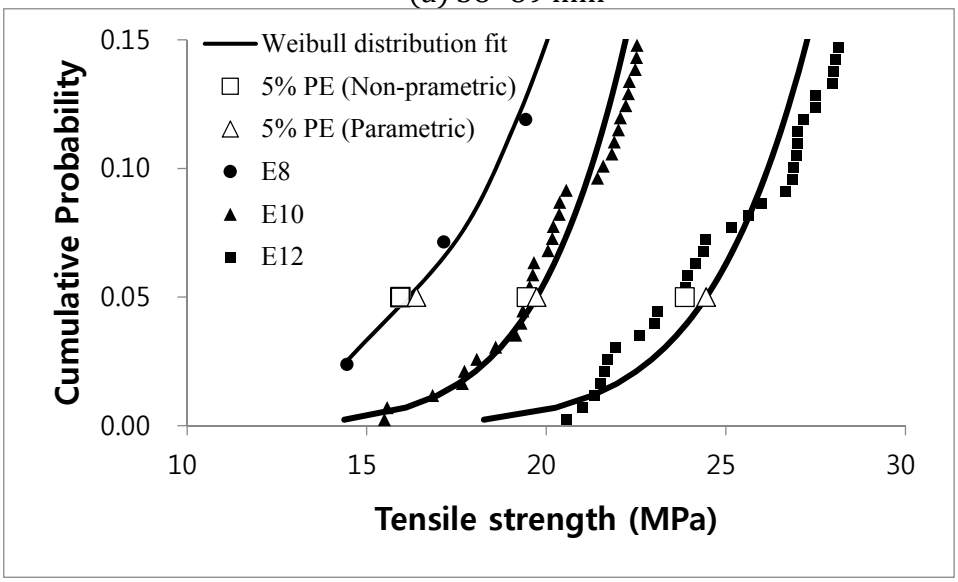

(b) 38×140 mm

Figure 5-4 Weibull distribution superimposed over data points of empirical cumulative distribution for lower 15% of data

The same grades between different dimension cross section lamination was compared. The tensile strength distribution of E8 grade of 38×89 mm dimension lamination seems like overlap on that of 38×140 mm dimension lamination (Figure 5-5 a), however, the distribution of the other grades of 38×89 mm lamination was placed right side of 38×140 mm lamination. Meanwhile, the mean of E8 grades from 38×89 mm is smaller than that of 38×140 mm and the mean of the other grades from 38×89 mm is higher than that of 38×140 mm (Figure 5-6). However, the standard deviation of the lower tensile strengths group also have smaller than that of higher tensile strengths group. Straight away equal variances cannot be assumed, and the sample sizes are also different.

Thus, in order to see whether the average tensile strength of each grades is statistically significant between the two cross section lamination or not, a 2-tailed 2 sample t-test, taking into account the inequality of variances and sample sizes, was carried out. The hypothesis was formally as Eq. (5.6) and (5.7), and tested at the α=0.1 level (90%) that there is not statistical difference between the mean values of a grade of 38×89 mm and that of 38×140 mm cross section.

$$H_0 : \overline{Y_1} - \overline{Y_2} = 0 \quad (5.6)$$

$$H_1 : \overline{Y_1} - \overline{Y_2} \neq 0 \quad (5.7)$$

$\overline{Y_1}$: a sample mean of tensile strength from 38 × 89 mm

$\overline{Y_a}$: a sample mean of tensile strength from 38 × 140 mm

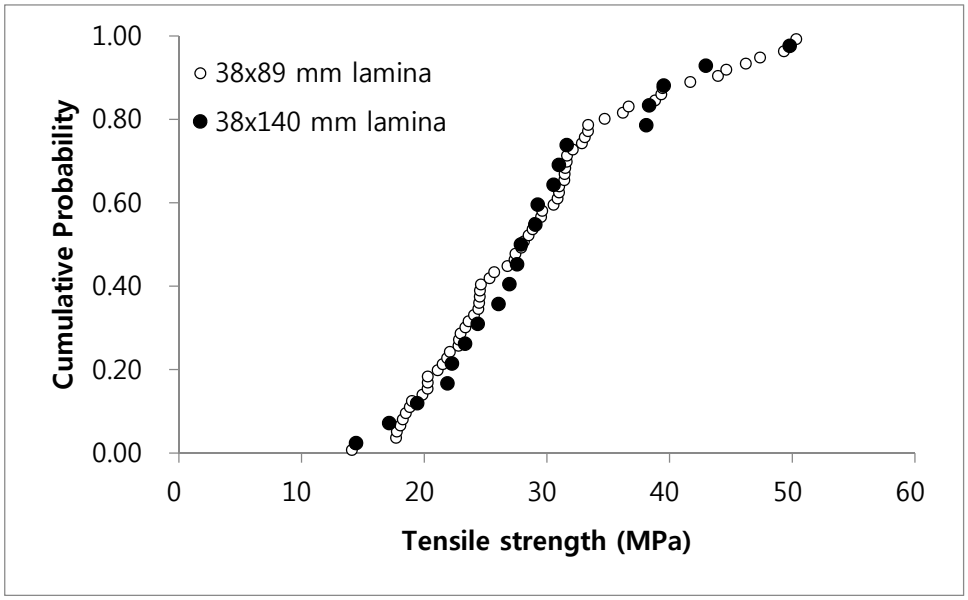
1.00
0.80
0.60
0.40
0.20
0.00
Cumulative Probability
38x89 mm lamina
38x140 mm lamina
0
10
20
30
40
50
60
Tensile strength (MPa)

(a) E8

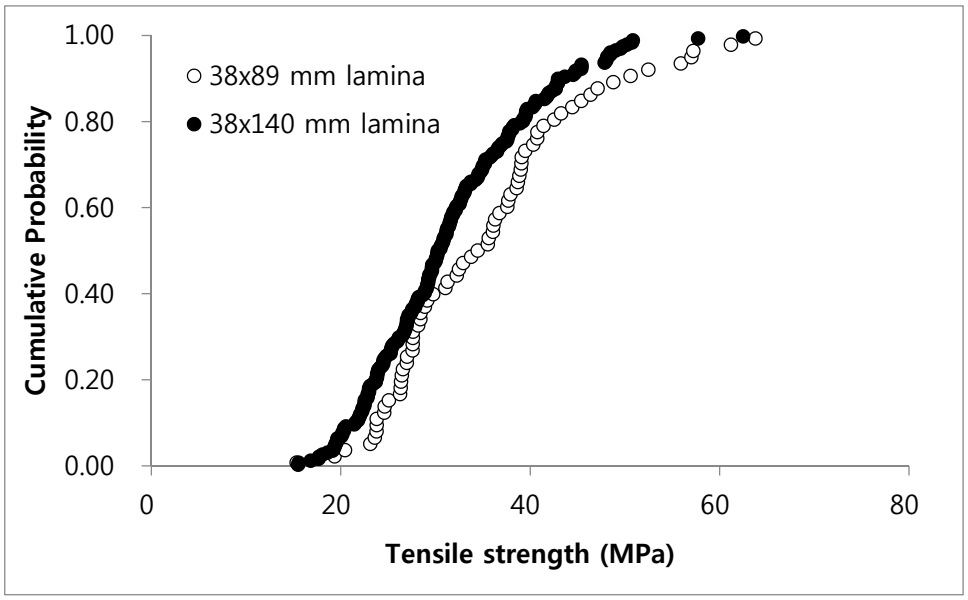
1.00
0.80
0.60
0.40
0.20
0.00
Cumulative Probability
38x89 mm lamina
38x140 mm lamina
0
20
40
60
80
Tensile strength (MPa)

(b) E10

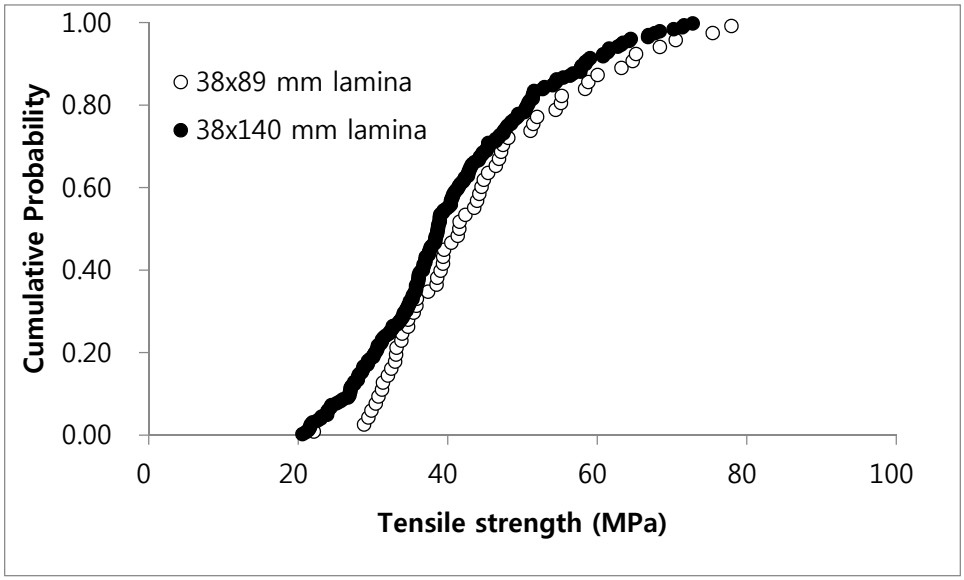

(c) E12

Figure 5-5 Comparison of same grades between 38×89 mm and 38×140 mm cross section

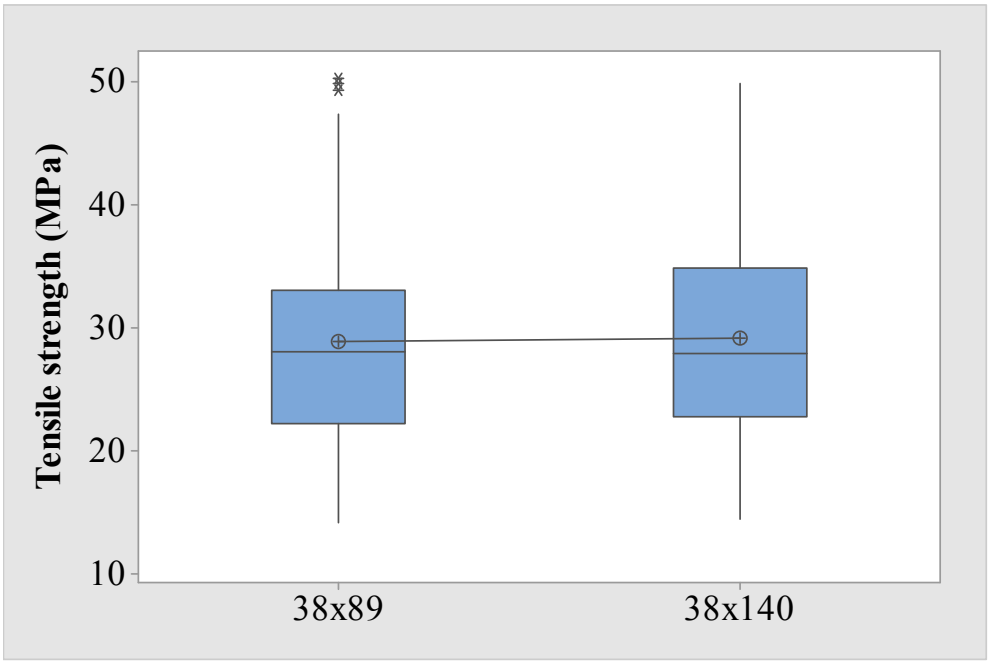
Tensile strength (MPa)
50
40
30
20
10
38x89
38x140

(a) E8

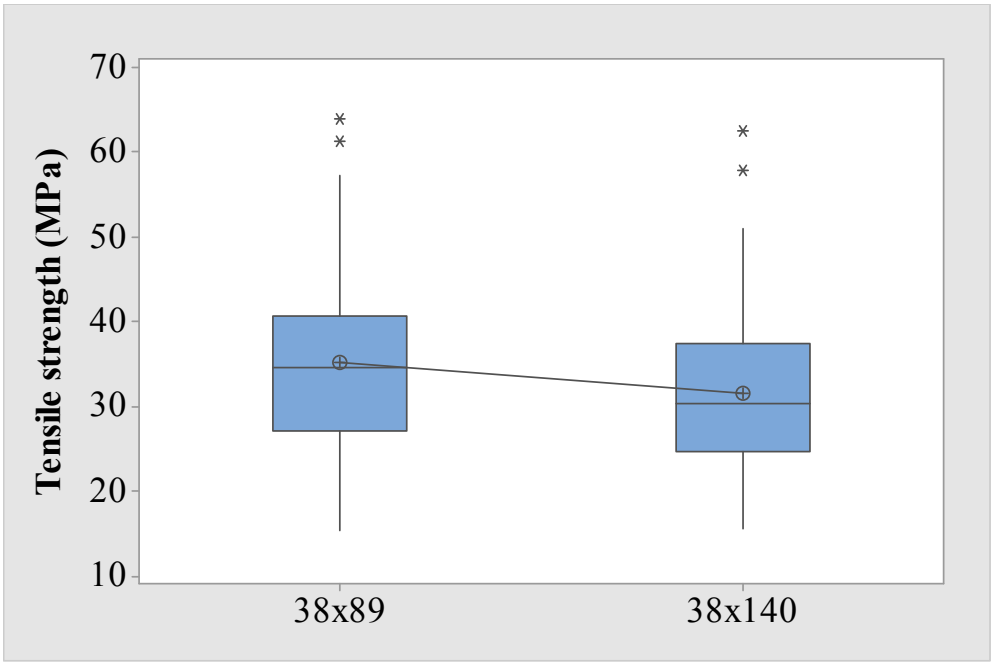
Tensile strength (MPa)
70
60
50
40
30
20
10
38x89
38x140

(b) E10

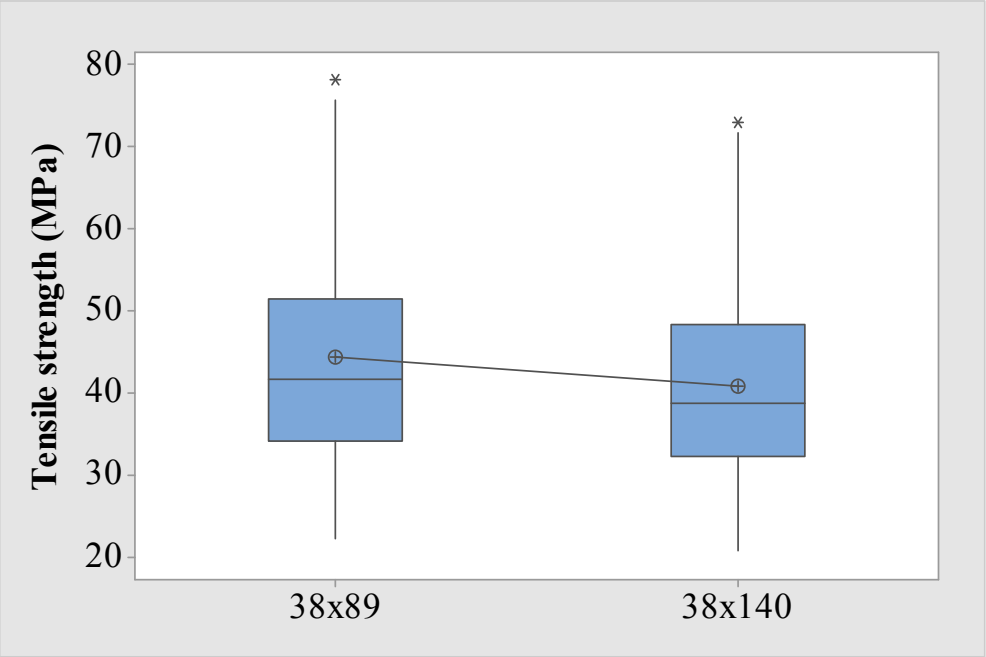

(c) E12

Figure 5-6 Boxplots of tensile strength from 38×89 mm and 38×140 mm cross section

The 2 sample t-test result shows that, except E8 grade, the p values of E10 and E12 grades was highly significant, therefore as p < α the null hypothesis (H_0) was rejected (Figure 5-5). Since a 2-tailed t-test was carried out, the actual α-value is α/2=0.05 and the result is not changed. The statistics indicate that the tensile strength distribution of E10 and E12 grades are statistically different.

Table 5-5 Two sample t-test result

Grade	*P*-value	Significance level (α)	Hypothesis
E8	0.913		H_0 accept
E10	0.010	0.1	H_0 reject
E12	0.065		H_0 reject

5.3.1.2 Tensile strength distribution of finger-jointed lamination

The finger joint has been used in manufacturing glulam for removal of the defect and extension of lamination in length. The finger-jointed lamination is used for manufacturing large scale glulam and it is known that a reduction in strength is 15-25% compared to the small clear specimens (Hoadley, 2000). Since the tensile strength of finger-jointed lamination is a main factor for determining both a bending strength of glulam and a tensile strength of lamination, the charactersitics of finger joint should be analyzed.

The tensile test of finger-jointed lamination shows that about 76 % of finger-jointed lamination was failed at finger joints (Figure 5-7). Especially, the failure at finger joint was increased in high grade (Figure 5-8). The tensile strength distribution of finger-jointed lamination was compared (Figure 5-9) and the distribution of higher grade placed on right side than that of lower grade. However, the low-tail distribution of each grades was not much different. Size effect on finger joint was not found (Figure 5-10) in this study. The tensile strength distribution of same grade was similar or the large size specimens are rather high. It shows that the width of finger-joined lamination does not significantly influence on the strength. The statistic characteristics of finger-jointed lamination are as shown in Table 5-6.

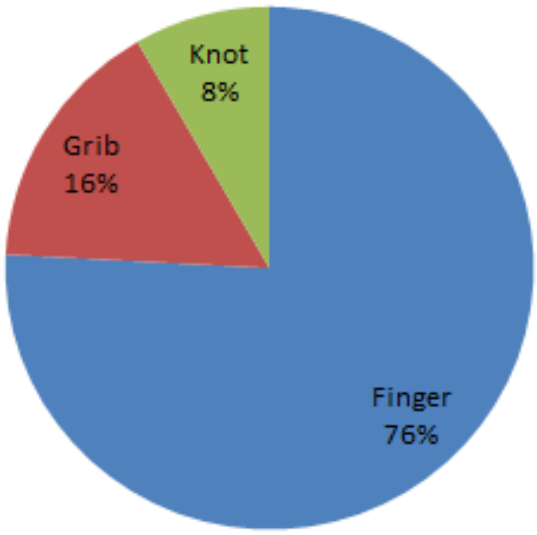

Figure 5-7 Failure modes of finger-jointed lamination (all grades)

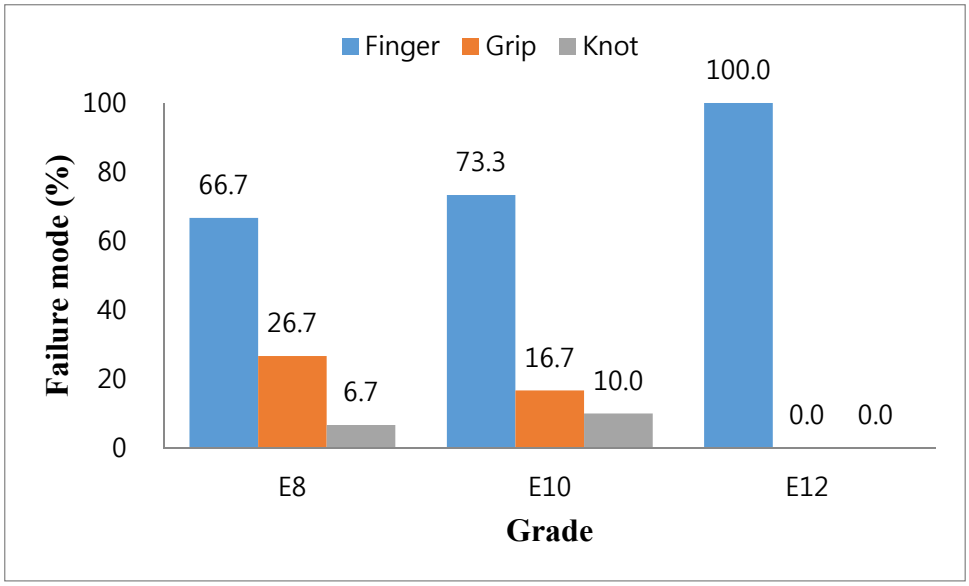

Figure 5-8 Failure modes of finger-jointed lamination at each grade

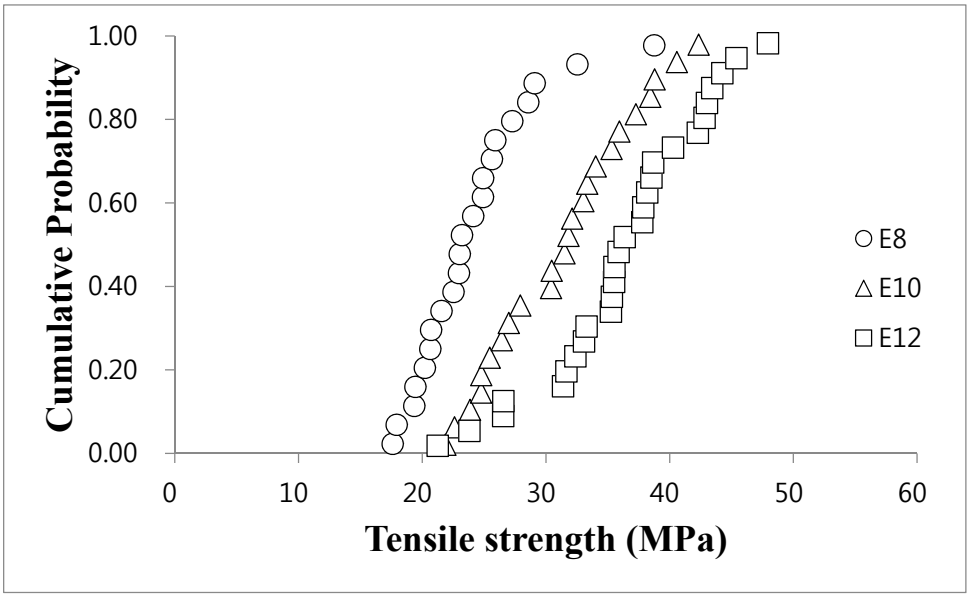

(a) 38×89 mm

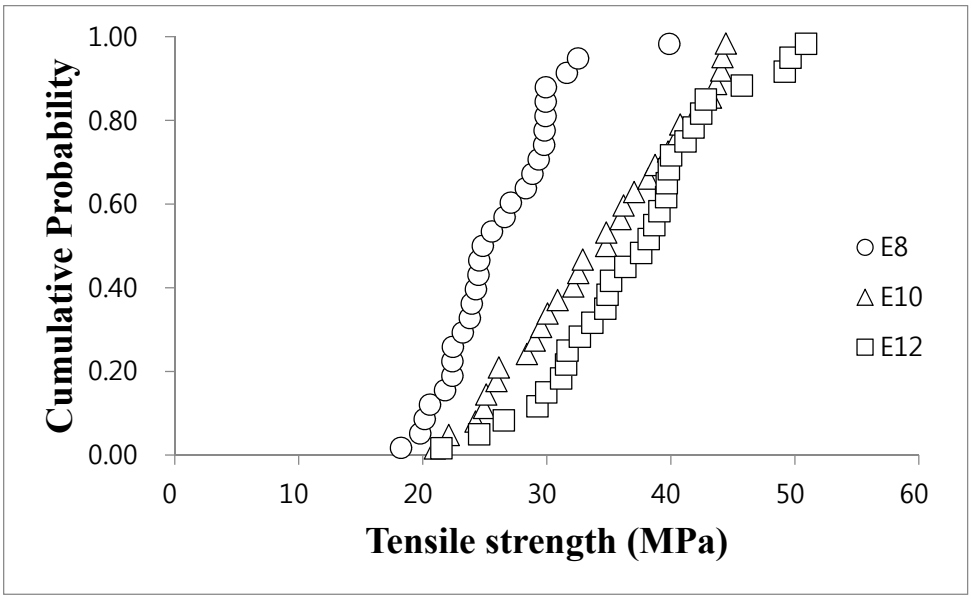

(b) 38×140 mm

Figure 5-9 Tensile strength distribution of finger-jointed lamination at same specimen size

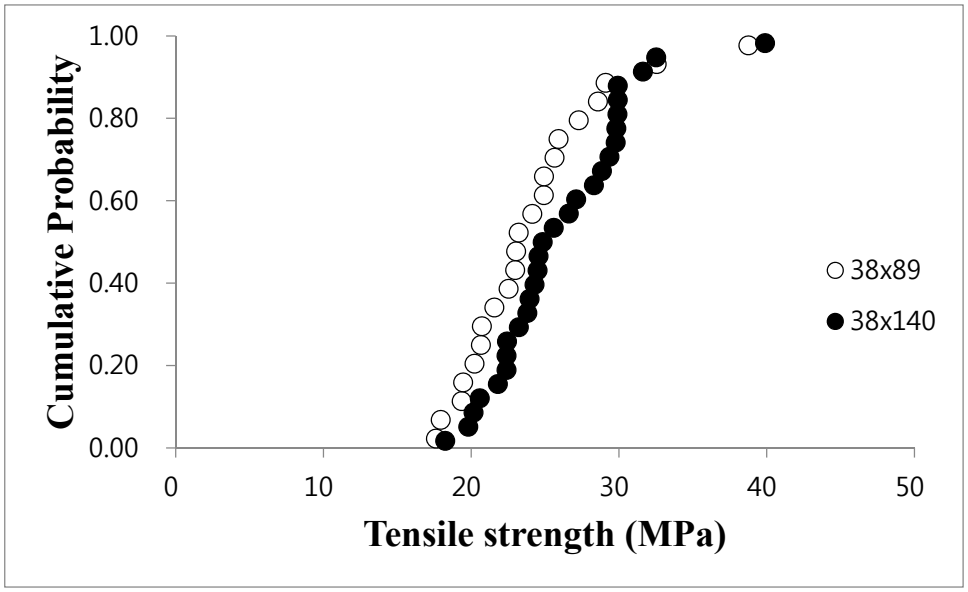
Cumulative Probability
1.00
0.80
0.60
0.40
0.20
0.00
0
10
20
30
40
50
Tensile strength (MPa)
38x89
38x140

(a) E8

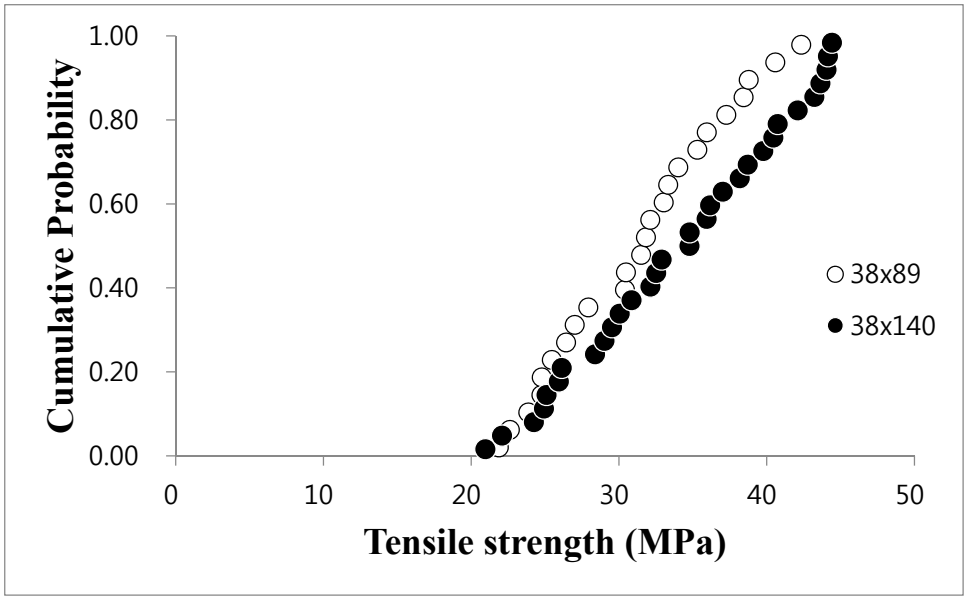
Cumulative Probability
1.00
0.80
0.60
0.40
0.20
0.00
0
10
20
30
40
50
Tensile strength (MPa)
38x89
38x140

(b) E10

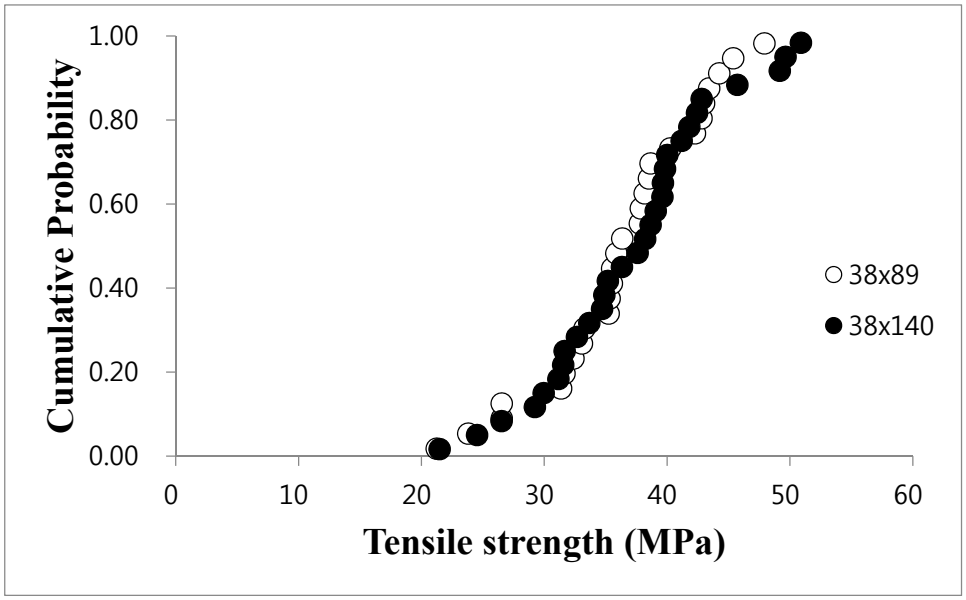

(c) E12

Figure 5-10 Comparison of finger-jointed lamination grades between 38×89 mm and 38×140 mm cross section

Table 5-6 Estimated tensile strengths and parameters of finger-jointed lamination

Specimen		5% NPE (MPa)	2P-Weibull		
			5% WPE	Shape	Scale
38×89 mm	E8	17.81	16.78	6.97	25.69
	E10	22.39	21.49	6.73	33.40
	E12	23.56	24.58	6.49	38.85
38×140 mm	E8	19.72	18.64	7.50	27.70
	E10	22.20	21.96	5.81	36.61
	E12	24.54	24.70	6.24	39.76

5.3.2 Validation of the glulam beam model

5.3.2.1 Validation of glulam without finger joints (Set 1)

One thousand virtual glulam beams were generated with input database of 38×89 mm lamination stock. The virtual glulam beams did not reflect a finger-jointed lamination and composed with two grades lamination, E12 and E8 (Figure 5-11). The lay-up of lamination grades corresponds to 10S-30B glulam grade in KS F3021.

Meanwhile, thirty actual glulam beams (Set 1) were manufactured and the glulam beams did not contain any finger joints. Bending test carried out for validating the simulated glulam bending strength and the most glulam specimens (27 EA) failed around a knot in tension zone (Figure 5-12 a). Meanwhile, shear failure appeared in three glulam specimens (Fig. Figure 5-12 b) and the maximum moment carrying capacity of the specimens was much higher than the other specimens that occurred tension failure. The shear failure would be caused by a high tensile strength of outmost lamination due to few knots and a low grain angle on the lamination. Since the maximum moment carrying capacity of the three glulam specimens was determined by shear failure, the moment carrying capacity of the glulam specimens by bending failure would be higher than the measured moment carrying capacity.

As a result, although this model was designed for predicting a glulam beam based on the tensile strengths of lamination and the shear failure was not considered, this concept is still reasonable, since the moment carrying capacity of the glulam by shear failure would be higher than that of glulam by tensile failure. If a tensile strength on lamination was lower than shear strength, tensile failure would be occurred.

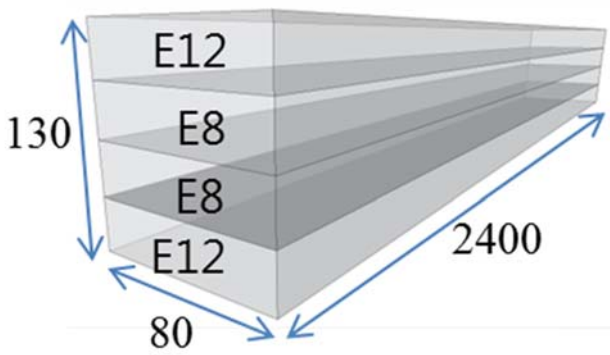

Figure 5-11 Lay-up of lamination grades for validating the basic virtual glulam beams that does not reflect a finger joints (Set 1)

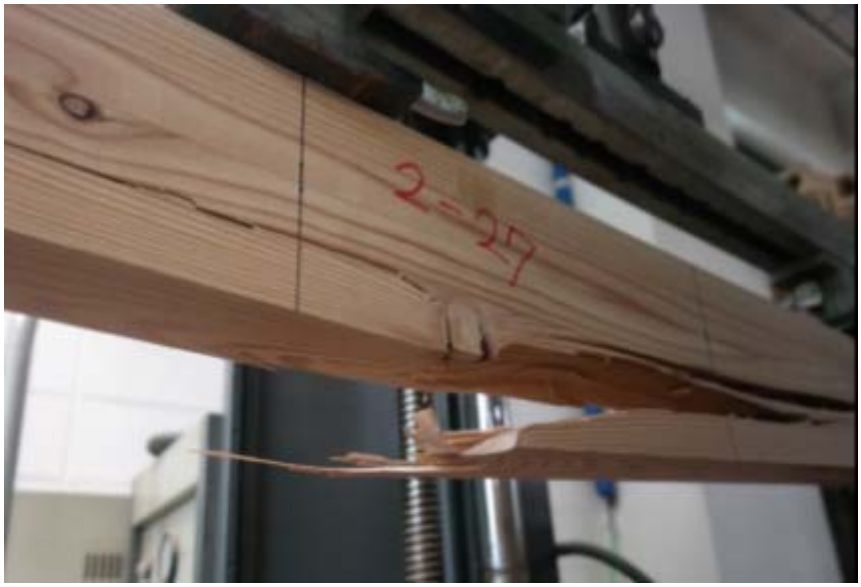

(a) Tension failure around knot in tension zone

(b) Shear failure

Figure 5-12 Figure modes of glulam set 1

The Kolmogorov-Smirnov two-sample test (K-S test) is one of the most useful and general nonparametric methods for comparing two samples, as it is sensitive to differences in both location and shape of the empirical cumulative distribution functions of the two samples. The Kolmogorov-Smirnov two-sample test (K-S test) was performed to test whether the simulated and actual cumulative distribution functions were significantly different. The K-S test shows that the test statistic was less than the critical value at significance level of 0.01 (Table 5-7). Thus, there was not sufficient evidence to conclude that the two distributions are different at significance level of 0.01. The difference of nonparametric 5% point estimate was approximately 1%.

The result of the Kolmogorov-Smirnov goodness-of-fit test shows that the assumption, failure criteria and tensile strength prediction, was reasonable. Especially, the low tail of the simulated bending strength distribution by the glulam model was fit very well with test data (Figure 5-13). The high tail of the simulated bending strength distribution was lower than the test data. It would be caused by the regression of material model and the reinforcing effect of lamination. First, in this model, in order to estimate localized tensile strength of lamination, regression of material models were used and the models were derived by KAR and MOE. It means that the regression was

optimized by large defects, since characteristics of clear part cannot be measured. Second, the high strength of specimens was happened at a glulam which has a good quality of lamination, low grain angle and little knots, in tensile section. High bending strength of glulam can be measured by reinforcing the good quality of lamination.

Table 5-7 Kolmogorov-Smirnov 2-sample test results (Set 1)

	Test data	Simulated data
No. of specimens (EA)	27	1000
Nonparametric 5% point estimate (MPa)	40.83	41.22
Coefficient of variation	0.22	0.17
K-S Test Statistic	0.265	
K-S Critical Value (significance level : 0.01)	0.317	

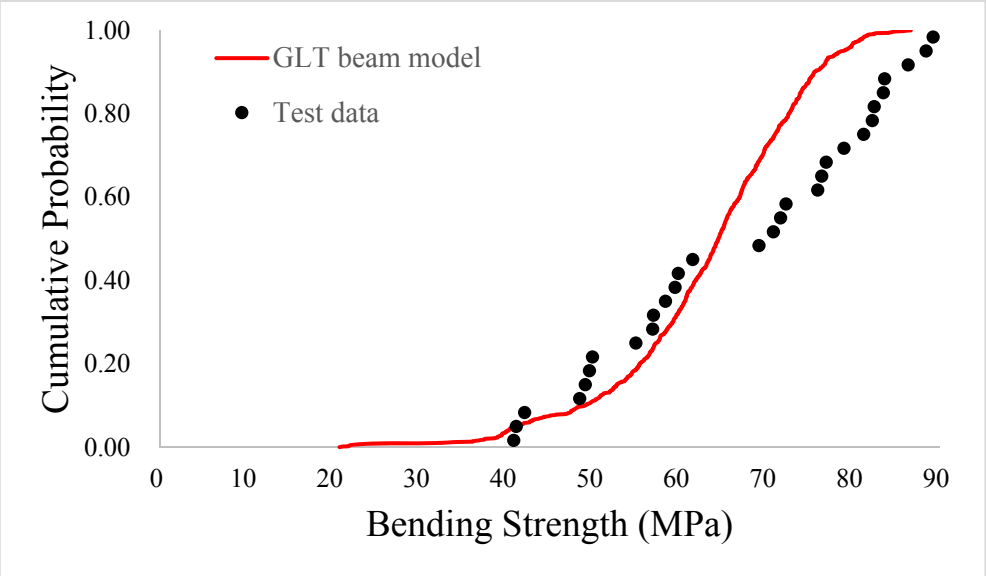

Figure 5-13 Comparison of the simulated and tested bending strength distribution (Set 1)

5.3.2.2 Validation of glulam containing finger joints (Set 2)

In order to check the glulam model whether reflecting an effect of finger joints in lamination or not, one thousand virtual glulam beams were generated with input database of 38×89 mm lamination stock. In manufacturing a finger-jointed lamination, about 40% of KAR on lamination is removed and the minimum length between finger joints was 800 mm, since too short span of lamination cannot be hold by the machine. Thus, a virtual glulam beam included a finger joint was generated as follows;

1) Knots, bigger than 40%, were replaced to finger joints of the same grades.
2) The minimum of distance between finger joints was 800 mm. If a lamination length was shorter than 800 mm, the lamination was removed.
3) At least one finger joints was forcibly placed in the middle of virtual glulam beam in order to simulate the actual glulam specimens.

Meanwhile, in order to validate the simulated glulam bending strength distribution, 30 pieces of actual glulam beams which include finger joints in lamination was manufactured. The arrangement and lay-up of lamination

grades was same with Set 1 (Figure 5-11). Especially, a finger joints was placed in the middle of outmost lamination in glulam specimens in order to lead to a failure in finger joints. Most of the failure of glulam specimens (28EA) were occurred in finger joints (Figure 5-14 a) and just two failure of specimens were occurred around knot in tension zone (Figure 5-14 b).

The K-S test result shows that the test statistic was less than the critical value (Table 5-8). Thus, the two distributions were not significantly different at significance level of 0.01. The difference of nonparametric 5% point estimate was approximately 1.1%. The coefficient of variation (COV) of actual test data was lower than that of simulated. It was caused by that the most of failure was occurred in the finger joints and the tensile strength variation of finger joints in glulam beams were not greater than tested tensile strength of finger-jointed lamination.

The comparison of simulated bending strength distribution and tested bending strength distribution shows that the lower tail distribution is fit well (Figure 5-15). It would be caused by the material regression model and the 15% lower-tail distribution for tensile strength of finger joints. The developed glulam model uses the material regression model for generating the tensile strength of

lamination. The material regression model could be developed by a weak strength since a high strength zone of lamination could not be fail. Thus, the material regression model reflects well the weak strength of lamination and the developed glulam model simulate well the lower bending strength distribution. In addition, since a tensile strength of finger joint is lower than clear lamination, a tensile strength of finger-jointed lamination failed in finger joint was placed in lower tail of tensile strength distribution. Thus, in order to reflect an experimental tensile strength of finger joint in virtual glulam beam, 15% lower-tail distribution of finger joint was used, and the lower-tail of simulated glulam bending strength distribution was fit well.

(a) Finger joint failure

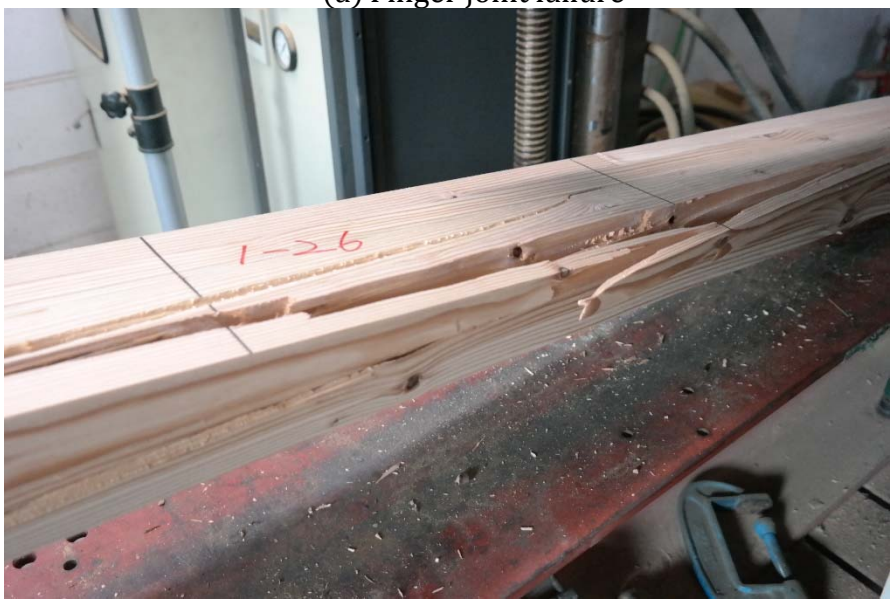

(b) Failure occurred around knot in tension zone

Figure 5-14 Figure modes of glulam Set 2

Table 5-8 Kolmogorov-Smirnov 2-sample test results (Set 2)

	Test data	Simulated data
No. of specimens (EA)	30	1000
Nonparametric 5% point estimate (MPa)	32.67	30.41
Coefficient of variation	0.18	0.25
K-S Test Statistic	0.259	
K-S Critical Value (significance level : 0.01)	0.302	

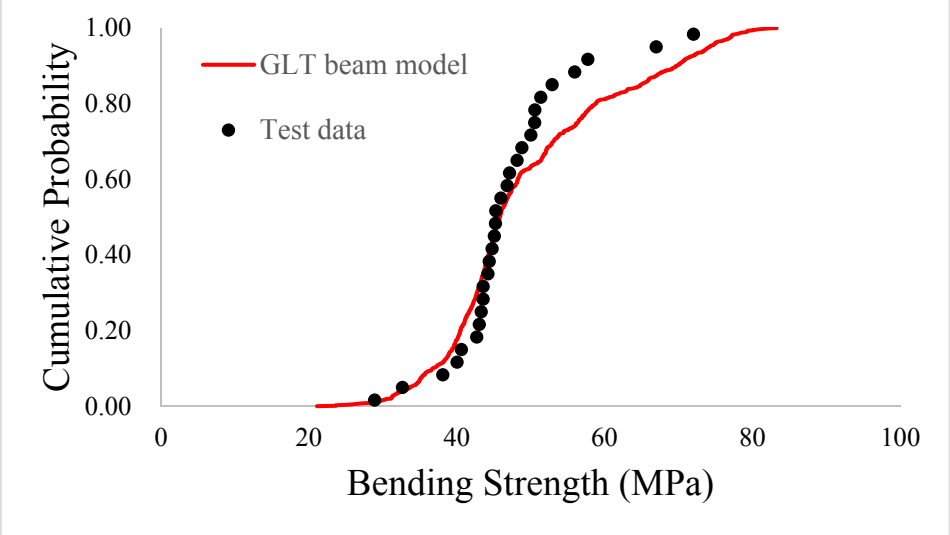

Figure 5-15 Comparison of the simulated and tested bending strength distribution (Set 2)

5.3.2.3 Validation of the different glulam size (Set 3)

The developed glulam beam model was designed for reflecting the natural growth irregularities of lamination. Moreover, using the scanning technology, the input database can be easily built. The width of 38×89 mm and 38×140 mm cross section lamination is different and the different cross section area includes the difference of physical characteristics, knot type, knot frequency, early wood/latewood ratio, and heartwood/sapwood ratio, etc. Moreover, the difference of lamination can be caused by a cutting method. Thus, in order to ensure that the developed model meet the other size glulam beam which were consisted of different lamination stock, the different size glulam beams were manufactured and validated with simulated bending strength.

One thousand virtual glulam beams were generated with input database of 38×140 mm lamination stock. The virtual glulam beams include finger joints and composed with three grades lamination, E12, E10, and E8 (Figure 5-16). The lay-up of lamination grades corresponds to 10S-30B glulam grade in KS F3021 like Set 1 and 2.

Meanwhile, thirty actual glulam beams for validating the simulated bending strength were manufactured. The bending test results show that 20 EA of

specimens were failed around finger joints (Figure 5-17 a) and 10 EA of specimens were failed around knot (Fig. Figure 5-17 b). The obvious fact is that all of the failure were occurred at tensile zone and the bending strength was governed by knots or tensile strength of finger joints.

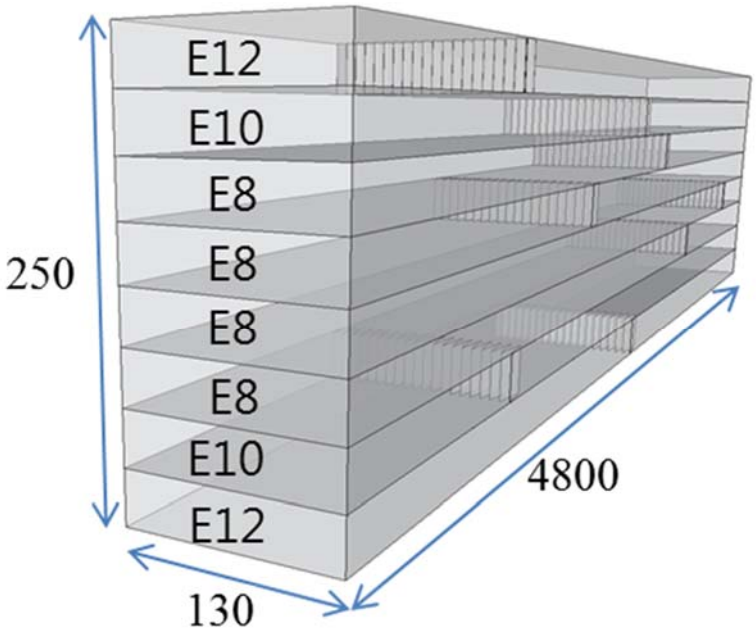

Figure 5-16 Lay-up of lamination grades for validating the different sized virtual glulam beam (Set 3)

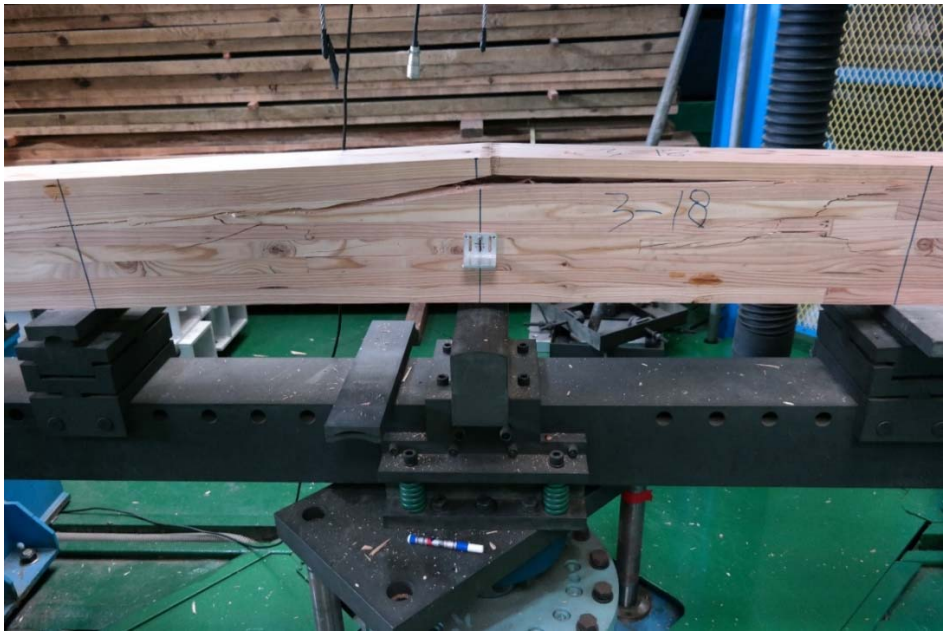

(a) Finger joint failure

(b) Failure occurred around knot

Figure 5-17 Figure modes of glulam Set 3

The K-S test result shows that the test statistic was less than the critical value and the two distributions were not significantly different at significance level of 0.01 (Table 5-9). The difference of nonparametric 5% point estimate was approximately 1.1% and the coefficient of variation (COV) of test data was also quite similar.

The simulated bending strength distribution was fit well with tested bending strength distribution (Figure 5-18). It shows that the applied failure criteria, material regression model was reasonable. Especially, the tested glulam beams were manufactured with the randomly sampled laminations which were used for establishing input database. Thus, the inherent characteristics of actual lamination stock were reflected well in both simulated and tested glulam bending strength. Thus, the results mean that the simulated glulam bending strength distribution is quite similar to the actual distribution of the glulam parent population can be manufactured by using the lamination grades in the input database.

Table 5-9 Kolmogorov-Smirnov 2-sample test results (Set 3)

	Test data	Simulated data
No. of specimens (EA)	30	1000
Nonparametric 5% point estimate (MPa)	31.91	29.06
Coefficient of variation	0.15	0.16
K-S Test Statistic	0.137	
K-S Critical Value (significance level : 0.01)	0.302	

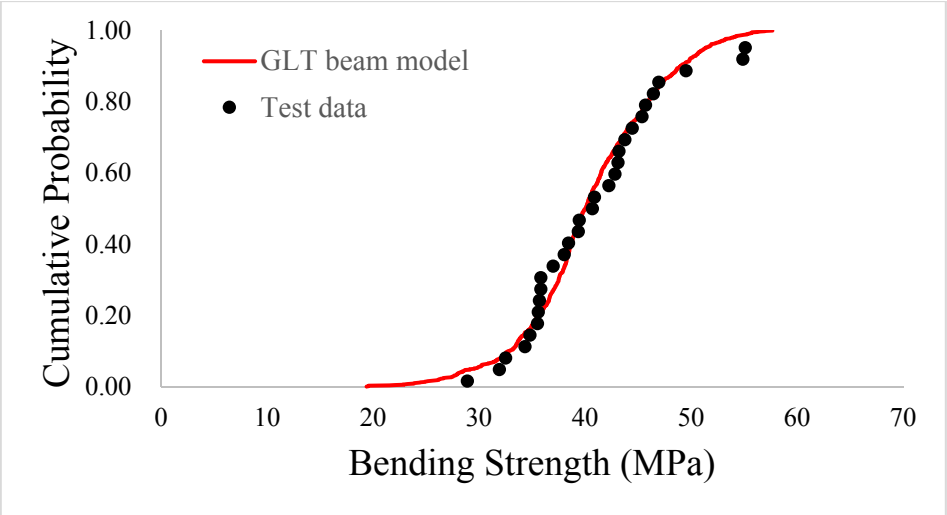

Figure 5-18 Comparison of the simulated and tested bending strength distribution (Set 3)

5.3.2.4 Validation for the different glulam grade (Set 4)

In order to ensure that the developed model meet another grade of glulam beam, 7S-27B glulam grade beams (Set 4) in KS F3021 was simulated using the developed model and manufactured for actual bending test. A thousand virtual glulam beams were generated with only E8 lamination grades of 38×89 mm lamination stock from input database (Figure 5-19). The bending test results of actual glulam beams show that 12 EA of specimens were failed around finger joints (Figure 5-20 a) and 18 EA of specimens were failed around knot (Figure 5-20 b). All of the failure were occurred at tensile zone, and the bending strength of glulam was governed by knots or finger joints like Set 3.

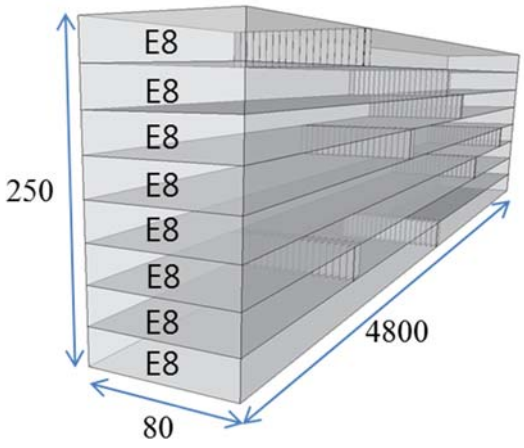

Figure 5-19 Lay-up of lamination grades for validating the different grade of virtual glulam beam (Set 4)

(a) Finger joint failure

(b) Failure occurred around knot

Figure 5-20 Figure modes of glulam Set 4

The K-S test result shows that the test statistic was less than the critical value and the two distributions were not significantly different at significance level of 0.01 (Table 5-10). The difference of nonparametric 5% point estimate was approximately 1.1% and the coefficient of variation (COV) of test data was also quite similar. Especially, the lower tail of simulated bending strength distribution was fit well with the tested bending strength distribution (Figure 5-21).

Table 5-10 Kolmogorov-Smirnov 2-sample test results (Set 4)

	Test data	Simulated data
No. of specimens (EA)	30	1000
Nonparametric 5% point estimate (MPa)	31.02	30.98
Coefficient of variation	0.16	0.15
K-S Test Statistic	0.19	
K-S Critical Value (significance level : 0.01)	0.302	

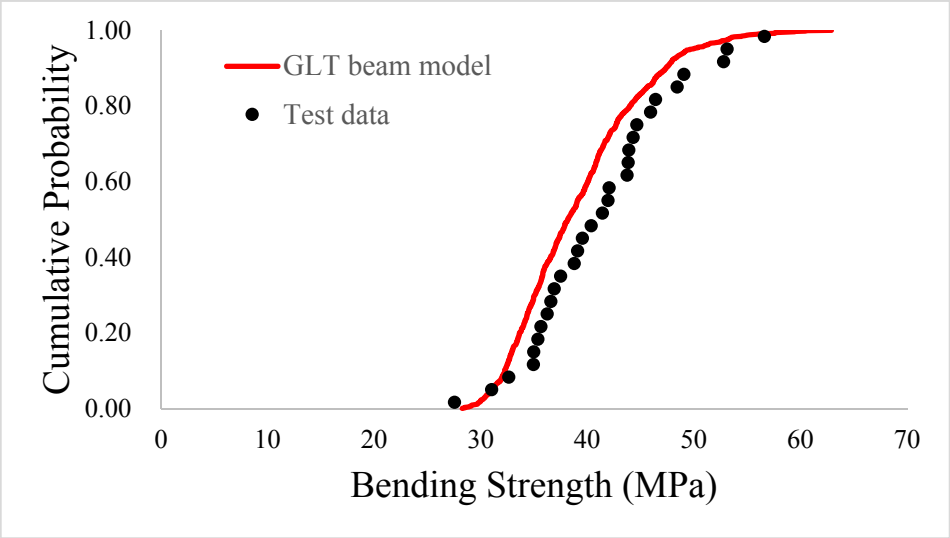

Figure 5-21 Comparison of the simulated and tested bending strength distribution (Set 4)

5.4 Conclusions

The bending strengths of four types of virtual glulam beams were simulated using the developed glulam model; (1) bending strengths of glulam beams without finger joints, (2) bending strengths of glulam beams with finger joints, (3) bending strengths of different glulam sizes, (4) bending strengths of different glulam grades. In order to validate the simulated bending strengths, the four types of actual glulam beams were manufactured as the same size with the four types of virtual glulam beams. The lamination was randomly selected from the lamination stock which used for building the input database.

The destructive bending test was carried out and brittle tensile failure was occurred finger joint or around knot in the most tested glulam specimens. It shows that the assumption of the model that the glulam beams were governed by the tensile strength of lamination was reasonable. Since the glulam beam model was designed for estimating bending strength distribution of glulam, the simulated bending strength distributions were validated with the experimental bending strength data and the K-S goodness-of-fit test was carried out. The K-S test result shows that the four types of simulated distributions were not significantly different with the corresponding experimental distribution at significance level of 0.01. In addition, the difference of nonparametric 5% point estimate was approximately 1 % in all cases.

Chapter 6. Model application using the developed glulam beam model

6.1 Size effect of the developed glulam beam model

6.2 Effect of knot size restriction on bending strength of glued laminated timber

6.3 Influence of material regression model on glulam bending strength distribution

6.4 Reliability analysis of glued laminated timber beam

6.1 Size effect of the developed glulam beam model

The main advantages of the developed glulam model are that the size effect of glulam beam can be investigated. Size effects must be quantified in order to adjust test strength for structural reliability analysis. In theory, as increasing beam size, the probability of the occurrence of a weak zone within a glulam beam increases and the bending strength decreases. The developed glulam beam model generates a virtual beam with (a) the number of lamination, (2) lamination thickness, and (3) lamination width. The length of virtual beam is determined automatically by 18 times the depth and the depth is determined by multiplying the number of lamination and lamination thickness.

The developed model was designed to consider the size effect by segmentation in length direction of lamination. By the segmentation, the resulting strength, the property variation within lamination would be considered in model. The occurrence of a weak link would be changed. Thus the resulting strength was expected to be changed with the size changes. In width direction, the model was expected to consider the width effect by inputting different set of input variables. The aim of this section is to check whether the developed model can consider the size effect or not.

6.1.1 Materials and methods

In order to simulate as close as possible to the actual glulam with actual lamination characteristics, the lamination thickness and lamination width for virtual glulam beam should be similar to the tested lamination size in input database. Since the structural performance of glulam depends on lamination arrangement, in case of large-size non-homogeneous glulam, same glulam grades in standards can be designed with various lamination combination and the actual strength characteristic would be different depending on the lamination combination. Thus, herein, the size effect was investigated with the validated homogeneous glulam, Set 4 glulam (Figure 5-19).

The simulated homogeneous glulam was validated with actual beams of Set 4. The Set 4 beams were consisted of 8 lay-up with only E8 lamination and the length was 4500 mm. For investigating the size effect, various size of glulam was generated with various E8 lamination lay-up (Table 6-1).

Table 6-1 5% point estimate on different size of glulam

Number of beam lay-up	Depth (mm)	Length (mm)	Width (mm)	5% PE (MPa)
4	125.0	2250	80	34.98
6	187.5	3375	80	31.76
8	250.0	4500	80	30.98
12	375.0	6750	80	29.17
24	750.0	13500	80	28.09

6.1.2 Results and discussion

The result shows that the bending strength of larger size glulam became lower and the distribution was placed the left side (Figure 6-1). Especially, the variation of bending strength was became smaller. It would be related to the possibility of including a weakest zone on lamination. The longer the virtual glulam, the greater the chances that it may include the largest defect on lamination in the virtual glulam.

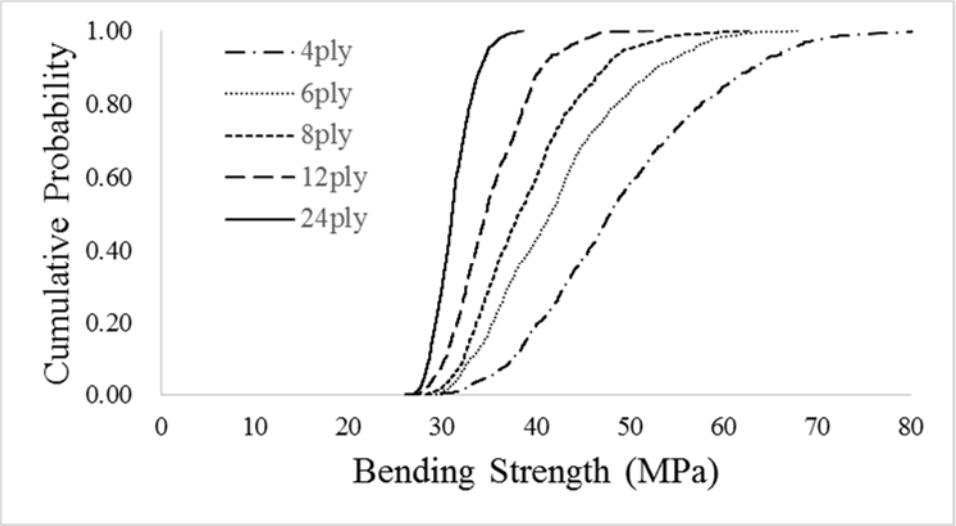

Figure 6-1 Bending strength distribution depends on different lamination lay-up

In structural design, the lower 5% point estimate (5% PE) of strength is used and the size effect also appeared at the 5% PE level (Figure 6-1). The size effects connected with failure parallel to grain have been represented using Eq. (6.1) and the equation is used as a design size adjustment factor for the characteristic strength (Foschi, 1992).

$$\sigma_1 = \sigma_2 \left(\frac{W_1\, T_1\, L_1}{W_2\, T_2\, L_2}\right)^{1/k_{volume}} \tag{6.1}$$

$$\ln\left(\frac{\sigma_1}{\sigma_2}\right) = \left(\frac{1}{k_{volume}}\right) \cdot ln\left(\frac{W_1\, T_1\, L_1}{W_2\, T_2\, L_2}\right) \tag{6.2}$$

where,

σ_1 = the strength of glulam 1 (MPa)

W_1 = width of glulam 1 (mm)

T_1 = thickness of glulam 1 (mm)

L_1 = length of glulam 1 (mm)

σ_2 = the strength of glulam 2 (MPa)

W_2 = width of glulam 2 (mm)

T_2 = thickness of glulam 2 (mm)

L_2 = length of glulam 2 (mm)

k_{size} = the size effect exponent

The size effect exponent, k, depends on the species in solid timber and can be obtained from statistical regression of logarithmic scale function with tested data (Eq. (6.2)). In case of glulam, the exponent, k, would be affected by lamination grade and lay-up of lamination as well, since the size effect related to the possibility of including week zone. In the logarithmic plots of size ratio and bending strength ratio curve (Figure 6-2), all points are distributed regularly and showed linear relationship. In Figure 6-2, the size ratio and bending strength ratio are the ratio of various simulated glulam to an 8 lay-up glulam which was validated with destructive test. Finally, the size effect exponent was determined as approximately 16.9. The calculated bending strength using the size effect function with the derived exponent value, Eq. (6.1), fits well with the simulated bending strength (Figure 6-3). In National Design Specification (NDS), for Southern Pine 20 is used as a size effect exponent, 10 is used for all other species. Shedlauskas et al. (1996) investigated the size effect for red oak glulam and the derived size effect exponent was 12.5.

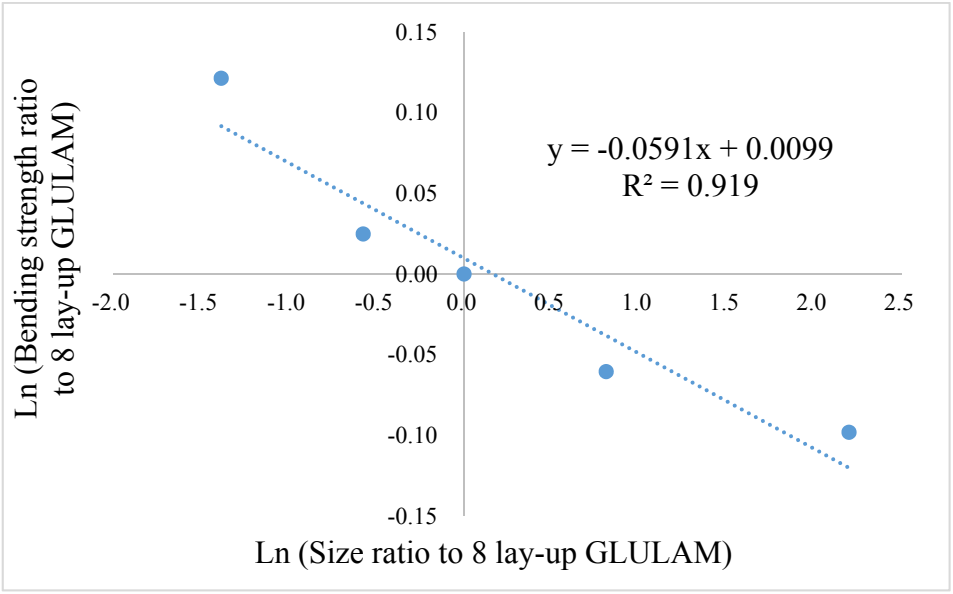

Figure 6-2 Relationship between size ratio and bending strength ratio

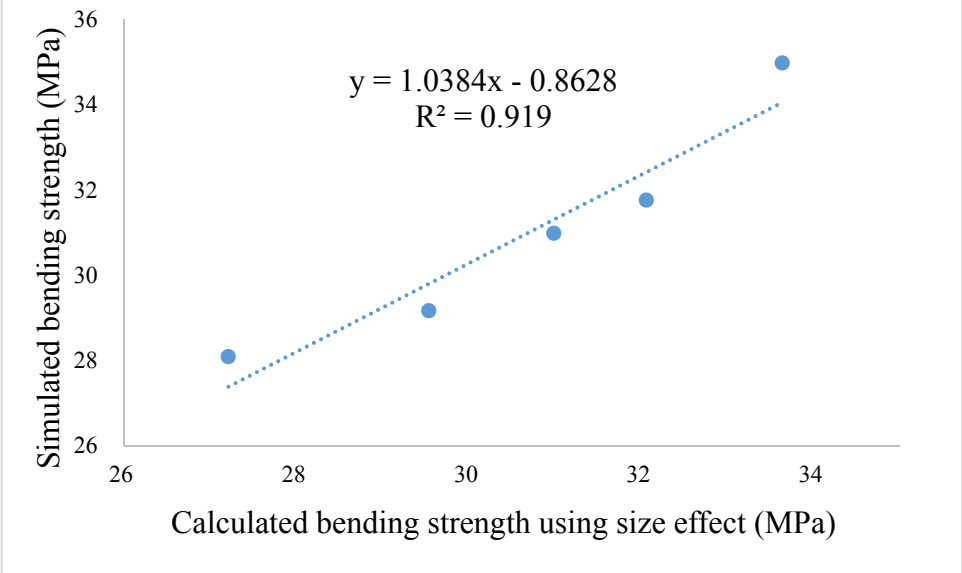

Figure 6-3 Simulated bending strength for various glulam size and calculated bending strength using Eq. (4.1) with the derived size effect exponent

6.1.3 Conclusions

In the developed model, the more number of lay-up of lamination, the larger glulam size, and the probability of weakest zones was increased in the larger size of virtual glulam beam. The size effect was investigated by comparing the bending strength distributions of various size glulam beams. The size effect exponent was as 16.95.

6.2 Effect of knot size restriction on bending strength of glued laminated timber

In glued laminated timber (glulam), finger joints are used for two purposes. First, finger joints connect the end of lamination for manufacturing a long span glulam. Second, after removing a large defect in lamination, finger joins are used for connecting the devided lamination. In this case, the aim of finger joint is to increase the strength of lamination in order to ensure the strength quality of glulam.

A tensile strength of finger joint is higher than that of lamination including a large defect. However, the tensile strength of finger joint is definitely lower than that of defect-free lamination which do not have any defects. The strength of finger joints is depends on the shape of finger joints, and 75~85% of defect-free wood (Hoadley, 2000). Thus, if a small defect removed and connected with a finger joint, the strength of lamination can be decreased.

One of the main advantages of the presented glulam model is that the influence of parameters on the glulam load-bearing capacity can be investigated. The developed glulam model uses localized tensile strength of lamination as an input parameter and the tensile strength is generated with localized KAR on actual lamination. In case of a finger joint, an experimental tensile strength of

finger-jointed lamination of the same grade was applied instead of a tensile strength generated by a KAR. Thus, the finger joints effect to glulam bending strength can be investigated by changing the KAR size to be removed using the developed glulam beam model.

The aim of this section is to investigate the glulam bending strength distribution depending on a knot size restriction to be removed and connected by finger joints in lamination.

6.2.1 Materials and methods

When glulam beams were consisted of various lamination grade, more accurate trend by finger joint effect can be investigated. Thus, in order to investigate the finger joint effect, non-homogeneous 8-ply glulam was simulated with various knot size restriction that knot to be removed. The lamination lay-up was same with Figure 5-16, since the virtual glulam which was consisted of various lamination grade and already validated with the Set 3 beams.

6.2.2 Results and discussions

A large defect, such as knot, bark, curved section, etc., on lamination is usually removed and the divided laminations are connected by a finger joint. Since the defect was removed, the variation in tensile strength of finger-jointed lamination was smaller than that of the same lamination grade, and the minimum tensile strengths of finger-jointed lamination tend to be higher than those of the same lamination grades (Table 6-2). It means that the glulam bending strength can be governed by the knot size restriction to be allowed in the lamination, since the glulam bending strength related to the tensile strength of lamination.

Table 6-2 Tensile strength ranges of lamination and finger-jointed lamination

Grade	Specimen size	Range of tensile strength (MPa)	
		Lamination	Finger-jointed lamination
E8	38×89 mm	14-50	17-39
	38×140 mm	14-50	18-30
E10	38×89 mm	15-64	21-39
	38×140 mm	15-63	21-39
E12	38×89 mm	21-78	21-43
	38×140 mm	20-73	21-40

The simulated glulam bending strength distributions show that the glulam bending strength is significantly affected by the KAR limitation (Figure 6-4 a). However, when the KAR limitation was 0.45, the lower tail distribution under 20% tend to be similar (Figure 6-4 b). It would be caused by that the lower glulam bending strength was governed by a finger joint. The minimum tensile strengths of finger-jointed lamination were not significantly different between three grades (Table 6-2).

When the KAR limitation was 0.25, the glulam bending strength distribution was decreased rather than when the high KAR limitation, 0.45, was applied. It means that the optimized KAR is existed for deriving a highest glulam bending strength distribution. Herein, the optimized KAR size for deriving highest glulam bending strength was 0.25.

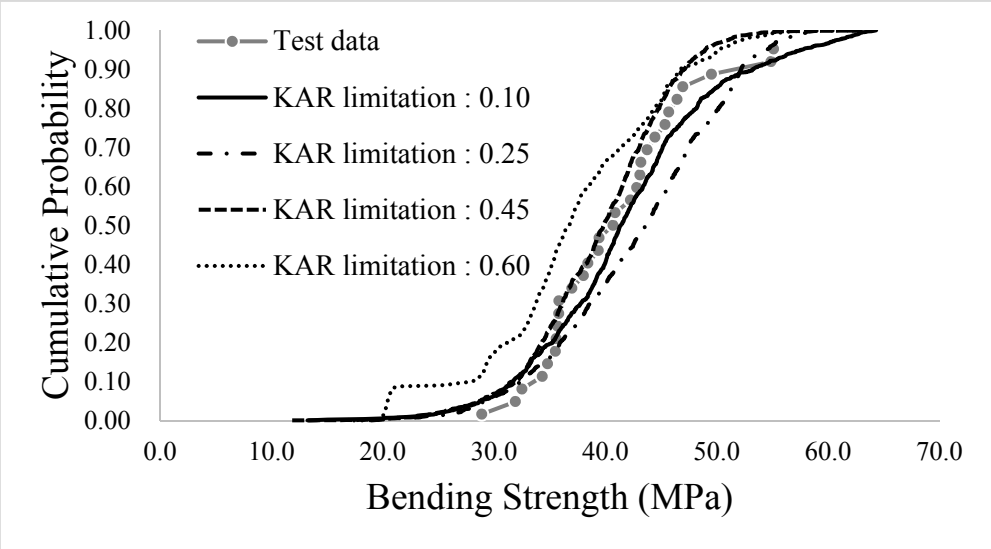

(a) Total distribution

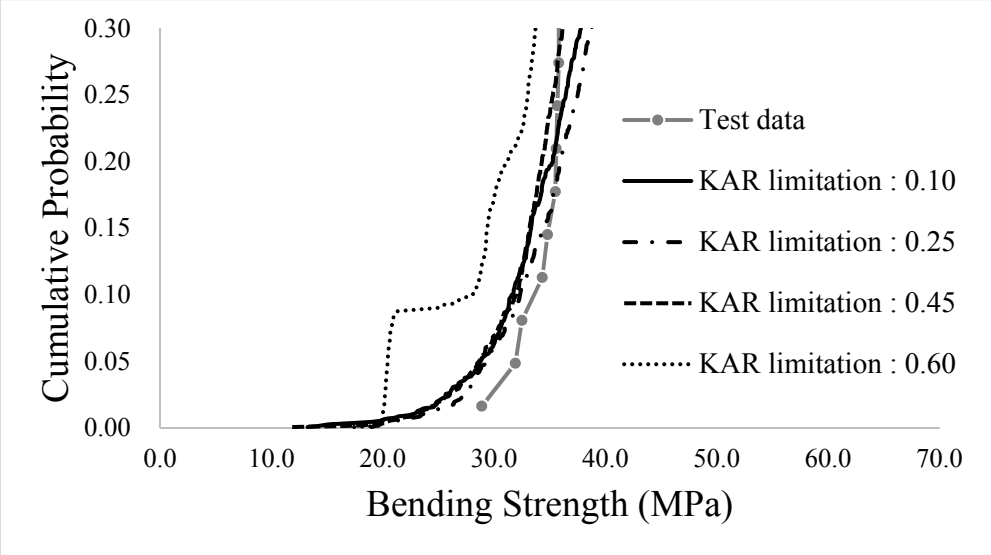

(b) Lower tail distribution

Figure 6-4 Bending strength distribution depending on various KAR limitation

Meanwhile, in case of the 5% point estimate (5% PE), when larger KARs than 0.45 were included in lamination, the 5% PE was significantly decreased (Figure 6-5). However, when the KAR sizes under 0.45 were removed, the 5% PE was not significantly different. It shows that the KAR criteria, 0.17, 0.25, 0.33, of existing standard is appropriate, but little bit strict.

An optimized KAR size for deriving highest 5% PE was also existed, herein, it was approximately 0.33. In addition, when the higher or lower KAR limitation than optimized KAR limitation was applied, a tendency was appeared that the 5% PE of simulated glulam beams were decreased. Especially, the tendency of decreasing 5% PE by the lower KAR limitation than optimized KAR limitation shows that if smaller KAR than a specific KAR is removed, the bending strength of manufactured glulam can be decreased as well, since the tensile and bending strength of finger joints can be lower than those of lamination which includes the smaller KAR.

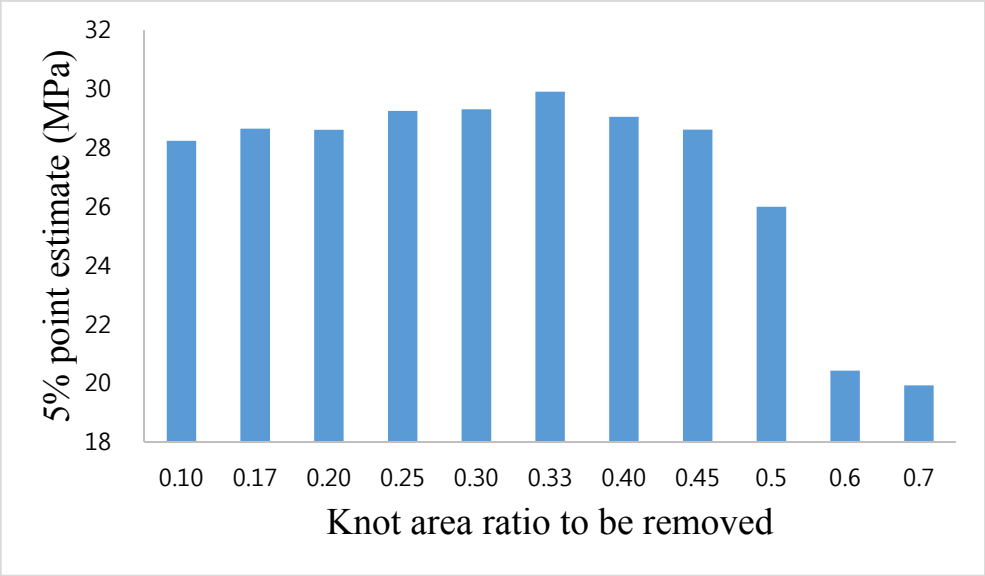

Figure 6-5 Relationship between 5% point estimates and KAR size to be removed

6.2.3 Conclusions

In the developed model, a tensile strength of finger joint is applied instead of lamination tensile strength generated by local KAR and MOE. Thus, the finger joint effect to the glulam bending strength can be investigated by changing the KAR restriction to be removed.

The tensile strength range of finger jointed lamination is shorter than that of the same lamination grade. In addition, the lowest tensile strength of finger joint lamination is higher than that of the same lamination grade. Thus, a specific KAR for deriving a highest glulam bending strength distribution should be existed. The optimized KAR for deriving a highest glulam bending strength distribution was 0.25. Meanwhile, a KAR criteria for deriving a highest 5% PE of glulam beams was 0.33.

The results show that there is a specified KAR limitation for optimizing the glulam bending strength due to the possibility of that the tensile strength of finger-jointed lamination inserted instead of knots can be lower than the original tensile strength. In addition, it means that the quality of finger joint is important, since the glulam bending strength can be increased as increasing the finger joint strength and reducing the strength variation.

6.3 Influence of material regression model on glulam bending strength distribution

The glulam beam model uses material regression model for generating localized tensile strength on lamination. Thus, the between-lamination and within-lamination correlation can be easily updated corresponding to new lamination grade. But it needs empirical equation to estimate tensile strength from KAR and MOE profiles. Folz's model, Bender's model, and Nakamura's model use only MOE profiles with the correlated random variables for generating tensile strength. Meanwhile, Foschi's model, Karlsruhe model, Lee's model, and Fink's model use KAR profiles for generating tensile strength.

In Chapter 4, three kinds of regression model was developed previously, (1) MOE-tensile strength model (MOE-model), (2) KAR-tensile strength model (KAR-model), and (3) Multiple regression model using both KAR and MOE (Multi-model). Thus, the three tensile strength prediction model can be used for generating a localized tensile strength on lamination and a bending strength of glulam beam.

The aim of this section is to investigate the influence of material regression with two input properties, MOE and KAR, on lamination for the glulam bending strength.

6.3.1 Materials and methods

The lamination lay-up of virtual glulam beam was same with Figure 5-11 to remove the influence of the finger joints. In addition, the simulated bending strength can be validated with the Set 1 beams.

Three kinds of developed regression model in Chapter 4 were used for generating tensile strength. The regression models and the ranges of input variables are in Table 6-3. The MOE-model reflects the lengthwise MOE distribution and localized MOE on lamination in a simulated glulam bending strength. The KAR-model reflects the lengthwise KAR distribution and localized KAR on lamination in a simulated glulam bending strength. The Multi-model reflects both lengthwise MOE and KAR distribution, and both localized MOE and KAR on lamination in a simulated glulam bending strength.

Table 6-3 Regression model for generating tensile strength and input variable ranges

Regression model (Tensile strength =)		Input variable range		Tensile strength range (MPa)
		KAR	MOE (GPa)	
(1) MOE-model	3.01×MOE+7.48		7-13	28.5-46.6
(2) KAR-model	-77.2×KAR+59.8	0-0.6		13.5-59.8
(3) Multi-model	-69.71×KAR+1.63×MOE +41.23	0-0.6	7-13	10.8-62.4

6.3.2 Results and discussion

By comparing three simulated bending strength distributions generated from three regression model, the influence of material model and input variables were investigated using same input variable database based on localized MOE and KAR. This can provide precious information for reviewing the difference of previously developed glulam models by several researchers.

Although the comparison of several glulam model is impossible due to the difference of the used input parameters and the used material properties, almost the models use MOE or KAR profiles for considering lengthwise variation of lamination. Thus, by comparing the influence of material models related to MOE or KAR, the influence of MOE or KAR for glulam bending strength can be investigated. In addition, the prediction accuracy of the several glulam models can be estimated indirectly.

Figure 6-6 shows that this glulam beam model is affected by material regression model. The expected bending strength of glulam beams using Multi-model was closer the results using KAR-model than using MOE-model. The expected tensile strength range using Multi-model is also closer to the results by KAR-model than by MOE-model (Table 6-1). It shows that the

glulam bending strength is very closely related to the tensile strength of lamination, and the lamination tensile strength is governed by a localized KAR than a localized MOE on lamination. Thus, when the KAR on lamination is reflected for predicting glulam bending strength, more accurate bending strength would be derived. The glulam models reflecting KAR information would provide more accurate bending strength than the others.

The root mean square error (RMSE) was calculated using Eq. (6.3) in order to check the differences between the empirical glulam bending strength distribution and the simulated glulam bending strength distributions derived by the three material regression models (Table 6-4). The results show that the simulated glulam bending strength distribution derived by Multi-model was the most similar to the empirical glulam bending strength distribution.

*The RMSE formula :

$$A = \begin{bmatrix} x_{1,1} \\ x_{1,2} \\ \vdots \\ x_{1,n} \end{bmatrix} \quad and \quad B = \begin{bmatrix} x_{2,1} \\ x_{2,2} \\ \vdots \\ x_{2,n} \end{bmatrix}$$

$$RMSE(A,B)=\sqrt{\frac{\sum_{i=1}^{n}(x_{1,i}-x_{2,i})^2}{n}} \tag{6.3}$$

Where,

A: empirical glulam bending strength (MPa)

B: simulated glulam bending strength by material regression models

Table 6-4 Root mean square error results

Model	Root mean square error
MOE-model	14.39
KAR-model	5.28
Multi-model	4.73

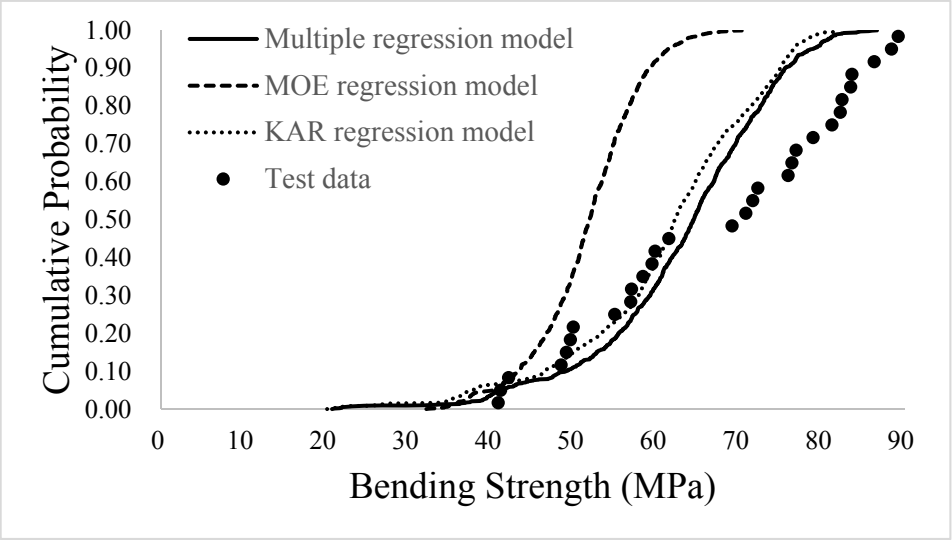

Figure 6-6 Comparison of the bending strength distribution using the material model

6.3.3 Conclusions

The influence of three material regression models with two input variables on lamination was investigated for glulam bending strength. Multi-model based on two variables (MOE, KAR) predicting equation provided much better accuracy in glulam beam prediction.

6.4 Reliability analysis of glued laminated timber beam

The design codes take the uncertainties into consideration to help engineers create safe and efficient designs to meet a level of safety deemed acceptable from experience/performance record and calculations. In Allowable Stress Design (ASD) codes, uncertainties are handled by a safety factor accounting for uncertainties in both load and capacity. In contrast, in limited state design (LSD) codes, uncertainties are handled by safety factors for loads (load factor) and for resistance (resistance factor).

Korean Building Code (KBC) provides structural design values of construction materials as well as design codes regulating the design and construction of structures. Timber design codes in KBC are based on the ASD codes. However, all other material (concrete, steel, and brick) design codes are based on the LSD codes. Thus, the differences of design principles make the engineers difficult to designs a building to meet a constant safety level.

The design values depend on the design codes. Most timber engineering codes (Eurocode 5, International Building Code, Canadian Standards Association, Australia standards, New Zealand standards) has been adopted LSD. In LSD codes, the uncertainties of material are reflected in resistance factor and 5%

value is used as the structural design value of timber. In ASD codes, a reduced 5% value, the 5% value is divided by reduction factors for the duration of load and the safety factor, is used as the structural design value of timber. As a result, the design value of timber in KBC is lower than the species of other countries. The lower tabulated design values of timber will be considered a timber of a low quality. The larger cross-section area makes overdesigned building which is economically poor and it prevents designing to optimize the efficiency of each member.

LSD codes are accepted by code agencies throughout the world. It is essential to convert the ASD codes to LSD codes for the cooperation of engineers with state-of-the-art technology and for using together with other domestic construction materials. Although researches for converting the design values of domestic timber have been attempted, the characteristic values of domestic glulam has never investigated.

In this section, reliability analysis of glulam beam in bending was carried out based on domestic design loads and bending strength distributions of glulam.

6.4.1 Materials and methods

6.4.1.1 Basic principles of reliability analysis

The performance of an engineering structure depends on the type and magnitude of the applied load and the structural strength. The conceptual basis for limited state design is founded in classical reliability theory (Freudenthal et al. 1966, Shinozuka, 1983) and the mathematical model relating the resistance and load variables for the specific limit state of interest is as follows:

$$G(\mathrm{X}) = G(X_1, X_2, \dots, X_N) \tag{6.4}$$

Where, $\mathrm{X} = (X_1, X_2, \dots, X_N)$ is random resistance or load variable

Random load variables will influence the *demand D* on the system, and random resistance variables will characterize the *capacity C* to withstand the demand. By convention, mathematical model *G* is written as

$$G = C - D \tag{6.5}$$

From the model with the random variables, the distribution of probability of the failure event, $G < 0$, and that of survival event, $G \geq 0$, can be calculated.

6.4.1.2 Structural reliability model for beam bending strength

The maximum bending moment of a simply supported beam in uniform load can be calculated using Eq. (6.6). The maximum bending stresses of a simply supported beam of rectangular cross-section can be calculated using Eq. (6.7). Thus, the mathematical model G_b for the bending failure limit state of a simply supported beam of rectangular cross-section can be written as Eq. (6.8).

$$M = \frac{Q_{DL}L^2}{8} \tag{6.6}$$

Where,

M : maximum bending moment (N · mm)

Q_{DL} : the uniformly distributed load (N)

L: the beam span (mm)

$$\sigma_b = \frac{My}{I} = \frac{Q_{DL}L^2}{8}\left(\frac{y}{I}\right) = Q_{DL}\frac{6L^2}{8WT^2} \tag{6.7}$$

Where,

σ_b : maximum bending stresses of a beam (MPa)

M : maximum bending moment (N · mm)

y : the distance from the neutral axis to the location of a extreme fiber stress (mm)

I : the moment of inertia (mm^4)

Q_{DL} : the uniformly distributed load (N)

L: the beam span (mm)

W and T : the beam width and thickness, respectively (mm)

$$G_b = R - (D + Q) \cdot \frac{6L^2}{8WT^2} \tag{6.8}$$

Where,

G_b : the bending failure limit state of a simply supported beam of rectangular cross-section

R: the bending strength (random variables) (MPa)

D: the uniformly distributed dead load (random variables) (N)

Q: the uniformly distributed live load (random variables) (N)

L: the beam span (mm)

W and T : the beam width and thickness, respectively (mm)

Meanwhile, the format for the ultimate strength limit state design equation is

$$(1.2D_n + 1.6Q_n) \cdot \frac{6L^2}{8WT^2} = \emptyset R_{0.05} \tag{6.9}$$

Where,

1.2 and 1.5: the dead and live load factors in Korean Building Code

D_n and Q_n: the design dead and live load (N)

L: the beam span (mm)

W and T : the beam width and thickness, respectively (mm)

$\emptyset$: the resistance factor

$R_{0.05}$: the characteristic strength (the nonparametric 5th percentile) (MPa)

If the ratio of the design dead load to the design live load is defined as Eq. (6.10), the Eq. (6.9) can be rewritten as Eq. (6.11) and mathematical model G_b, Eq.(6.8), can be rewritten as Eq. (6.12). Finally, structural reliability model for beam bending (Eq. (6.13)) can be derived combining Eqs. (6.11) and (6.12).

$$\gamma = \frac{D_n}{Q_n} \tag{6.10}$$

Where,

γ : dead-live load ratio, a deterministic parameter and herein chosen to be 0.25, 0.5, 1, 1.5, 2 (KICT, 1989)

D_n and Q_n: the design dead and live load (N)

$$Q_n = \frac{8WT^2}{6L^2}\left(\frac{\emptyset R_{0.05}}{1.2\gamma + 1.6}\right) \tag{6.11}$$

Where,

Q_n: the design live load (N)

W and T : the beam width and thickness, respectively (mm)

L: the beam span (mm)

$\emptyset$: resistance factor, a deterministic parameter for calibrating a probability of failure

$R_{0.05}$: 5% point estimate, a deterministic parameter from simulated data (MPa)

γ : dead-live load ratio, a deterministic parameter and herein chosen to be 0.25, 0.5, 1, 1.5, 2 (KICT, 1989)

$$G_b = R - \frac{6L^2}{8WT^2} \cdot Q_n \cdot \left(\frac{D}{D_n}\gamma + \frac{Q}{Q_n}\right) \quad (6.12)$$

Where,

G_b : the bending failure limit state of a simply supported beam of rectangular cross-section

R: the bending strength (random variables) (MPa)

L: the beam span (mm)

W and T : the beam width and thickness, respectively (mm)

Q_n: the design live load (N)

D and Q: the uniformly distributed dead and live load (random variables) (N)

D_n and Q_n: the design dead and live load (N)

$$G_b = R_g - \left(\frac{\emptyset R_{0.05}}{1.2\gamma + 1.6}\right) \cdot (d\gamma + q) \quad (6.13)$$

Where,

G_b : the bending failure limit state of a simply supported beam of rectangular cross-section

R_g : random variables taken from simulated glulam bending strength (MPa)

$\emptyset$: resistance factor, a deterministic parameter for calibrating a probability of failure

$R_{0.05}$: 5% point estimate, a deterministic parameter from simulated data (MPa)

γ : dead-live load ratio, a deterministic parameter and herein chosen to be 0.25, 0.5, 1, 1.5, 2 (KICT, 1989)

d and q : random variables, the dead and live loads normalized with respect to their corresponding design values

$$d = \frac{D}{D_n} \qquad q = \frac{Q}{Q_n}$$

6.4.1.3 Load and resistance distribution

The probability distributions of load and resistance for beam element were generated using Monte Carlo simulation, 500,000 times. The random variables for the dead and live loads were taken from the domestic load distribution developed by KICT (1989). The statistical parameters for beam element of 50-year loads are in Table 6-5.

The bending strength of glulam beams was randomly taken from a simulated bending strength distributions and the distributions were simulated by the developed glulam model. The lay-up arrangement of virtual glulam beams was composed with 8 lamination (Figure 6-7) and the material properties, localized MOE, KAR, and tensile strength of finger joints, were taken from 38×140 mm lamination database.

Table 6-5 Statistical parameters and distributions for beam element

Variables		Mean	COV	5% PE (MPa)	Distribution
Load	Live (*d*)	1.038	0.239		Type-1 Gumbel
	Dead (*q*)	1.050	0.100		Normal
Resistance	Type 1 (All E8 lamination)	38.90	0.127	32.11	Simulated bending strength distribution
	Type 2 (All E10 lamination)	40.12	0.125	33.16	
	Type 3 (All E12 lamination)	40.46	0.120	36.13	
	Type 4 (E8, E10, E12 lamination)	40.44	0.163	29.06	

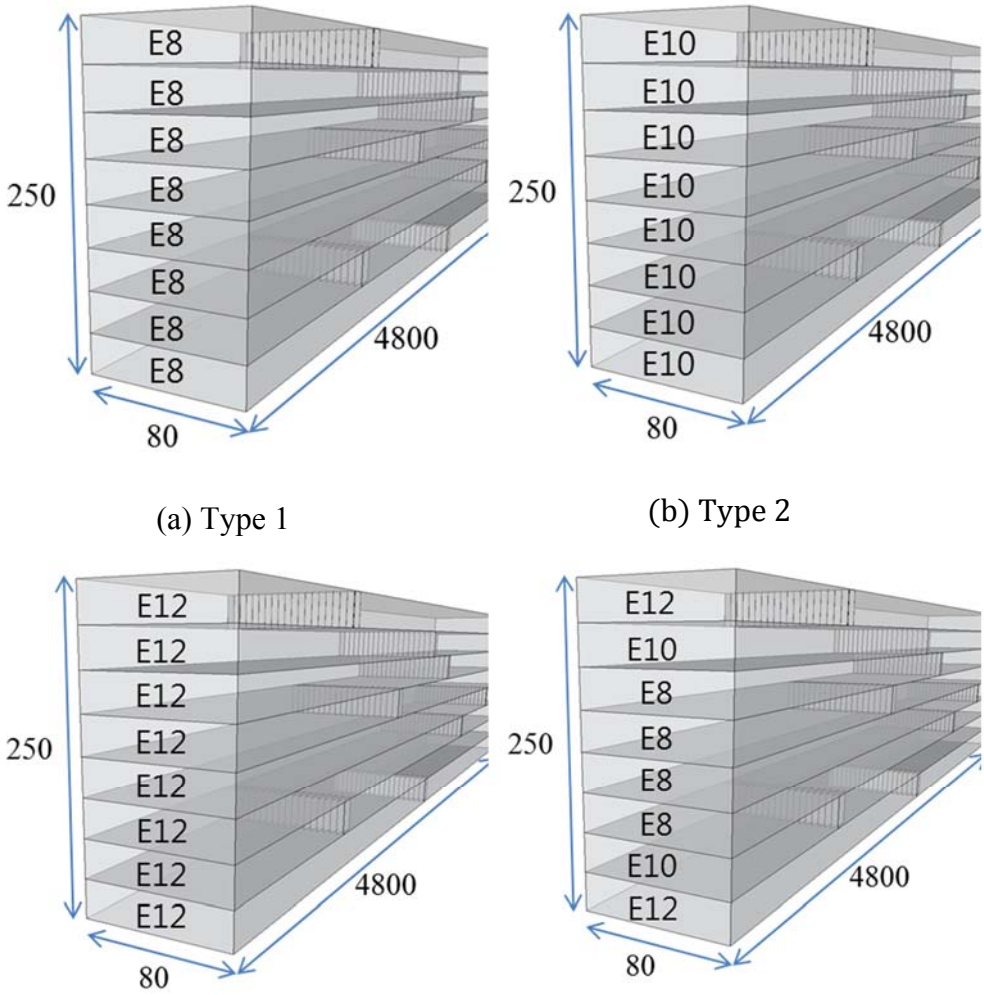

(a) Type 1

(b) Type 2

(C) Type 3

(d) Type 4

Figure 6-7 Lay-up of virtual glulam beams for generating the glulam bending strength distribution

6.4.2 Results and discussion

The reliability analysis implies the determination of the probability that the structural reliability model,$G_{bending}$, is negative (failure). This probability is calculated using the structural reliability model, Eq. (6.13), with Monte Carlo simulation and is related to the reliability index, β, is represented by Eq. (6.14).

$$\beta = \Phi^{-1}(1 - P_f) \tag{6.14}$$

where,

Φ^{-1} = the inverse cumulative distribution function (CDF) of the standard normal distribution.

P_f = the probability of failure, $G_{bending} \leq 0$ in Eq. (6.13)

The reliability index, β, depends on the resistance factor, ∅, and they have negative relationship. In the larger γ, the ratio of design dead load to the design live load, the negative relationship was more great (Figure 6-8). A reliability index β = 3.0 indicates that the probability of failure is approximately 0.001 and is usually used for target reliability index. The ∅ should be chosen to ensure a target reliability index and is usually defined as a single value for representing a material for the convenience of structural

design. In order to determine single ϕ, the β was used at the lowest dead-live load ratio, γ=0.25, since the β was greater in the larger γ (Table 6-6).

When the ϕ was less than 0.9, all of the β was more than 3.0 in Types 1 and 2. In Types 3 and 4, when the ϕ was less than 0.8, all of the β was more than 3.0. Thus, the ϕ = 0.8 is suitable for representing the all simulated glulam beam types.

Table 6-6 Reliability index depending on various resistance factors and dead-live load ratios, γ

	Resistance factor	Reliability index				
		ϒ : 0.25	ϒ : 0.50	ϒ : 1.00	ϒ : 1.50	ϒ : 2.00
Type 1	1.0	2.8	2.9	3.0	3.1	3.1
	0.9	3.2	3.4	3.5	3.7	3.8
	0.8	3.7	3.8	4.0	4.3	
	0.7	4.0	4.3			
Type 2	1.0	2.9	3.0	3.1	3.2	3.3
	0.9	3.3	3.4	3.6	3.9	4.2
	0.8	3.7	3.9	4.2		
	0.7	4.1				
Type 3	1.0	2.5	2.6	2.7	2.8	2.9
	0.9	2.9	3.1	3.3	3.5	3.7
	0.8	3.4	3.6	3.9	4.3	
	0.7	4.0	4.4			
Type 4	1.0	2.4	2.4	2.4	2.3	2.2
	0.9	2.7	2.7	2.7	2.6	2.6
	0.8	3.1	3.1	3.2	3.1	3.1
	0.7	3.5	3.5	3.6	3.6	3.7

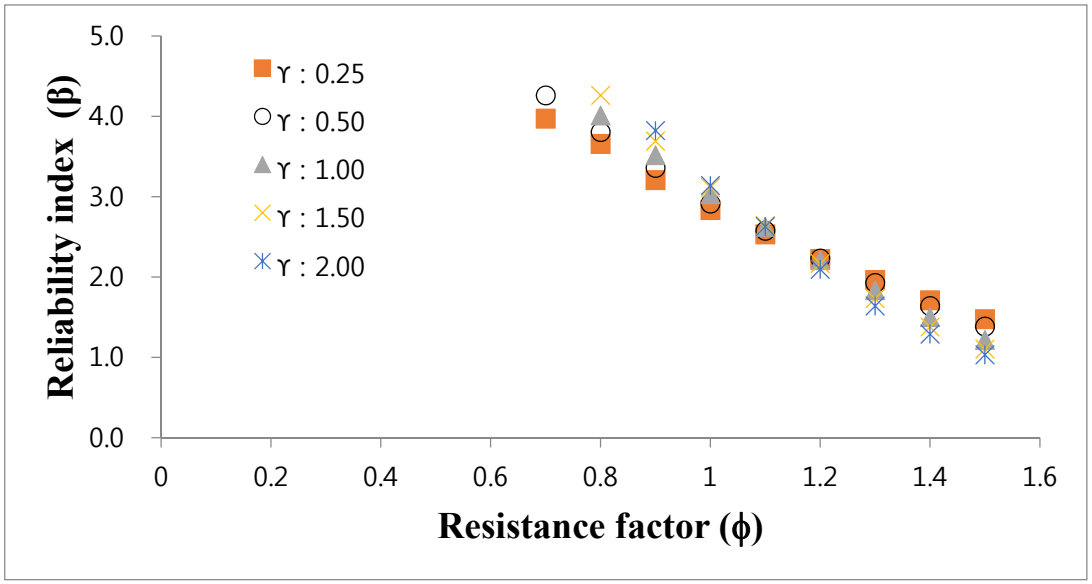

(a) Type 1

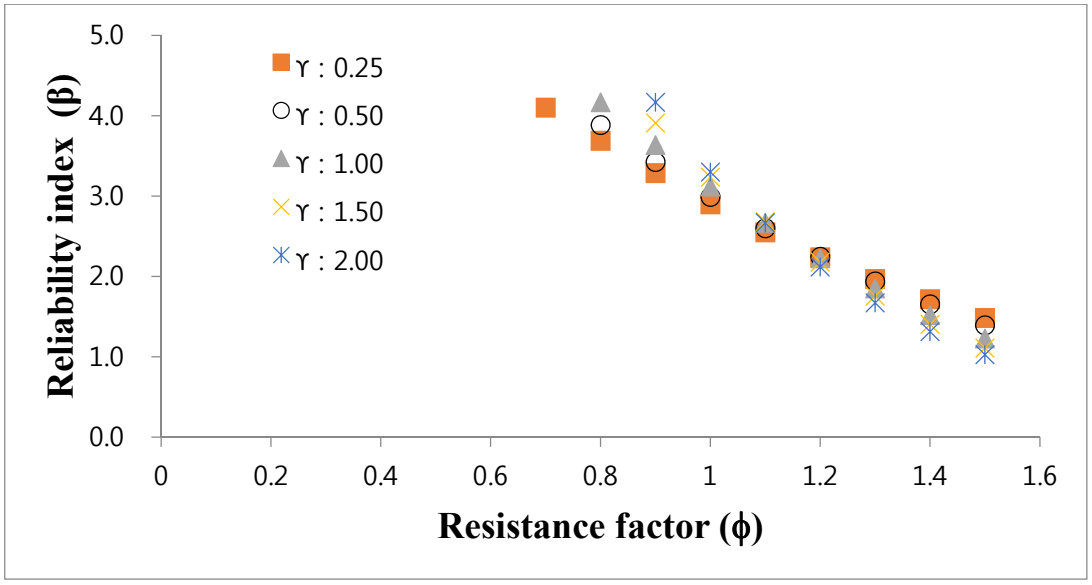

(b) Type 2

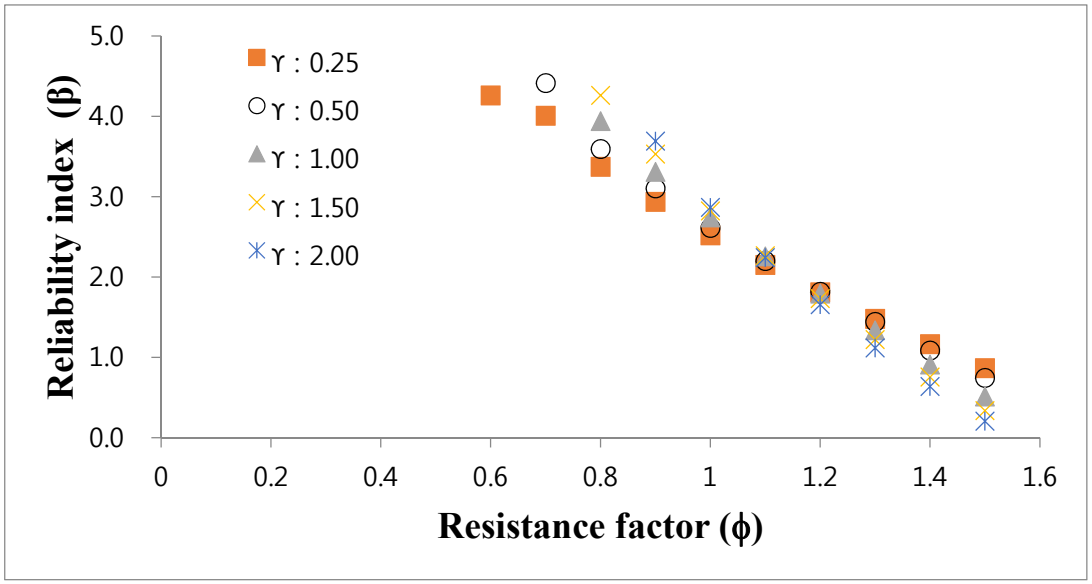

(c) Type 3

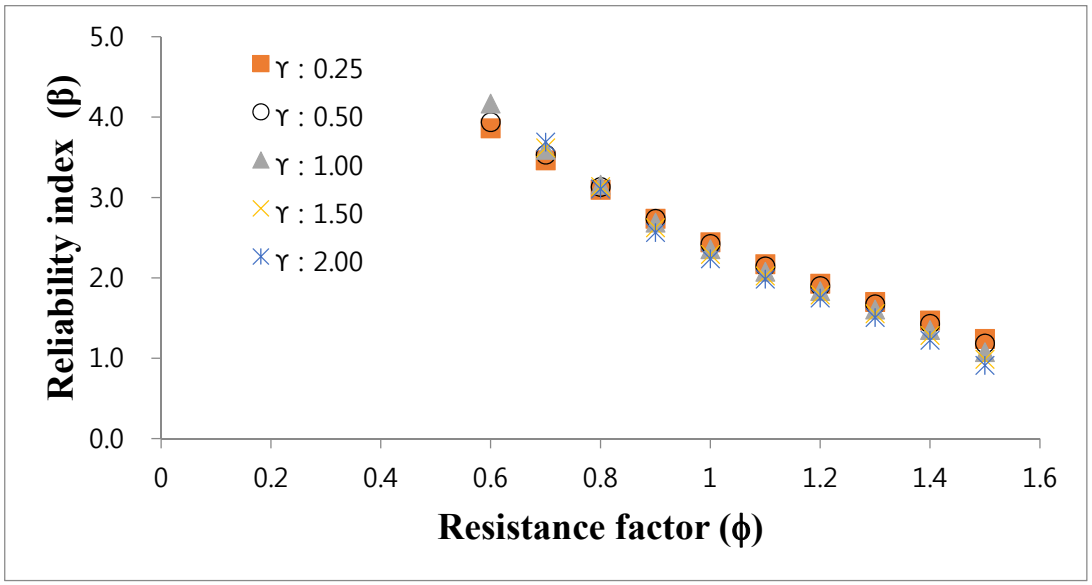

(d) Type 4

Figure 6-8 Relationship between reliability index and resistance factor in various γ, the ratio of design dead load to the design live load

When $\emptyset$ =0.8 and γ=0.25, the β of each glulam Types was different depending on the glulam Types. In order to insure the constant target reliability index, 3.0, regardless of the glulam Types, The 5% PE of all glulam Types should be calibrated. Thus, at $\emptyset$=0.8 and γ=0.25, the reliability indexes were simulated again by changing the 5% PE using Eq. (6.13) so that the β = 3.0. The results show that as the β is decreased which means that the probability of failure is increased, the 5% PE is increased. Especially, the increment of 5% PE was greater in the higher β and the gap of 5% PE became greater between beam Types (Table 6-7).

Table 6-7 Five percent (5%) PE depending on the reliability index

	Before calibration of β		After calibration of β	
	β	5% PE (MPa)	β	5% PE (MPa)
Type 1	3.7	32.11	3.0	38.5
Type 2	3.7	33.16	3.0	39.5
Type 3	3.4	36.13	3.0	42.5
Type 4	3.1	29.06	3.0	32.5

If a glulam beam is consisted with a high tensile strength lamination, the bending strength of the beam should be higher than a beam consisted with a low tensile strength lamination. This phenomenon is observed by comparing Type 1, Type2, and Type3 (Figure 6-9).

If a beam is reinforced by a high tensile strength lamination at the outmost layer, the bending strength of the beam should be higher than that of a beam that a high tensile strength lamination is not placed at the outmost layer. Meanwhile, the lamination grades is determined by the average localized MOE on flatwise lamination and the correlation between the flatwise MOE and tensile strength is low. Thus, actually, the higher grade lamination does not mean that the lamination always has high tensile strength. In other words, the tensile strength of high lamination grades can be equal or lower than that of the low lamination grades (Table 6-8).

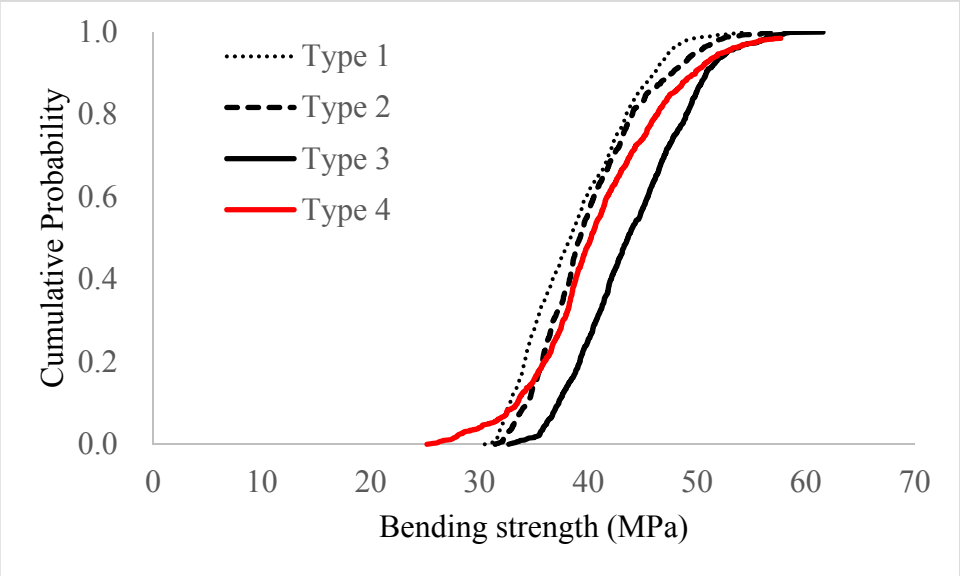

Figure 6-9 Bending strength distribution of 4 types glulam beams

Table 6-8 glulam bending strength ratio depends on tensile strength ratio of lamination grades (MPa)

Tensile strength of lamination			Bending strength of glulam		
E8	E12	Ratio (E12 to E8)	Type 1	Type 2	Ratio (Type 2 to Type 1)
26.50	26.50	1.00	30.29	27.53	0.91
26.50	27.50	1.04	30.29	28.56	0.94
26.50	29.15	1.10	30.29	30.28	1.00
26.50	30.00	1.13	30.29	31.16	1.03
26.50	32.00	1.21	30.29	33.24	1.10

If the increment of tensile strength ($f_{t,i}$) of outmost lamination is not higher than the increment MOE (E_i) of layer, the moment carrying capacity of beam can be decreased as shown in Eq. (6.15) derived from Eq. (3.3).

$$M_{ult,s} = \frac{f_{t,i}}{y_{i,t}} \cdot \frac{E_T I_T}{E_i} \tag{6.15}$$

As a result, the bending strength distribution of Type 4 placed on the right side than that of Type 1, but the lower bending strength was appear in Type 4 rather than Type 1 (Figure 6-9). It shows the possibility of lower bending strength in non-homogeneous glulam beams. If the tensile strength of lamination is not increased as much as the MOE increment of the lamination, the bending strength of glulam beam (Type 2) consisted with high lamination grade (E12) at outmost layer can be lower than that of glulam beam (Type 1) which is not consisted with the high lamination grade (Figure 6-9). In other words, it shows that the glulam bending strength is sensitively governed by the tensile strength than the MOE on lamination. Thus, the tensile strength of lamination should be increased than the MOE of lamination for reinforcing a glulam beam consisted with low lamination grades. In this study, when the tensile strength of E12 grade was at least 10% higher than that of E8 lamination, the glulam bending strength of Type 2 was higher than that of Type 1 (Figure 6-10).

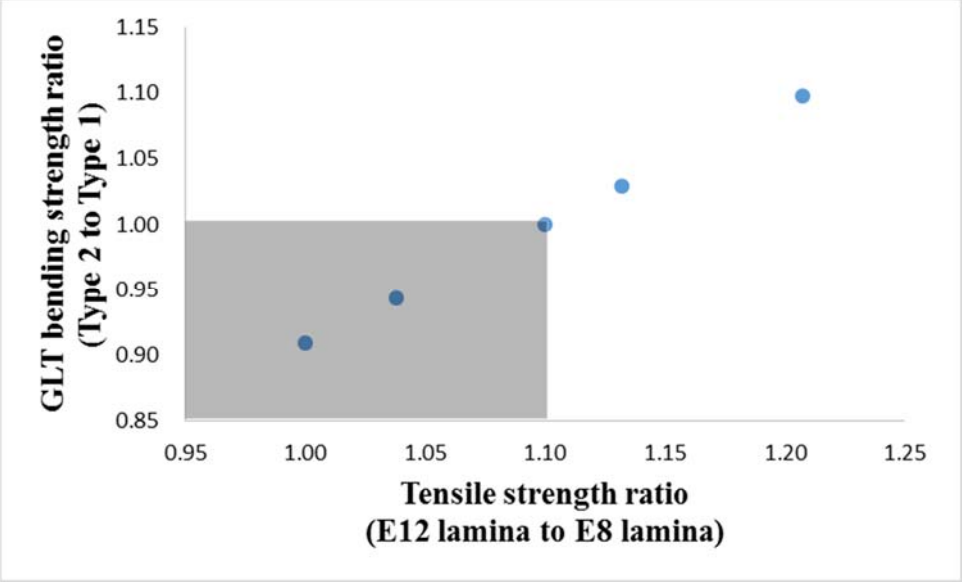

Figure 6-10 Area that glulam bending strength of Type 2 is lower than Type 1

6.4.3 Conclusions

Reliability analysis has been carried out with the domestic load distribution and the simulated glulam bending strength distribution. The reliability indexes for probability of failure have been investigated by changing resistance factors and, herein, the reliability index of four types glulam beams was more than 3.0 at the resistance factor, 0.8.

Since the reliability indexes of four types glulam beams were different, the reliability indexes were adjusted to a target reliability index, 3.0, and the 5% PE were increased after the calibration. The target reliability index, 3.0 (the probability of failure : 1/1000), commonly uses for structural design. Thus, the derived 5% PE has reasonable probability of failure under the domestic load distribution condition.

Chapter 7. Conclusions

The probabilistic glulam model has been developed for predicting the glulam bending strength distribution. Bending strength distributions of 4 types glulam beams have been simulated and validated with actual bending strength distributions derived by destructive tests with full-size glulam beams. The K-S test results shows that the simulated bending strength distributions fit well with actual bending strength distribution. Especially, the difference of 5% PE was approximately 1%.

The developed glulam model reflects non-destructively the lamination longitudinal variation using two machine system, machine stress grader (MSR) and image processing system. Thus, the size effect of CLT can be investigated using the developed glulam model. In this study, the size effect was investigated with the homogeneous virtual glulam beams and the size effect exponent was determined as approximately 16.9.

In case of the finger joints, the empirical tensile strength distributions of finger-joined lamination grades were applied instead of the tensile strength generated by local KAR, local MOE, and Multi regression model. Thus, by controlling the KAR limitation, the influence of finger joint can be

investigated using the developed glulam model. The results show that there is a specified KAR limitation for optimizing the glulam bending strength due to the possibility of that the tensile strength of finger-jointed lamination inserted instead of knots can be lower than the tensile strength generated by KAR. In other words, the phenomenon means that the quality of finger joint is important since the glulam bending strength can be increased as increasing the finger joint strength and reducing the strength variation.

Reliability analysis has been carried out using the domestic load distributions and the simulated glulam bending strength distributions. Reliability indexes of 4 types glulam beams was more than 3.0 at the resistance factor, 0.8. The target reliability index, 3.0 (the probability of failure : 1/1000), commonly uses for structural design. Thus, the derived 5% PE has reasonable probability of failure under the domestic load distribution condition.

The developed model can be used for determining the design value of glulam. The lower 5% PE of strength is used for the design value of glulam and the lower tail distributions of the developed model were fit well.

References

American Forest & Paper Association. 2011, National Design Specification (NDS) for Wood Construction Supplement: Design Values for Wood Construction 2012 Edition.

ASTM D-198, 1994, Standard Methods of Static Tests of Lumber in Structural Sizes.

ASTM D-1990. 2007. Standard practice for establishing allowable properties for visually-graded dimension lumber from in-grade tests of full-size specimens.

ASTM D-2915. 2010. Standard practice for sampling and data-analysis for structural wood and wood-based products.

ASTM D-3737, 2008, Standard practice for establishing allowable properties for structural glued laminated timber (glulam)

Astrup, T., Clorius, C. O., Damkilde, L., & Hoffmeyer, P. 2007, Size effect of glulam beams in tension perpendicular to grain. Wood Science and Technology, 41(4), 361-372.

AS/NZS 4063.2. 2010. Characterization of structural timber part 2: determination of characteristic values.

AF&PA/ASCE 16-96. 1996. Standard for load and resistance factor design (LRFD) for engineered wood construction

Ang, A. H. S., & Cornell, C. A., 1974, Reliability bases of structural safety and design. Journal of the Structural Division, ASCE. vol.100 (9), pp.1755-1769.

Barrett, J. D., Jones, E. D., & Lau, W., 1994. Canadian lumber properties. Canadian Wood Council : p.81

Bender D.A., Woeste F.E., Schaffer E.L., and Marx C.M., 1985, Reliability formulation for the strength and fire endurance of glued laminated beams. Research paper FPL460, Forest Products Laboratory, Madison, WI, USA.

Colling, F, 1990. Bending strength of laminated timber beams in relation to size effect: Development of a statistical model. Holz Roh-Werkst. vol.48, pp.269-273.

Cornell, C. A., 1969, Structural safety specifications based on second-moment reliability analysis. Dept. of civil engineering, Massachusetts Institute of Technology, Cambridge, Mass.

CSA O86-09. 2009. Engineering Design in Wood. Canadian Standards Association, Mississauga, Ontario, Canada.

Ehlbeck J, Colling F, Go¨rlacher R (1985a) Einfluss keilgezinkter Lamellen auf die Biegefestigkeit von Brettschichtholztra¨gern. Eingangsdaten fu¨r das

Rechenmodell [Influence of finger-jointed lamellae on the bending strength of GLT beams. Input data for the computer model; Published in German]. Holz Roh- Werkst 43:369–373

Ehlbeck J, Colling F, Go¨rlacher R (1985b) Einfluss keilgezinkter Lamellen auf die Biegefestigkeit von Brettschichtholztra¨gern. Entwicklung eines Rechenmodells [Influence of finger-jointed lamellae on the bending strength of GLT beams. Development of a computer model; Published in German]. Holz Roh- Werkst 43:333–337

Ehlbeck J, Colling F, Go¨rlacher R (1985c) Einfluss keilgezinkter Lamellen auf die Biegefestigkeit von Brettschichtholztra¨gern. U¨ berpru¨fung des Modells mit Hilfe von Tra¨gerversuchen [Influence of finger-jointed lamellae on the bending strength of GLT beams. Verification of the computer model by bending tests; Published in German]. Holz Roh- Werkst 43:439–442

Ellingwood, B., Galambos, T. V., MacGregor, J. G., and Cornell, C. A., 1980, Development of a probability based load criteria for American National Standard Committee A58, Special Publication No. 577, Nat. Bureau of Standards, Washington, D.C.

Falk, R. H., and Colling, F. 1995, Laminating effects in glued laminated timber beams. Journal of structural engineering, vol.121(12), pp.1857-1863.

Falk, R. H., Solli, K. H., and Aasheim, E. 1992, The performance of glued laminated beams manufactured from machine stress graded Norwegian spruce. Rep. no. 77, Norwegian Institute of Wood Technology, Oslo, Norway.

Folz, B. and Foschi, R.O. 1992. Stochastic finite element analysis of laminated beams. Annual Conference of the Canadian Society for Civil Engineering, Quebec, May 27-29.

Folz, B. and Foschi, R.O. 1993. ULAG: Ultimate load analysis of glulam-user's manual. Version 1.0, Department of Civil Engineering, The University of British Columbia, Vancouver, Canada. 23p.

Folz, B. and Foschi, R.O. 1994. Stochastic finite element analysis of progressive failure in a laminated wood beam, in: Schueller, Shinozuka, Yao (Eds.), International Conference on Structural Safety and Reliability, ICOSSAR 93, Balkema, Rotterdam, 1994. pp.585-592.

Folz, B.R. 1997. Stochastic finite element analysis of the load-carrying capacity of laminated wood Beam-Columns. Ph.D. Thesis, The University of British Columbia, Vancouver, Canada.

Foschi, R. O. and Barrett, J.D. 1980. Glued laminated Beam Strength: A Model. Journal of the Structural Division, ASCE, 106(ST8), pp.1735-1754.

Foschi, R. O., Folz, B. and Yao, F.Z., 1989. Reliability-based design of wood structures. Structural Research Series, Report No. 34, Department of Civil Engineering, The University of British Columbia, Vancouver, Canada.

Forest Products Society, 1997. Machine-graded lumber. Madison, WI: Forest Products Society. Wood Design Focus. 8(2) : 1-24

Freas, A. D., & Selbo, M. L., 1954. Fabrication and design of glued laminated wood structural members. Technical Bulletin No. 1069, USDA Forest Service, Forest Products Laboratory, Madison, WI

Frese, M., Chen, Y., and Blaß, H. J., 2010. Tensile strength of spruce glulam. European Journal of Wood and Wood Products, vol.68(3), pp.257-265.

Freudenthal, A.M. 1947. Safety of structures, Transactions, ASCE, vol.112 (1), pp.125–159

Glos, P.; Heimeshoff, B. 1982: Möglichkeiten und Grenzen der Festigkeitssortierung von Brettlamellen für den Holzleimbau. In: Ingenieurholzbau in Forschung und Praxis. Bruderverlag Karlsruhe: 41–47

Haldar, A., and Mahadevan, S., 2000, Probability, reliability, and statistical methods in engineering design. John Wiley & Sons, New York, NY

Hasofer, A. M., & Lind, N. C., 1974, Exact and invariant second-moment code format. Journal of the Engineering Mechanics Division, ASCE. vol.100 (1), pp.111-121.

Hernandez, R., Bender, D.A., Richbur, B.A. and Kline, K.S. 1992. Probabilistic modeling of glued laminated timber beams. Wood and Fiber

Science, The Society of Wood Science and Technology, vol.24(3) pp.294-306.

Huh, J., & Haldar, A., 2001, Stochastic finite-element-based seismic risk of nonlinear structures. Journal of structural engineering, vol.127(3), pp.323-329.

ISO 13910. 2005. Structural timber – characteristic values of strength-graded timber – sampling, full-size testing and evaluation.

Jang, S. J. 2010 Calibration of Resistance Factors of Load and Resistance Factor Design for Drilled Shafts Embedded in Weathered Rock. Ph.D. Thesis, Seoul National University, Seoul, Korea.

Johansson C. J., 1990, Strength and stiffness of glulam with laminations of machine stress graded timber, SP RAPPORT 1990:22. Swedish National Testing and Research Institute, Sweden

Johansson, C. J. 2003. Grading of timber with respect to mechanical properties. In timber engineering, pp.29

Kim, B. N., Lee, H. W., Kim. K. M. 2009, The Development of Image Processing System Using Area Camera for Feeding Lumber, Journal of the Korean wood science and technology, vol.37(1), pp.37-47

Kim, B. N., Kim, K. M., Shim. K. B., Lee, H. W., Shim, S. R. 2009, The Verification of Image Merging for Lumber Scanning System, Journal of the Korean wood science and technology, vol.37(6), pp.556-565

Kim, G. C., Lee, J. J. 2000, Effects of Finger Joint and Strength of Lamination on the Estimation of Strength Properties of Glulam, Journal of the Korean wood science and technology, vol.28(1), pp.8-17

Kim, G. C. 2009, A basic research for the probability based design of wood structures, Journal of the Korea furniture society, vol.20(4), pp.339-357

Kim, J. S., Kim, J. H., 2011, Calibration of Load and Resistance Factors in KCI Code Based on Domestic Data, Journal of the Korea concrete institute, vol.23(4), pp.495-501

Kim, J. S., Kim, J. H., 2011, Calibration of Load and Resistance Factors in KCI Code Based on Domestic Data, Journal of the Korea concrete institute, vol.23(4), pp.495-501

Korea Institute of Civil Engineering and Building Technology (KICT). 1989, Reliability evaluation of structures : a case of reinforced concrete buildings under dead, live, and wind loads

Larsen, H. J., 1982, Strength of glued laminated beams. Part 5. Report no. 8201, Institute of Building Technology and Structural Engineering, Aalborg Univertity, Aalborg, Denmark.

Lee, J. J., Park, J. S., Kim. K. M., Oh, J. K., 2005, Prediction of bending properties for structural glulam using optimized distributions of knot characteristics and laminar MOE, Journal of wood science vol.51, pp.640-647

Lee, J. J., Kim, G. C., Kim, K. M., Oh, J. K., 2003. Distribution characteristics of bending properties for visual graded lumber of Japanese larch. Journal of the Korean wood science and technology, vol.31(5) pp.72-79.

Lee, J. J., Kim, G. C., Kim, K. M., Oh, J. K., 2003. Distribution characteristics of bending properties for visual graded lumber of Japanese larch. Journal of the Korean wood science and technology, vol.31(5) pp.72-79.

Lee, S. H. 2014 Calibration of the load-resistance factors for the reliability-based design of cable-supported bridges. Ph.D. Thesis, Seoul National University, Seoul, Korea.

Lim, J. A., Oh, J. K., Yeo, H. M., Lee, J. J., 2010. Feasibility of Domestic Yellow Poplar (Liriodendron tulipifera) Dimension Lumber for Structural Uses. Journal of the Korean wood science and technology, vol.38(6) pp.470-479.

Madsen, B., & Buchanan, A. H. 1986. Size effects in timber explained by a modified weakest link theory. Canadian Journal of Civil Engineering, vol.13(2), pp.218-232.

Mihashi, H., Itagaki, N. 1998. Probabilistic design of performance in glued laminated timber. In PROBAMAT-21st Century: Probabilities and Materials, pp.333-345

Moody, R., Falk, R., & Williamson, T., 1990, Strength of glulam beams-size effects. In Proceedings of the 1990 International Timber Engineering Conference, vol.1, pp.176-182

Nakamura, N., and Fujita, K., 2011, Simulation method to generate the strength of glulam using correlated random variables. Journal of wood science, vol.57(3), pp.203-207.

Oh, C. Y. 1995. Assignment of the allowable design values for domestic softwood structural lumber _Structural 1-grade_. Journal of the Korean wood science and technology, vol.24(1) pp.11-16.

Oh, J. K., Kim, K. M., Lee, J. J. 2010. Use of Adjacent Knot Data in Predicting Bending Strength of Dimension Lumber by X-Ray. Wood and Fiber Science vol.24(1) pp.10-20.

Oh, S. C., Park, M., J., Shim, K., 1993, Stress grading of domestic softwood 2x4 lumber, Journal of the Korea furniture society, vol.4(1), pp.8-13.

Pang, S. J., Oh, J. K., Park, C. Y., Park, J. S., Park, M. J., Lee, J. J., 2011, Characteristic Evaluation of Bending Strength Distributions on Revised Korean Visual Grading Rule, Journal of the Korean wood science and technology, vol.39(1) pp.1-7

Pang, S. J., Park, J. S., Hwang, K. H., Jeong, G. Y., Park, M. J., Lee, J. J., 2011, Bending Strength of Korean Softwood Species for 120 x 180 mm Structural

Members, Journal of the Korean wood science and technology, vol.39(5) pp.444-450

Pang, S. J., Oh, J. K., Park, C. Y., Kim, C. K., Kim, H. K., Lee, J. J., Park, J. S., Park, M. J., 2012, Bending Strength Distributions and LRFD Code Conversion of Korean Softwood Species, International Conference on Biobase Material Science and Engineering (BMSE) 2012, pp.311-315

Pang, S. J., Lee, J. J., Oh, J. K., 2013a, Effect of test zone selection for evaluating bending strength of lumber, Journal of the Korean wood science and technology vol.41(5) pp.392-398

Pang, S. J., Lee, J. J., Oh, J. K., 2013b, Evaluation of Allowable Bending Stress of Dimension Lumber; Confidence Levels and Size-adjustment, Journal of the Korean wood science and technology, vol.41(5) pp.432-439

Park, C. Y., Kim, H. K. and Lee, J. J. 2004. Study on soft conversion from ASD to RBD code in larch. Journal of the Korean wood science and technology, vol.23(5) pp.45-50.

Park, C. Y., Pang, S. J., Park, J. S., Kim, K. M., Park, M. J. and Lee, J. J. 2010. Study of the distribution properties and LRFD code conversion in Japanese larch. Mokchae Konghak vol.38(2) pp.94-100.

Park, M. J., Kim, G. C. 2009, Methods for wooden structural design _ A comparative research between deterministic design and probability based design, Journal of the Korea furniture society, vol.20(4), pp.358-373

Park, J. H. 2011 Resistance factor calibration and bayesian implementation for LRFD of axially-loaded driven steel pipe piles. Ph.D. Thesis, Seoul National University, Seoul, Korea.

Pugsley, A. 1955. Report on structural safety, Structural engineer, vol.33(5), pp.141–149

Rackwitz, R., & Flessler, B., 1978, Structural reliability under combined random load sequences. Computers & Structures, vol.9(5), pp.489-494.

Renaudin, P. 1997. Approche probabiliste du comportement mecanique du bois de structure, prise en compte de la variabilite biologique. Doctoral thesis, LMT, ENS Cachan, Paris, France

Samson, M., and Blanchet, L. 1992. Effect of knots on the flatwise bending stiffness of lumber members. Holz als Roh-und Werkstoff, 50(4), 148-152.

Serrano, E. 2003. Mechanical performance and modelling of glulam. In timber engineering, pp.67-79

Serrano, E., Gustafsson, J., and Larsen, H. J. 2001. Modeling of finger-joint failure in glued laminated timber beams. Journal of Structural Engineering, vol.127(8), pp.914-921.

Serrano, E., and Larsen, H. J. 1999. Numerical investigations of the laminating effect in laminated beams. Journal of Structural Engineering, vol.125(7), pp.740-745.

Shin, D. K., Kim, C. Y., Rho, J. S., and Park, Y. S. 2007. Flexural Resistance Statistics of Composite Plate Girders, Journal of Korean Society of Steel Construction, vol.19(2) pp.139-146.

Smulski, S., 1997. Engineered Wood Products: A guide for specifiers, designers and users. PFS Research Foundation.

Weibull W., 1939. A statistical theory of the strength of materials. Nr. 151, Proc. Royal Swedish Institute for Engineering Research, Stockholm, Sweden.

Wen, Y. K., 2001. Reliability and performance-based design. Structural safety, vol.23(4), pp.407-428.

West Coast Lumber Inspection Bureau, 2004. Tension/Bending Ratios of Machine Stress-rated Lumber. Technical Report No. 2 : p.8

초 록

본 논문에서는 여러 개의 층재를 접착시켜 제조되는 구조용집성재를 대상으로 한계상태설계를 위해 요구되는 휨강도분포를 도출하고, 도출된 휨강도분포와 국내 하중분포를 사용하여 집성재 보의 신뢰성해석을 수행하였다. 특히, 실험적 평가를 통한 집성재의 강도분포 도출은 층재의 치수, 등급, 크기, 조합의 다양성으로 인한 한계가 있기 때문에 집성재의 휨강도성능을 예측할 수 있는 모델을 개발하고 검증하였다.

본 연구에서 개발한 집성재 휨강도 예측 모델은 층재의 생장특성(길이방향 변이)과 가공특성(핑거조인트)를 반영하고, 층재의 기준조건 변화에 따른 집성재의 휨강도 변화 추이를 검토할 수 있도록 개발하였다. 예를 들어, 층재의 길이방향 MOE 와 옹이면적비(Knot Area Ratio, KAR)가 기본입력변수로 사용되기 때문에, 특정 KAR 이상의 옹이를 제거하고 핑거조인트로 연결함으로써 야기되는 집성재의 휨강도 변화를 검토할 수 있다. 또한, 층재의 길이방향 MOE 와 KAR 이 입력변수로 사용되기 때문에 입력되는 층재의 길이가 늘어나면 weak zone 이 포함될 가능성이 높아진다. 이는 집성재의 크기가 커지면 강도가 감소하는 치수효과(size effect)를 검토할 수 있음을 의미한다.

본 모델의 입력변수는 구간의 MOE (localized MOE), 구간의 KAR (localized KAR), 핑거조인트의 인장강도이다. 기본입력변수인 길이방향 MOE, KAR 은 각각 기계등급구분기기(MSR machine)와 화상이미지 분석기기를 이용하여 측정하였다. MOE 와 KAR 로 인장강도를 예측하기 위한 다변량회귀모델을 개발하였으며, 이 모델로 각 층재의 구간 MOE 와 구간 KAR 을 구간의

인장강도로 전환하였다. 핑거조인트 인장강도의 경우, 인장강도가 높아 그립에서 파괴되는 시험편은 핑거조인트의 실제 인장강도를 적절히 반영하지 못한다. 따라서 핑거조인트의 인장강도는 실대재 인장강도의 하위 15% 분포를 사용하였다.

각 등급별로 구축된 입력변수 데이터베이스와 집성재 휨강도 예측 모델로 도출한 집성재 휨강도분포의 적합도를 검증하고자, 개발된 집성재 휨강도 예측 모델로 4 종류의 집성재(무핑거집성재, 핑거조인트가 포함된 집성재, 다른 크기의 집성재, 다른 등급의 집성재)에 대하여 각각의 휨강도분포를 도출하였다. 그리고 4 종류의 집성재에 대한 각각의 검증용 실대재 집성재를 30 개씩 제작한 후 휨파괴실험을 수행하여 휨강도분포를 도출하였다. 예측과 실험에 의한 휨강도 분포간의 적합도를 평가하고자 Kolmogorov-Smirnov test 를 수행한 결과, 4 종류의 휨강도분포 모두 1% 유의수준에서 적합한 것으로 나타났고, 5%하한치의 오차는 약 1%였다.

예측된 휨강도분포와 실험에 의한 휨강도분포의 높은 적합도는 예측된 휨강도분포가 구축된 데이터베이스의 층재로 제작하는 집성재의 휨강도분포를 잘 반영하고 있음을 의미한다. 왜냐하면, 구축된 입력변수 데이터베이스에서 무작위로 추출된 층재의 구간 MOE 와 KAR 정보로 집성재의 휨강도를 예측하였고, 입력변수의 데이터베이스 구축에 사용된 층재 중 일부를 무작위로 추출하여 검증용 집성재를 제작하였기 때문이다. 또한, 이것은 만약 입력변수 데이터베이스가 해당 수종 및 층재의 모집단을 잘 반영한다면, 예측된 집성재의 휨강도분포가 해당 수종 및 층재로 제작한 집성재의 휨강도분포를 매우 정확하게 반영할 수 있음을 의미한다.

다른 등급으로 구성되는 집성재는 집성재의 크기 증가에 의한 강도감소뿐만 아니라 추가되는 층재 등급의 MOE 및 인장강도가 집성재의 휨강도에 영향하기 때문에 분석이 난해하다. 그래서 같은 등급(E8)으로 구성된 집성재를 대상으로 층재의 개수가 늘어남에 따른 치수효과지수(size effect exponent)의 변화 추이를 검토하였다. 개발된 휨강도 예측 모델을 통해 보의 크기가 커짐에 따라 집성재 휨강도분포의 변이가 줄어들고, 5% 하한치 또한 작아짐이 확인되었다. 이는 집성재의 크기가 커짐에 따라 weak zone 이 포함될 가능성이 커짐을 의미하고, 본 모델이 weakest link theory 에 의한 치수효과를 잘 반영하고 있음을 의미한다. 본 연구에서 도출된 치수효과지수는 약 16.9 이다.

개발된 집성재 예측 모델로 특정 KAR 이상의 옹이를 제거하고 핑거조인트로 연결함으로써 야기되는 집성재의 휨강도 변화를 조사한 결과는 다음과 같다. KAR 0.25 이상인 옹이를 제거하고 핑거로 연결할 때, 집성재의 휨강도 분포가 가장 높게 나타났고, KAR 0.33 이상인 옹이를 제거하고 핑거로 연결할 때, 집성재의 5%하한치가 가장 높게 나타났다. 이는 집성재의 휨성능을 극대화하기 위해 제거되어야 할 특정크기의 옹이가 존재함을 의미한다. 본 예측 모델에서는 층재의 인장강도로 집성재의 휨강도를 예측하기 때문에 이러한 현상이 일어나는 이유는 다음과 같다. 옹이에 의한 강도손실이 큰 경우에는 핑거조인트의 인장강도가 무핑거층재의 인장강도보다 높지만, 옹이에 의한 강도손실이 작을 경우는 핑거조인트의 인장강도가 무핑거층재의 인장강도 보다 오히려 작아지게 된다. 그러므로 집성재의 휨성능을 극대화하기 위해 제거되어야 하는 옹이가 존재하게 된다. 한편, 이는 무핑거 층재와

핑거조인트의 인장강도 차이에 의해 발생하므로, 핑거조인트의 품질관리가 중요함을 의미한다.

국내외에서 보편화된 설계법으로 인식되고 있는 한계상태설계법은 하중분포와 저항분포에 대한 신뢰성 분석을 기반으로 한다. 특히, 타 건설재료에 비해 큰 강도 변이를 가지는 목재의 경우, 신뢰성 분석을 통한 구조적 안전성 확보가 더욱 요구된다. 본 연구에서는 국내하중분포와 집성재 휨강도 예측모델로 도출한 집성재의 휨강도분포를 사용하여 집성재 보의 신뢰성분석(파괴확률)을 수행하였다. 그 결과, 저항계수로 0.8 을 사용할 때, 분석에 사용된 모든 집성재 보의 신뢰성지수가 구조물의 보편적인 신뢰성지수로 적용하고 있는 3.0 이상인 것으로 나타났다. 이는 국내하중분포조건에서 집성재 보의 파괴확률이 약 1/1000 이하임을 의미한다.

Appendix

For calculating knot area in cross-section automatically, the type of global knot was determined according to the surface including knots (Table X-1). The types of knot were classified by ASTM D3737 (Figure X-1).

Table X-1 Classification of knot according to the surface including knots

No.	Surface					Type		
	Top	Side1	Bottom	Side2	Pith			
1	0				0	7a		
2		0			0	7a		
3			0		0	7a		
4				0	0	7a		
5	0		0			1		
6		0		0		5		
7	0	0			7b	4	9(TiYe=w)	7b
8	0			0	7b	4	9(TiYs=0)	7b
9		0	0		7b	4	9(BiYs=0)	7b
10			0	0	7b	4	9(BiYe=w)	7b
11	0	0	0			2(TiYe=w, BiYs=0)	3	5(TiYs=0, TiYe=w)
12	0		0	0		2(TiYs=0, BiYe=w)	3	5(BiYs=0, BiYe=w)
13	0	0	0	0		6(TiYs=0)	6(TiYe=w)	

0: Presence of knot on a surface

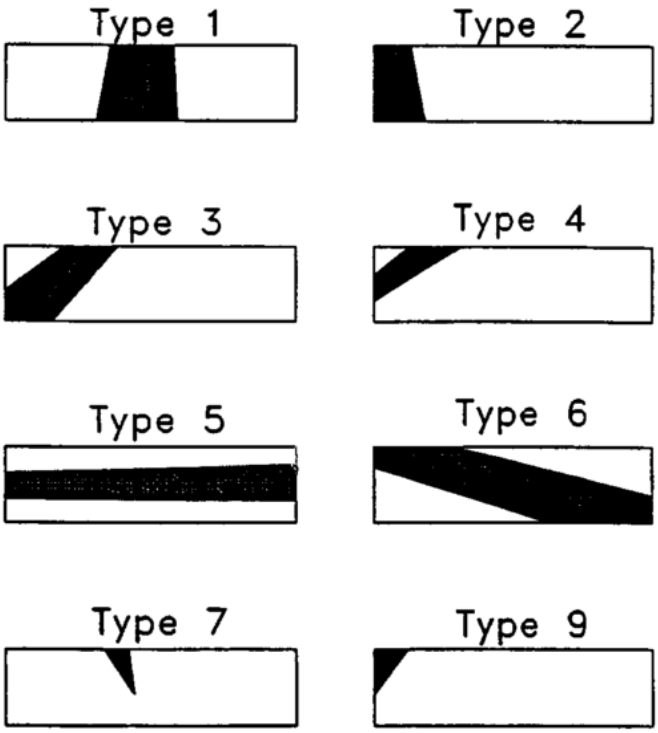

Figure X-1 Types of knot area ratio depending on the appearances on surface (adopted from ASTM D3737)

In each knot, the lengthwise position of knot (Knot X) was calculated with X-coordinates (*xS*, *xE*, Figure 4-9). The knot area ratio of each knot was calculated with crosswise grain (widthwise and thickwise) position of knot (*yS*, *yE*, Figure 4-9). The detailed calculation of knot type is as follow.

1) Type 1

KAR = ((Top_yE - Top_yS) + (Bottom_yE - Bottom_yS))/(2×w)

Knot_x = (Top_xS + Top_xE + Bottom_xS + Bottom_xE)/4

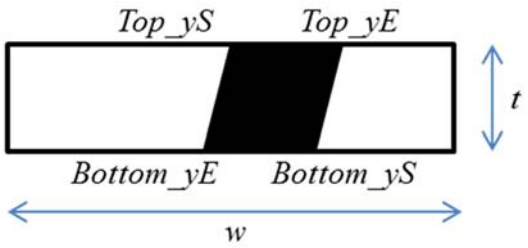

Figure X-2 Knot area ratio of Type 1

2) Type 2

KAR = ((Top_yE - Top_yS) + (Bottom_yE - Bottom_yS))/(2×w)

Knot_x = (Top_xS + Top_xE + Bottom_xS + Bottom_xE)/4;

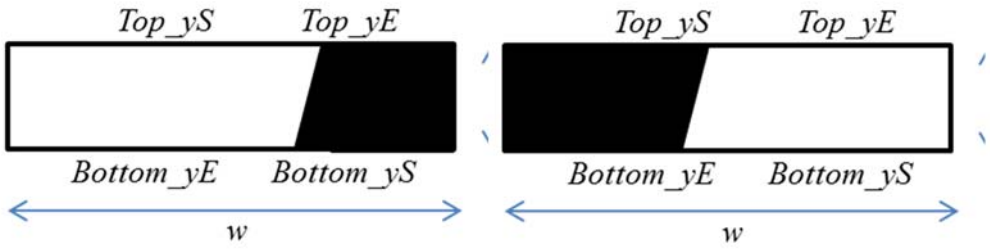

Figure X-3 Knot area ratio of Type 2

3) Type3

(a)

KAR = ((Top_yE - Top_yS)×Side1_yS/2 + (Bottom_yE - Bottom_yS)×t/2 + (Side1_yE-Side1_yS)×(w - Top_yS)/2)/(w×t)

Knot_x = (Top_xS + Top_xE + Bottom_xS + Bottom_xE + Side2_xS + Side2_xE)/6

(b)

KAR = ((Top_yE - Top_yS)×t/2 + (Bottom_yE - Bottom_yS)×t/2 + (Side1_yE-Side1_yS)×Bottom_yS/2)/(w×t)

Knot_x = (Top_xS + Top_xE + Bottom_xS + Bottom_xE + Side1_xS + Side1_xE)/6

(c)

KAR = ((Top_yE - Top_yS)×t/2 + (Bottom_yE - Bottom_yS)×t/2 + (Side2_yE-Side2_yS)×Top_yS/2)/(w×t)

Knot_x = (Top_xS + Top_xE + Bottom_xS + Bottom_xE + Side2_xS + Side2_xE)/6

(d)

KAR = ((Top_yE - Top_yS)×t/2 + (Bottom_yE - Bottom_yS)×Side2_yS/2 + (Side2_yE-Side2_yS)×(w-Bottom_yS)/2)/(w×t)

Knot_x = (Top_xS + Top_xE + Bottom_xS + Bottom_xE + Side2_xS + Side2_xE)/6

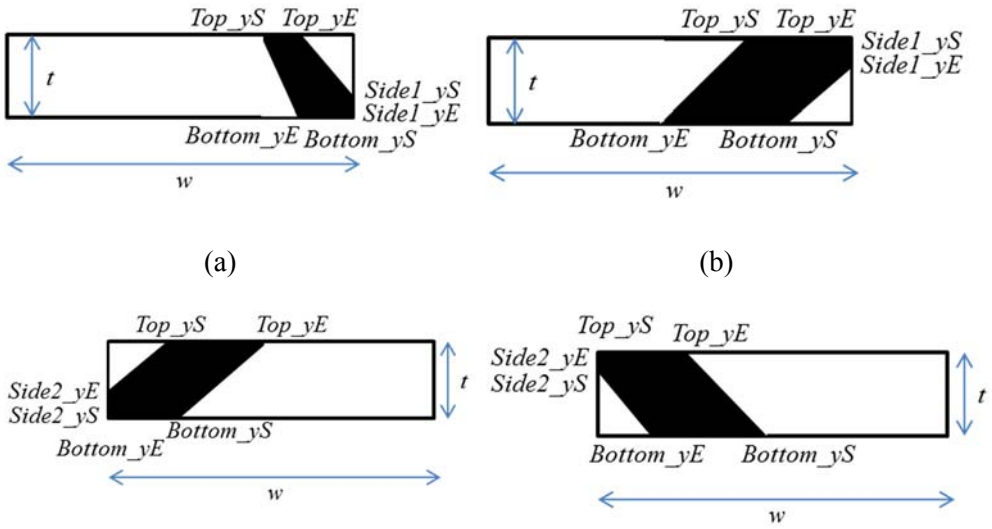

Figure X-4 Knot area ratio of Type 3

4) Type4

(a)

KAR = ((Top_yE - Top_yS)×(t-Side2_yS)/2 + ((Side2_yE-Side2_yS)×Top_yS/2))/(w×t)

Knot_x = (Top_xS + Top_xE + Side2_xS + Side2_xE)/4

(b)

KAR = ((Top_yE - Top_yS)×Side1_yS/2+(Side1_yE-Side1_yS)×(w-Top_yS)/2)/(w×t)

Knot_x = (Top_xS + Top_xE + Side1_xS + Side1_xE)/4

(c)

KAR = ((Bottom_yE - Bottom_yS)×Side2_yS/2 + (Side2_yE - Side2_yS) × (w-Bottom_yS)/2) / (w×t)

Knot_x = (Bottom_xS + Bottom_xE + Side2_xS + Side2_xE)/4

(d)

KAR = ((Bottom_yE - Bottom_yS) × (t-Side1_yS)/2 + (Side1_yE-Side1_yS) × Bottom_yS/2) / (w×t)

Knot_x = (Bottom_xS + Bottom_xE + Side1_xS + Side1_xE)/4

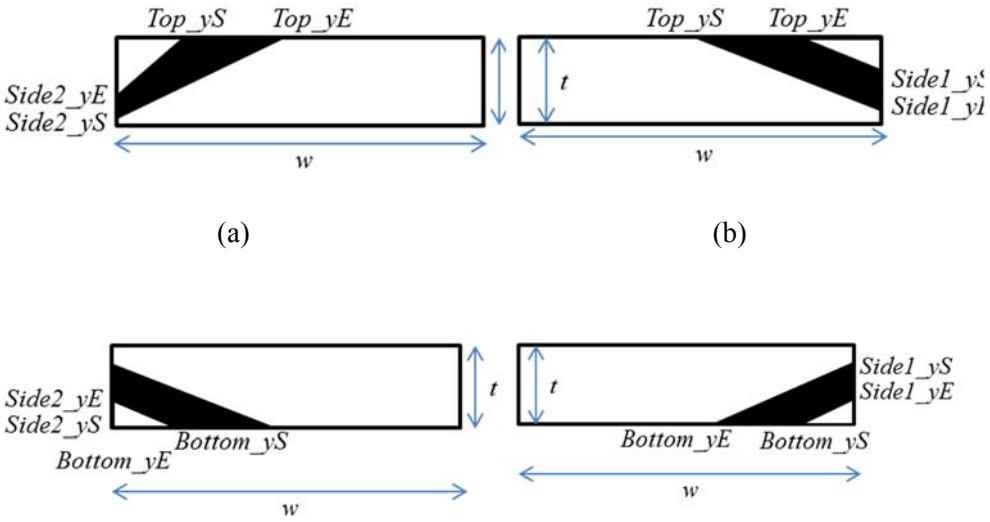

Figure X-5 Knot area ratio of Type 4

5) Type5

KAR = ((Side1_yE - Side1_yS) + (Side2_yE - Side2_yS))/(2×t)

Knot_x = (Side1_xS + Side1_xE + Side2_xS + Side2_xE)/4

(a)

(b)

(c)

Figure X-6 Knot area ratio of Type 5

6) Type6

(a)

KAR = ((Top_yE - Top_yS)×Side1_yS/2 + (Bottom_yE - Bottom_yS)×Side2_yS/2 + (Side1_yE-Side1_yS)×w/2 + (Side2_yE - Side2_yS)×w/2)/(w×t)

Knot_x = (Top_xS + Top_xE + Bottom_xS + Bottom_xE + Side1_xS + Side1_xE + Side2_xS + Side2_xE)/8

(b)

KAR = ((Top_yE - Top_yS)×t/2 + (Bottom_yE - Bottom_yS)×t/2 + (Side1_yE-Side1_yS)×Bottom_yS/2 + (Side2_yE - Side2_yS)×Top_yS/2)/(w×t)

Knot_x = (Top_xS + Top_xE + Bottom_xS + Bottom_xE + Side1_xS + Side1_xE + Side2_xS + Side2_xE)/8;

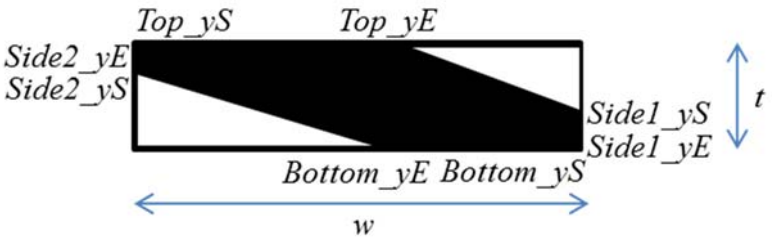

(a)

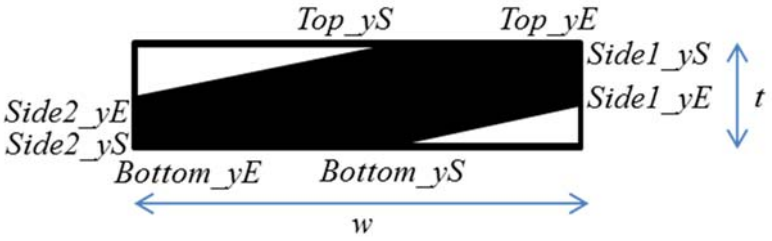

(b)

Figure X-7 Knot area ratio of Type 6

7) Type 7

(a)

KAR = ((Top_yE - Top_yS)×(t-P1)/2)/(w×t)

Knot_x = (Top_xS + Top_xE)/2

(b)

KAR = ((Bottom_yE- Bottom_yS)×(P1)/2)/(w×t)

Knot_x = (Bottom_xS + Bottom_xE)/2

(c)

KAR = ((Side2_yE - Side2_yS) × P2/2)/(w×t)

Knot_x = (Side2_xS + Side2_xE)/2

(d)

KAR = ((Side1_yE - Side1_yS) × (w-P2)/2)/(w×t)

Knot_x = (Side1_xS + Side1_xE)/2

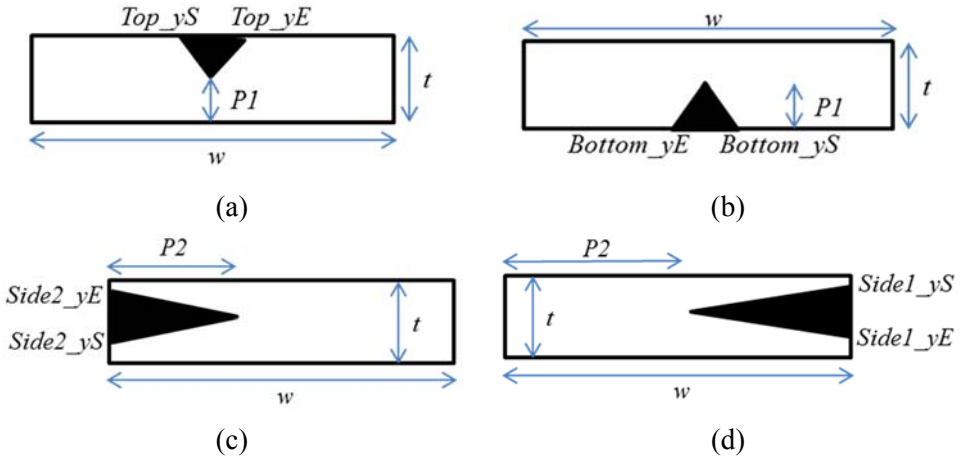

Figure X-8 Knot area ratio of Type 7(1)

(e)

KAR = ((Top_yE-Top_yS)×(t-P1)/2 + (Side2_yE-Side2_yS)×P2/2)/(w×t)

Knot_x = (Top_xS + Top_xE + Side2_xS + Side2_xE)/4

(f)

KAR = ((Top_yE-Top_yS)×(t-P1)/2 + (Side1_yE-Side1_yS) × (w-P2)/2)/(w×t)

Knot_x = (Top_xS + Top_xE + Side1_xS + Side1_xE)/4

(g)

KAR = ((Bottom_yE - Bottom_yS) × (P1)/2 + (Side2_yE-Side2_yS)×P2/2)/(w×t)

Knot_x = (Bottom_xS + Bottom_xE + Side2_xS + Side2_xE)/4

(h)

KAR = ((Side1_yE - Side1_yS) × (w-P2)/2 + (Bottom_yE-Bottom_yS) × P1/2)/(w×t)

Knot_x = (Bottom_xS + Bottom_xE + Side1_xS + Side1_xE)/4

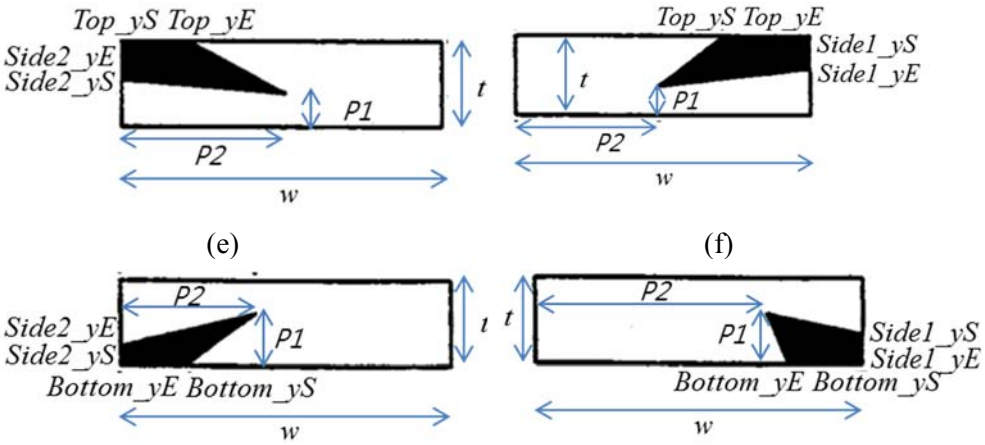

Figure X-9 Knot area ratio of Type 7(2)

8) Type 9

(a)

KAR = ((Top_yE - Top_yS) × (Side2_yE - Side2_yS))/(2×w×t)

Knot_x = (Top_xS + Top_xE + Side2_xS + Side2_xE)/4

(b)

KAR = ((Top_yE - Top_yS) × (Side1_yE - Side1_yS))/(2×w×t)

Knot_x = (Top_xS + Top_xE + Side1_xS + Side1_xE)/4

(c)

KAR = ((Bottom_yE - Bottom_yS) × (Side2_yE - Side2_yS))/(2×w×t)

Knot_x = (Bottom_xS + Bottom_xE + Side2_xS + Side2_xE)/4

(d)

KAR = ((Bottom_yE - Bottom_yS) × (Side1_yE - Side1_yS))/(2×w×t)

Knot_x = (Bottom_xS + Bottom_xE + Side1_xS + Side1_xE)/4

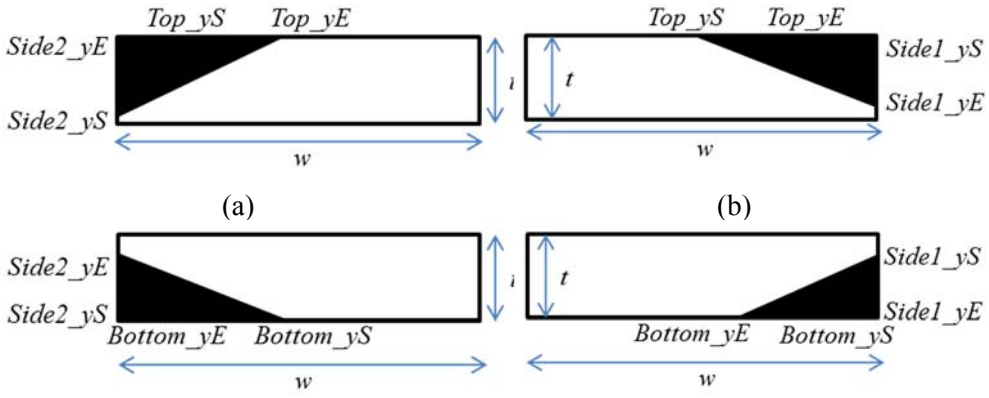

Figure X-10 Knot area ratio of Type 9

9) Pith position

If pith presents on the end of cross-section, the pith position was recorded by three-dimensional coordinates (Figure X-11). A pith position within lamination was calculated with the recorded two point (Pith_Start, Pith_End in Figure X-11). If a Line *l* is parallel to $\overrightarrow{Pith_{Start}\ Pith_{End}}$ = (3600, P2e-P2s, P1e-P1s) and passes Pith_Start (0, P2s, P1s), the parameter equation of Line *l* is as follows:

$$x = 3600l$$
$$y = P2s + (P2e - P2s)l$$
$$z = P1s + (P1e - P1s)l$$

Thus, at any *x* position,

$$P1 = P1s + (P1e - P1s)(\frac{x}{3600})$$
$$P2 = P2s + (P2e - P2s)(\frac{x}{3600})$$

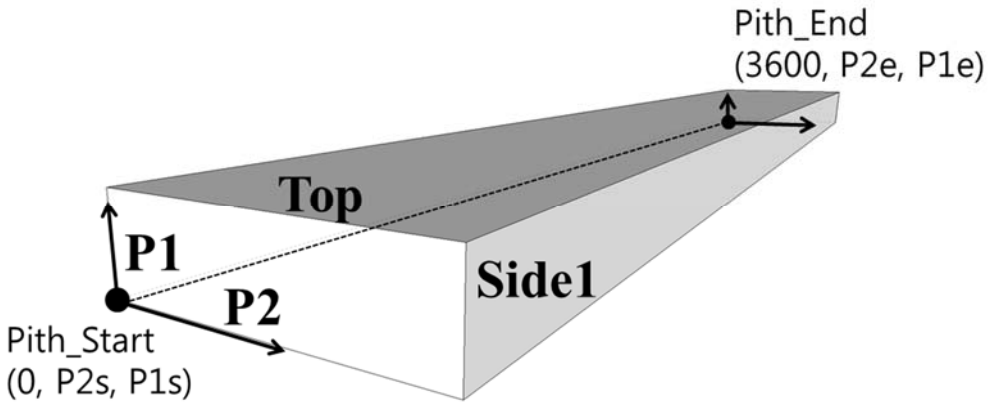

Figure X-11 Pith position on the end of cross-section of lamination